Synthesis and characterization of fiber Bragg gratings

Johannes Skaar

November 7, 2000

Abstract

This thesis is mainly a study of theoretical issues in the field of fiber Bragg gratings. The synthesis problem of gratings is investigated in detail. This applies to synthesis based on desired, complex spectra in reflection as well as in transmission. In addition, methods for characterization of fiber gratings are proposed.

For the synthesis problem of gratings, a genetic algorithm and a layer-peeling method are used. The genetic algorithm follows the principle of evolution from nature. As with nature, the evolution gives good results, but the synthesis process is extremely slow. On the other hand, the layer-peeling approach is extremely efficient, and the performance of the designed filters is very good. As the name indicates, one retrieves one layer at a time using a simple causality argument, and peels off the layers until the whole structure is reconstructed from the reflection response. We derive, analyze and compare two variants of the method that have appeared in the literature, a discrete and a continuous version. The discrete version is simplified and shown to be superior to the continuous version when it comes to stability and computing time. The continuous version offers some advantages in flexibility. To demonstrate the generality of the layer-peeling algorithm, we also apply it for synthesis of thin-film filters.

When designing gratings for use in transmission, one must have the minimum phase restriction in mind. Despite this restriction, it turns out that it is still possible to realize a complex response inside a limited bandwidth. The minimum phase condition is then satisfied by the behavior of the transfer function outside that interval. We propose a general method for synthesizing limited bandwidth minimum phase filters, and apply it in particular to design fiber gratings with specified transmission coefficients.

Several methods for characterization of fiber gratings are treated in the thesis. It is showed that phase reconstruction from reflectivity alone is not possible in general. Even if such reconstruction is possible for a certain type of grating, this method is not suitable for experimental gratings owing to bad stability against grating imperfections. Different kinds of *a priori* information can resolve this problem; one possibility is to use information of the index modulation amplitude. The resulting method is particularly useful for intragrating sensing since the index modulation amplitude is unchanged when the fiber is exposed to a spatial variation of strain or temperature. One can also retrieve the complex reflection spectrum of a grating by measuring the interference spectrum of the grating and a bare fiber end reflection. The group delay of the grating is obtained from the periodicity of the resulting Fabry-Perot spectral fringes. Finally, one can measure the complex reflection spectrum using low-coherence interferometry. By probing the grating at different positions, one gets the impulse response, from which the complex reflection spectrum can be determined through a Fourier transform.

Acknowledgements

Contents

Chapter 1

Introduction

1.1 Background

A fiber Bragg grating is an optical fiber for which the refractive index in the core is perturbed forming a periodic or quasi-periodic index modulation profile. A narrow band of the incident optical field within the fiber is reflected by successive, coherent scattering from the index variations. When the reflection from a crest in the index modulation is in phase with the next one, we have maximum mode coupling or reflection. Then the Bragg condition is fulfilled, i.e.

$$\lambda_B = 2n_{\mathrm{eff}}\Lambda, \tag{1.1}$$

where λ_B is the Bragg wavelength, n_{eff} is the effective modal index and Λ is the perturbation period. By modulating the quasi-periodic index perturbation in amplitude and (or) phase, we may obtain different optical filter characteristics.

The formation of permanent gratings by photosensitivity in an optical fiber was first demonstrated by Hill *el al.* in 1978 [1]. Photosensitivity means that exposure of UV light leads to a rise in the refractive index of certain doped glasses. Typical values for the index change are ranging between 10^{-6} to 10^{-3}, dependent on the UV-exposure and the dopants in the fiber. By using techniques as hydrogen loading [2], an index change as high as 10^{-2} can be obtained. The physical mechanism behind photosensitivity is not yet fully understood.

Fiber gratings are nowadays usually fabricated by a variant of the transverse holographic method first proposed by Meltz *et al.* [3]. By exposing the fiber to a UV interference pattern from the side, the pattern is "printed" into the fiber [4], see Fig. 1.1. Only the core is usually doped (for example with germanium), and consequently the grating is only formed in the core and not in the cladding. In order to write nonuniform gratings with advanced characteristics, one can use the scheme suggested by Stubbe *et al.* [5, 6].

Because a fiber Bragg grating can be designed to have an almost arbitrary, complex reflection response, it has a variety of applications, well described by Hill and Meltz among others [4]. For telecommunications, the probably most promising applications have been dispersion compensation [7] and wavelength selective devices [8]. Examples of the latter are filters for Wavelength Division Multiplexing (WDM) [9]. Fiber Bragg
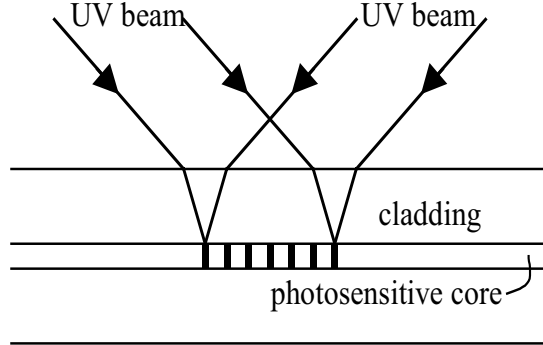
Figure 1.1: The transverse holographic method for writing fiber gratings. Two coherent UV beams produce an interference pattern in the fiber. The periodicity of the resulting grating is dependent on the angles of the incident beams.

gratings have also become popular as sensing devices, ranging from structural monitoring to chemical sensing [10]. Any change in the fiber properties, such as strain, temperature, or polarization which varies the modal index or grating pitch, will change the Bragg wavelength. Thus, by determining the peak reflectivity wavelength of the grating, we will get information about the sensing parameters. Distributed sensing is also possible for instance by recording the entire reflection spectrum. By applying an inverse scattering approach, it is possible to determine the grating structure, and thereby the distributed sensing parameters along the fiber (see Chapter 5). Another noteworthy application of fiber gratings is to use them as reflectors for fiber lasers [11].

In order to design fiber gratings for various applications, it is crucial to have tools for analysis, synthesis and characterization of fiber gratings. The most common mathematical model that governs wave propagation in gratings is the coupled-mode theory [12]. The analysis of gratings based on coupled-mode theory is well understood; a review is given in Chapter 2. The synthesis problem of gratings amounts to finding the grating structure (grating amplitude and phase) from a specified, complex spectrum. The synthesis problem will be treated in this thesis; both the design of gratings based on a desired reflection spectrum (Chapter 3) and based on a desired transmission spectrum (Chapter 4). Similarly, the task of characterizing fiber gratings is important to monitor the fabrication process or to monitor the grating as it is exposed to different physical perturbations as strain or temperature gradients. This problem is not always trivial as the reflection phase response spectrum is required in addition to the power spectrum for a complete characterization. Chapter 5 contains a description of methods for obtaining complete characterization of gratings.

The fiber Bragg grating is analogous to many other physical situations involving coupling between counter-propagating waves as transmission lines, thin-film filters, and acoustic filters. Therefore, many of the results in this thesis can be used in other fields.

2

An example of this is the layer-peeling synthesis method of fiber gratings which has been adopted for the synthesis of thin-film filters in Section 3.3.

1.2 Thesis history and outline

1.2.1 History

This thesis work was originated as a continuation of my diploma work 1997, which was about analysis and synthesis of fiber Bragg gratings. The work on the present thesis started in January 1998. During several stays at the Institute of Optical Research in Stockholm in 1998, I had the opportunity to test some of the grating theory in practice. At their grating lab facilities, we developed a low-coherence system for characterization of fiber gratings (Section 5.4). Back in Trondheim, I worked on phase retrieval of fiber gratings and application to characterization and distributed sensing (Sections 5.1 through 5.3). During the summer 1999, I was with the Institute of Optics, University of Rochester, Rochester NY. We investigated the layer-peeling inverse scattering method in detail and applied it to the synthesis of gratings and thin-film filters (Sections 3.2 and 3.3). Also, the new idea about synthesis of gratings for use in transmission was born (Chapter 4).

1.2.2 Outline

It is the author's intention that it should be possible to read the thesis if one has a general background in physics and mathematics. Therefore, a relatively thorough introduction to the field of fiber Bragg gratings is given in Chapter 2. First the coupled-mode theory is reviewed and the connection between the mathematical model and the physical quantities is described. In Section 2.2 the coupled-mode equations are solved analytically for two situations, uniform gratings and weak gratings. Section 2.3 contains the most convenient methods for solving the coupled-mode equations numerically. Both the numerical integration method (Runge-Kutta) and the common transfer-matrix method are described in addition to a new variant of the transfer-matrix method that is the counterpart to the discrete layer-peeling method for the corresponding inverse problem. Chapter 2 is ended by a brief discussion of the most important mathematical properties of the grating reflection and transmission spectra, and the properties of the transformation that exists between the grating structure and the spectra. The material in the Sections 2.1 through 2.3.2 is well-known, while the last Sections 2.3.3 through 2.4.2 contain less known theory.

Chapter 3 is devoted to the synthesis problem of gratings. The first article is about a genetic algorithm for the synthesis. The idea is to design the grating structure by numerical optimization using a certain merit function and a goal spectrum. In the second article, more direct design methods (layer-peeling algorithms) are described. The layer-peeling algorithm is a general, inverse scattering algorithm, and to show its powerfulness and generality, it is also applied for the synthesis of thin-film filters in the last paper of this chapter.

In Chapter 4 we treat a related synthesis problem, namely how to design a grating

with an arbitrarily transmission response. Because the transmission coefficient is a minimum phase-shift function, we limit the bandwidth of consideration to a finite interval. Then it turns out that the problem becomes that of finding a minimum phase transfer function with a desired complex response inside a finite frequency interval. The response outside that interval is unspecified. The problem is treated in a general context in the first article, and the next article shows how the theory can be applied to the synthesis of practical gratings. Both articles stand on their own.

The last group of papers deals with characterization of fiber gratings and intragrating sensing. Intragrating sensing basically means to read out the local Bragg wavelength profile of the grating, and consequently we can treat this application as a special case of characterization. The first two papers are about situations where it is possible to reconstruct the complex reflection coefficient from the power reflectivity, given some *a priori* information. The numerical stability is treated. The next paper is about a simple characterization method that utilizes the interference between the grating and a bare fiber end reflection, whereas the final paper describes a low-coherence approach to the characterization.

Finally, the thesis is summed up and lines are drawn into the future in Chapter 6.

Chapter 2

Fiber Bragg grating model

In this chapter, we describe the mathematical model of fiber Bragg gratings (FBG) that is used in the thesis. The results from coupled-mode theory are briefly reviewed together with the common numerical techniques for computing the reflection and transmission spectra of fiber gratings. Finally, we summarize the main properties of grating spectra and properties of the transformation that exists between the grating structure and the reflection spectrum.

The contents in Section 2.1 through 2.3.2 are well-known. There are already two books in the field of fiber Bragg gratings [13, 14], and in addition, there are several review articles and other articles, see e.g. [4, 12] and the references therein. The numerical algorithm in Section 2.3.3 and the theoretical grating properties listed in Section 2.4 are less known although most of the results have been published previously.

2.1   Coupled-mode theory

The relation between the spectral dependence of a fiber grating and the corresponding grating structure is usually described by the coupled-mode theory. While other techniques are available, we consider only coupled-mode theory since it is straightforward, it is intuitive, and it accurately models the optical properties of most fiber gratings of interest. Coupled-mode theory is described in a number of texts; detailed analysis can be found in [12, 15, 16, 17, 18]. The notation in this section follows most closely that of Snyder and Love [15] and Poladian [18]. Throughout this thesis, we assume that the fiber is lossless and single mode in the wavelength range of interest. In other words, we consider only one forward and one backward propagating mode. Moreover, we assume that the fiber is weakly guiding, i.e. the difference between the refractive indices in the core and the cladding is very small. Then the electric and magnetic fields are approximately transverse to the fiber axis, and we can ignore all polarization effects due to the fiber structure and consider solely the scalar wave equation [15]. The fiber axis is oriented in the $+z$ direction and we assume that the electric field is x-polarized. The implicit time dependence is $\exp(-i\omega t)$; a forward propagating wave with propagation constant $\beta > 0$ and frequency $\omega > 0$ has thus the form $\exp[i(\beta z - \omega t)]$.

The grating is treated as a perturbation on the fiber. The unperturbed fiber has refractive index profile $\overline{n}(x, y)$ and the perturbed fiber has the z-dependent index $n(x, y, z)$.

Both fibers are weakly guiding so we assume $\overline{n} \cong n \cong n_{\text{eff}} \cong n_{\text{cl}}$ where n_{cl} is the index in the cladding and n_{eff} is the effective index of the supported mode in the absence of the grating. We write the total electric field as a superposition of the forward and backward propagating modes,

$$E_x(x,y,z) = b_1(z)\Psi(x,y) + b_{-1}(z)\Psi(x,y), \tag{2.1}$$

where the coefficients $b_{\pm 1}$ contain all the z-dependence of the modes. It is clear that $b_{\pm 1}$ are dependent on frequency since they include the harmonic propagation factor $\exp(\pm i\beta z)$ with $\beta = \beta(\omega) = n_{\text{eff}}\omega/c = n_{\text{eff}}k$ as the scalar propagation constant. The transverse dependence is described by the function Ψ, which satisfies the scalar wave equation for the unperturbed fiber,

$$\{\nabla_t^2 + k^2\overline{n}^2(x,y) - \beta^2\}\Psi = 0, \tag{2.2}$$

where $\nabla_t^2 = \partial^2/\partial x^2 + \partial^2/\partial y^2$, and $k = \omega/c$ is the vacuum wavenumber. The total electric field E_x must satisfy the scalar wave equation for the perturbed fiber, i.e.

$$\{\nabla_t^2 + k^2 n^2(x,y,z) + \partial^2/\partial z^2\}E_x = 0. \tag{2.3}$$

By substituting (2.1) into (2.3), and using (2.2), we obtain

$$\frac{d^2}{dz^2}(b_1 + b_{-1})\Psi + [\beta^2 + k^2(n^2 - \overline{n}^2)](b_1 + b_{-1})\Psi = 0. \tag{2.4}$$

Multiplication by Ψ and integration over the xy-plane leads to

$$\frac{d^2 b_1}{dz^2} + \frac{d^2 b_{-1}}{dz^2} + (\beta^2 + 2kn_{\text{co}}D_{11}(z))(b_1 + b_{-1}) = 0, \tag{2.5}$$

where we have defined the coefficient D_{11} as

$$D_{11}(z) = \frac{\frac{k}{2n_{\text{co}}}\int(n^2 - \overline{n}^2)\Psi^2 dA}{\int \Psi^2 dA}. \tag{2.6}$$

The refractive index $n_{\text{co}} \approx n_{\text{eff}}$ is an approximate value for the index in the fiber core, and the integrations extend over the entire xy-plane. Eq. (2.5) can be decomposed into the following set of first order differential equations [15]

$$\frac{db_1}{dz} - i(\beta + D_{11})b_1 = iD_{11}b_{-1}$$
$$\frac{db_{-1}}{dz} + i(\beta + D_{11})b_{-1} = -iD_{11}b_1, \tag{2.7}$$

as is readily realized by differentiation and summation of the two equations in (2.7). This decomposition corresponds to separating the total field in (2.1) into its forward and backward propagating components. Indeed, when $n = \overline{n}$, we observe that the solution of (2.7) reduces to $b_{\pm 1}(z) = B_{\pm 1}\exp(\pm i\beta z)$ with constant $B_{\pm 1}$, i.e. $b_{\pm 1}$ correspond to the forward and backward propagating modes. In the absence of the grating, $n = \overline{n}$,

6

the modes propagate without affecting each other; otherwise the modes will couple to each other through the quantity $D_{11}(z)$.

For a fiber grating, the z-dependence of the index perturbation is approximately quasi-sinusoidal in the sense that it can be written

$$n^2 - \overline{n}^2 = \Delta\epsilon_{r,\text{ac}}(z)\cos\left(\frac{2\pi}{\Lambda}z + \theta(z)\right) + \Delta\epsilon_{r,\text{dc}}(z) \tag{2.8}$$

where Λ is a chosen design period so that $\theta(z)$ becomes a slowly varying function of z compared to a period Λ. The functions $\Delta\epsilon_{r,\text{ac}}(z)$ and $\Delta\epsilon_{r,\text{dc}}(z)$ are real and slowly varying, and satisfy

$$|\Delta\epsilon_{r,\text{ac}}(z)| << n_{\text{co}}^2, \qquad |\Delta\epsilon_{r,\text{dc}}(z)| << n_{\text{co}}^2. \tag{2.9}$$

It is therefore convenient to express D_{11} as a quasi-sinusoidal function

$$D_{11}(z) = \kappa(z)\exp\left(i\frac{2\pi}{\Lambda}z\right) + \kappa^*(z)\exp\left(-i\frac{2\pi}{\Lambda}z\right) + \sigma(z) \tag{2.10}$$

where $\kappa(z)$ is a complex, slowly varying function of z and $\sigma(z)$ is a real, slowly varying function that accounts for the dc index variation from $\epsilon_{r,\text{dc}}(z)$. In order to simplify (2.7), we define new field amplitudes u and v by setting

$$b_1(z) = u(z)\exp\left(+i\frac{\pi}{\Lambda}z\right)\exp\left(+i\int_0^z \sigma(z')dz'\right)$$

$$b_{-1}(z) = v(z)\exp\left(-i\frac{\pi}{\Lambda}z\right)\exp\left(-i\int_0^z \sigma(z')dz'\right). \tag{2.11}$$

By substituting (2.10) and (2.11) into the equations (2.7), ignoring the terms that are rapidly oscillating since they contribute little to the growth and decay of the amplitudes, we arrive at the coupled-mode equations

$$\frac{du}{dz} = +i\delta u + q(z)v$$

$$\frac{dv}{dz} = -i\delta v + q^*(z)u. \tag{2.12}$$

In (2.12) we have defined the wavenumber detuning $\delta = \beta - \pi/\Lambda$ and the coupling coefficient q of the grating

$$q(z) = i\kappa(z)\exp\left(-2i\int_0^z \sigma(z')dz'\right). \tag{2.13}$$

Note that all phase factors in (2.11) are independent of the propagation constant β and therefore the frequency. Hence, we can simply treat the new variables u and v as the fields themselves once the reference planes have been fixed, since they differ only from $b_{\pm 1}$ by constant phase factors. For example, the reflection coefficient $b_{-1}(z_0)/b_1(z_0)$ can as well be computed by the expression $v(z_0)/u(z_0)$ once the position z_0 has been fixed because the two expressions only differ by a constant phase factor. Also note that all

the functions u, v and q are slowly varying with z compared to the period Λ because $\beta \approx \pi/\Lambda$ when the wavelength is close to the Bragg wavelength $\lambda_B = 2n_{\text{eff}}\Lambda$.

To get a feeling of the physical interpretation of the coupling coefficient, we will examine the relation between the coupling coefficient and the grating parameters. Usually for a fiber Bragg grating, the induced index change happens in the fiber core only, i.e. $n = \overline{n}$ in the cladding. Moreover, if we assume that the index change is created uniformly in the core, then (2.6) yields

$$D_{11}(z) = \frac{k}{2n_{\text{co}}}(n^2 - \overline{n}^2)\eta \tag{2.14}$$

where η is the fraction of the modal power that is contained in the fiber core. By substitution of (2.8) into (2.14), and comparison to (2.10), we obtain $2|\kappa| = \eta k \Delta \epsilon_{r,\text{ac}}/2n_{\text{co}}$, $\theta = \arg \kappa$, and $\sigma = \eta k \Delta \epsilon_{r,\text{dc}}/2n_{\text{co}}$. Because the index change is small we can set $\Delta \epsilon_r = \Delta(n_{\text{co}}^2) = 2n_{\text{co}}\Delta n$, and use (2.13) to obtain

$$|q(z)| = \frac{\eta \pi \Delta n_{\text{ac}}(z)}{\lambda}$$
$$\arg q(z) = \theta(z) - 2\eta k \int_0^z \Delta n_{\text{dc}}(z')dz' + \frac{\pi}{2}. \tag{2.15}$$

Note that since the index perturbation is small, (2.8) can be written

$$n - \overline{n} = \Delta n_{\text{ac}}(z) \cos\left(\frac{2\pi}{\Lambda}z + \theta(z)\right) + \Delta n_{\text{dc}}(z), \tag{2.16}$$

where $\Delta n_{\text{ac}}(z)$ and $\Delta n_{\text{dc}}(z)$ are the "ac" and "dc" index change, respectively, and we have used the approximation $n^2 - \overline{n}^2 \approx 2n_{\text{co}}(n - \overline{n})$. We can therefore interpret the coupling coefficient in the following way: The modulus of q is proportional to the index modulation amplitude or the peak-to-peak modulation of the index variation, see Fig. 2.1. The phase of q corresponds to the excess optical phase or phase envelope of the grating; the term $\theta(z)$ is the spatial grating phase and the integral term in (2.15) gives the optical modification to the spatial phase due to the increased dc index. The derivative of $\arg q$ gives the extra effective spatial frequency of the grating in addition to $2\pi/\Lambda$,

$$d\arg q/dz = d\theta/dz - 2\eta k \Delta n_{\text{dc}}(z). \tag{2.17}$$

This translates into an effective grating periodicity of

$$\Lambda_{\text{eff}}(z) = \Lambda \left(1 + \frac{\Lambda}{2\pi}\frac{d\theta}{dz} - \eta\frac{\Delta n_{\text{dc}}(z)}{n_{\text{eff}}}\right)^{-1} \tag{2.18}$$

for $\lambda \approx \lambda_B$. In the literature, the impact of the dc index change is sometimes incorporated in $\theta(z)$. In that case we would have $q = i\kappa$. Note however, that κ is defined in different ways, and may or may not include the grating phase and/or the phase due to the dc index change.
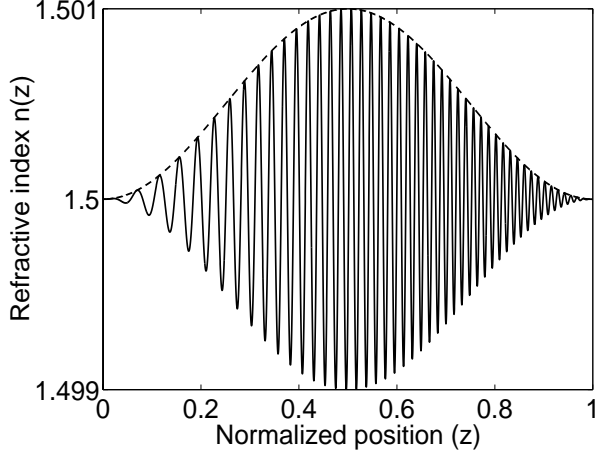
Figure 2.1: The solid line shows the refractive index profile of a chirped, apodized grating. Chirp and apodization mean that the grating period and strength are varying with z. For a typical fiber grating, the period would be much smaller compared to the grating length than at this plot. The unperturbed index is set to $\overline{n} = 1.5$. The dashed line corresponds to the ac index modulation envelope $\Delta n_{\mathrm{ac}}(z)$ added to $\overline{n}$.

We summarize the grating model as follows. The Bragg grating is characterized by the following quantities: The design Bragg wavelength λ_B, the effective refractive index n_{eff}, and the slowly varying complex coupling coefficient $q(z)$. The modulus of the coupling coefficient determines the grating strength or the index modulation amplitude, and the phase corresponds to the grating phase envelope. The forward and backward propagating field envelopes are mutually coupled by the coupled mode equations

$$\frac{du(z;\delta)}{dz} = +i\delta u + q(z)v$$
$$\frac{dv(z;\delta)}{dz} = -i\delta v + q^*(z)u, \tag{2.19}$$

where δ is proportional to the frequency detuning with respect to the design Bragg frequency,

$$\delta = \beta - \pi/\Lambda = (\omega - \omega_B)n_{\mathrm{eff}}/c, \qquad \omega_B = 2\pi c/\lambda_B. \tag{2.20}$$

This model forms the basis for the rest of this thesis.

2.2 Analytical solutions to the coupled-mode equations

Any solution $\{u, v\}$ to the coupled-mode equations must satisfy (2.19) and two appropriate boundary conditions. For example, the boundary conditions $u(0; \delta) = 1$ and $v(L, \delta) = 0$ give the reflection coefficient $r(\delta) = v(0; \delta)$ and the transmission coefficient $t(\delta) = u(L; \delta)$ of a grating located in $0 \leq z \leq L$. There are two well-known, important cases where it is possible to find simple closed-form solutions to the coupled-mode equations. The two cases are weak gratings for which we can use the first order Born approximation [16], and uniform gratings where $q(z) = \text{const.}$ [19]. We will use the boundary conditions above in both cases.

2.2.1 Weak gratings

A weak grating has small influence on the propagating waves. In the limit $q \to 0$, the coupled-mode equations yield the zeroth order, trivial solutions $u = u_0 \exp(i\delta z)$ and $v = v_0 \exp(-i\delta z)$. By the boundary conditions above, these solutions reduce to $u = \exp(i\delta z)$ and $v = 0$. The first order Born approximation will in this case mean that the forward propagating wave u is unaffected by the grating, that is $u = \exp(i\delta z)$. This expression in turn is substituted into the last equation in (2.19). By integrating the resulting first order differential equation using the boundary conditions $v(0, \delta) = r(\delta)$ and $v(\infty; \delta) = 0$, we obtain

$$r(\delta) = -\frac{1}{2} \int_0^\infty q^* \left(\frac{z}{2}\right) \exp(i\delta z) dz \tag{2.21}$$

Hence, in the first order Born approximation, the functions $r(\delta)$ and $-\frac{1}{2}q^* \left(\frac{z}{2}\right)$ form a Fourier transform pair, and

$$-\frac{1}{2}q^* \left(\frac{z}{2}\right) = \int_{-\infty}^\infty r(\delta) \exp(-i\delta z) d\delta. \tag{2.22}$$

As a rule of thumb, these weak grating relations are valid when the top reflectivity of the grating is less than about 10-40% or if the area of the coupling coefficient, $\int_0^\infty |q(z)| dz$, is less than about 0.3 to 1.0. Although the Fourier relations break down for stronger gratings, much of the intuition from Fourier analysis remains still valid as will be shown in Section 2.4.2.

2.2.2 Uniform gratings

A uniform grating has constant coupling coefficient over a limited range $0 \leq z \leq L$, where L is the grating length. In this situation, the coupled-mode equations can be solved analytically. By differentiation of (2.19) and substitution of the derivatives from the original equations, we obtain $d^2u/dz^2 = (|q|^2 - \delta^2)u$ and $d^2v/dz^2 = (|q|^2 - \delta^2)v$. By solving these simple equations, we obtain expressions for u and v involving 4 constants.
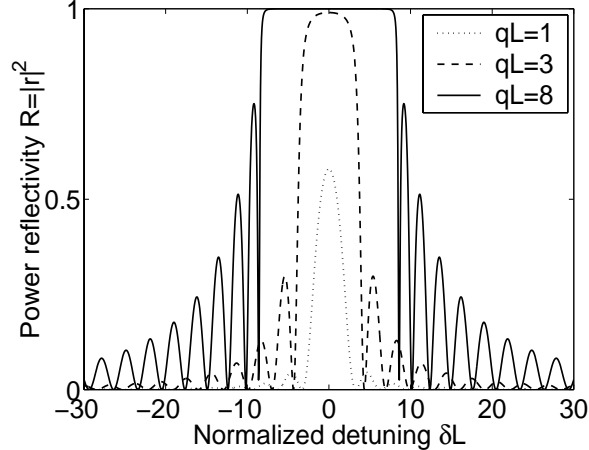
Figure 2.2: The power reflectivity $R = |r|^2$ of a uniform grating with three different values of the strength qL. When $qL = 1$, the spectrum is very near to the sinc²-like spectrum predicted by the Born approximation. For a 1cm grating at the Bragg wavelength $\lambda_B = 1550$nm, a detuning of 30cm^{-1} corresponds to a bandwidth of about $\Delta\lambda = 0.8$nm in a normal fiber.

These constants are determined by substituting the expressions into the original coupled-mode equations and applying the two boundary conditions. The resulting reflection coefficient is

$$r(\delta) = \frac{-q^* \sinh(\gamma L)}{\gamma \cosh(\gamma L) - i\delta \sinh(\gamma L)} \tag{2.23}$$

where we have defined the parameter $\gamma^2 = |q|^2 - \delta^2$. The transmission coefficient becomes

$$t(\delta) = \frac{\gamma}{\gamma \cosh(\gamma L) - i\delta \sinh(\gamma L)}. \tag{2.24}$$

We note that both coefficients are meromorphic functions. While the reflection coefficient has both poles and zeros, the transmission coefficient is zero-free everywhere. As we will see later, this is typical for all (nonuniform) fiber gratings. Moreover, we note that in the weak grating limit, the reflection coefficient reduces to $r(\delta) = -q^* L \exp(i\delta L) \operatorname{sinc} \delta L$, where $\operatorname{sinc} x = \sin x / x$, in consistency with the Fourier relation (2.21). In Fig. 2.2.2 the power reflectivity $R(\delta) = |r(\delta)|^2$ of a uniform grating is plotted for different values of the grating strength. We observe that the spectra are sinc²-like, but as the strength increases, the top reflectivity is pressed down so that it never gets larger than 1.

2.3   General numerical solution techniques

There is a variety of methods to compute the reflection and transmission spectra for nonuniform gratings. Here we will only present the two most extensively used methods in addition to another less known method. In the first method, the coupled-mode equations are integrated using Runge-Kutta algorithms, whereas in the other, often-preferred transfer matrix method, one divides the grating into smaller sections [12]. The sections are treated as uniform gratings, yielding the overall spectra by transfer matrix multiplication. Finally, we present a less known method in which the grating model is discretized into a stack of discrete, complex reflectors. The overall spectrum is then found using a simple recursion expression. The algorithm is in some sense similar to Rouard's method of thin-film optics which has been applied to corrugated waveguide filters previously [20]. The difference between the approach in [20] and the present approach is that they divided the grating into as many sections as there are grating periods, while in the present approach we will only use as many sections as necessary to represent the (slowly varying) coupling coefficient with a sufficient accuracy. As we will see in Section 3.2, the discretized grating model method is the direct counterpart to the layer-peeling reconstruction or synthesis algorithm [21].

2.3.1   Direct numerical integration

Define $r(z; \delta) = v(z; \delta)/u(z; \delta)$. By differentiation of $r(z; \delta)$ with respect to z and substituting from the coupled-mode equations (2.19), we get the following Riccati equation

$$\frac{dr(z; \delta)}{dz} = -2i\delta r - q(z)r^2 + q^*(z). \tag{2.25}$$

By applying the boundary condition $r(L; \delta) = 0$ we can start at the end of the grating and use Runge-Kutta methods to work the equation backwards to $z = 0$. The reflection coefficient of the grating becomes $r(\delta) = r(0; \delta)$. Even though this method is simple, the number of steps of the Runge-Kutta routine must be large to ensure convergence. Therefore, in some cases the algorithm might be slow compared to the next two methods.

2.3.2   Transfer matrix method

Divide the grating into a sufficient number N of sections so that each section can be approximately treated as uniform. Let the section length be $\Delta = L/N$. By applying the appropriate boundary conditions and solving the coupled-mode equations similar to the procedure in Section 2.2.2, we find the following transfer matrix relation between the fields at z and at $z + \Delta$

$$\begin{bmatrix} u(z + \Delta) \\ v(z + \Delta) \end{bmatrix} = \begin{bmatrix} \cosh(\gamma\Delta) + i\frac{\delta}{\gamma}\sinh(\gamma\Delta) & \frac{q}{\gamma}\sinh(\gamma\Delta) \\ \frac{q^*}{\gamma}\sinh(\gamma\Delta) & \cosh(\gamma\Delta) - i\frac{\delta}{\gamma}\sinh(\gamma\Delta) \end{bmatrix} \begin{bmatrix} u(z) \\ v(z) \end{bmatrix}. \tag{2.26}$$

Hence, we can connect the fields at the two ends of the grating through

$$\begin{bmatrix} u(L) \\ v(L) \end{bmatrix} = \mathbf{T} \begin{bmatrix} u(0) \\ v(0) \end{bmatrix}, \tag{2.27}$$

where $\mathbf{T} = \mathbf{T}_N \cdot \mathbf{T}_{N-1} \cdot \dots \cdot \mathbf{T}_1$ is the overall transfer matrix. The matrix $\mathbf{T}_j$ is the transfer matrix written in (2.26) with $q = q_j = q(j\Delta)$ the coupling coefficient of the jth section. As a result, $\mathbf{T}$ is a 2×2 matrix with elements

$$\mathbf{T} = \begin{bmatrix} T_{11} & T_{12} \\ T_{21} & T_{22} \end{bmatrix}. \tag{2.28}$$

Once $\mathbf{T}$ is found, the reflection coefficient from the left and the transmission coefficient are calculated by the relations

$$\begin{aligned} r(\delta) &= -T_{21}/T_{22} \\ t(\delta) &= 1/T_{22}, \end{aligned} \tag{2.29}$$

obtained by substitution of the appropriate boundary conditions into (2.27). The advantages with this method are that it is stable and also efficient since relatively few sections are required for analyzing most common gratings accurately.

2.3.3 Discretized grating model method

Instead of making the piecewise uniform discretization as above, we can discretize such that the whole grating becomes a stack of complex, discrete reflectors. Each of the transfer matrices above are then replaced by $\mathbf{T}^\Delta \cdot \mathbf{T}_j^\rho$, where

$$\mathbf{T}^\Delta = \begin{bmatrix} \exp(i\delta\Delta) & 0 \\ 0 & \exp(-i\delta\Delta) \end{bmatrix} \tag{2.30}$$

is the pure propagation matrix obtained by letting $q \to 0$ in the matrix in (2.26), and

$$\mathbf{T}_j^\rho = (1 - |\rho_j|^2)^{-1/2} \begin{bmatrix} 1 & -\rho_j^* \\ -\rho_j & 1 \end{bmatrix} \tag{2.31}$$

is the discrete reflector matrix obtained by letting $q \to \infty$ holding $q\Delta$ constant. The discrete reflection coefficient is given by $\rho_j = -\tanh(|q_j|\Delta)q_j^*/|q_j|$. It is straightforward to show that the task of transferring the fields using $\mathbf{T}^\Delta \cdot \mathbf{T}_j^\rho$, similar to (2.26), is equivalent to the recursion

$$r(z; \delta) = \frac{\rho_j + r(z + \Delta; \delta) \exp(2i\delta\Delta)}{1 + \rho_j^* r(z + \Delta; \delta) \exp(2i\delta\Delta)}, \tag{2.32}$$

analogously to (2.25). The reflection coefficient of the grating is obtained by setting $r(L; \delta) = 0$ and then working (2.32) backwards to $z = 0$, yielding the spectrum $r(\delta) = r(0; \delta)$. In contrast to the direct numerical integration method, the propagation of $r(z; \delta)$ is exact for the discrete model, and the numerical stability is therefore as good as for the transfer matrix method. In addition, the discrete method based on (2.32) is very fast as one only needs to evaluate a hyperbolic function $\mathcal{O}(N)$ times in contrast to $\mathcal{O}(N^2)$ times when using (2.26).

The two latter methods are exact once the grating model has been discretized; the computational error arises in the model discretization. In the ordinary transfer-matrix

13

approach, the coupling coefficient is assumed to be piecewise uniform, i.e. $q(z)$ has a staircase-like shape. In contrast, $q(z)$ has a comb shape in the discretized model. In the weak grating limit (Fourier), it is clear that the latter discretization is most accurate in the relevant bandwidth. This is realized from the fact that provided $q(z)$ is sampled with a sufficient number of points according to the Nyquist theorem, the spectrum is represented exactly in the relevant bandwidth (that is inside one period of the repeated spectra, principal range). The spectrum of the piecewise uniform approximation will be the exact spectrum multiplied by a (wide) sinc-function, and hence there will also be inaccuracies in the principal range. For strong gratings, the situation is opposite because the Fourier relation breaks down, and the piecewise uniform approximation models more accurately the multiple reflections inside each section. This conclusion has been supported by numerical calculations.

2.4 Theoretical constraints

In this section, we will give a summary of the most important mathematical properties of the grating spectra and the transformation between the coupling coefficient (grating structure) and the reflection spectrum. Most of the results in this section are either given in Song [22] or Poladian [23].

2.4.1 Properties of the reflection and transmission spectra

A fiber grating is a two-port device with scattering matrix [24]

$$\mathbf{S}(\delta) = \begin{bmatrix} r_1 & t \\ t & r_2 \end{bmatrix},$$
(2.33)

where $r_1 = r$ and r_2 are the reflection coefficients from the left and the right, respectively, and t is the transmission coefficient. The transmission coefficient is equal for both directions due to reciprocity. Since the device is assumed to be lossless, the scattering matrix must be unitary, i.e.

$$\mathbf{S}^T \mathbf{S}^* = \mathbf{I}.$$
(2.34)

From (2.34) we obtain the relations

$$|r_{1,2}|^2 + |t|^2 = 1$$
$$\frac{r_1}{r_2^*} = -\frac{t}{t^*}.$$
(2.35)

The first equation expresses the trivial lossless condition. The latter relation connects the phases of the two reflection coefficients and the transmission coefficient, and was stated previously in [22, 23].

The transfer matrix of a general grating is determined from the scattering matrix by the following expression

$$\mathbf{T}(\delta) = \begin{bmatrix} t - \frac{r_1 r_2}{t} & \frac{r_2}{t} \\ -\frac{r_1}{t} & \frac{1}{t} \end{bmatrix},$$
(2.36)

which is readily obtained from the transfer matrix relation (2.27). For a lossless grating, we can use the properties (2.35) to simplify $\mathbf{T}$, writing

$$\mathbf{T}(\delta) = \begin{bmatrix} \frac{1}{t^*} & \frac{r_2}{t} \\ -\frac{r_1}{t} & \frac{1}{t} \end{bmatrix} = \begin{bmatrix} \frac{1}{t^*} & -\frac{r_1^*}{t^*} \\ -\frac{r_1}{t} & \frac{1}{t} \end{bmatrix}. \tag{2.37}$$

We observe that $\det \mathbf{T} = 1$ and that the elements of $\mathbf{T}$ satisfy $T_{22} = T_{11}^*$ and $T_{21} = T_{12}^*$, as required from the lossless and reciprocity conditions.

It can be shown that the transmission coefficient has no zeros in the complex ω plane [25, 23, 26], and thus that it satisfies the minimum phase condition. If one sets the input and output reference planes to the same position, the asymptotic behavior of the transmission coefficient is $t(\omega) \to 1$ as $\omega \to \infty$. Then the amplitude and phase response in transmission are uniquely related by means of a logarithmic Hilbert transform,

$$\arg t(\omega) = \mathcal{H}[\ln |t(\omega')|]. \tag{2.38}$$

The sign in the integral expression of the Hilbert transform $\mathcal{H}$ is dependent on the sign convention of the Fourier transform. Note that in this context, it is more convenient to use ω rather than δ as the frequency variable. This is due to the fact that some of the dispersion relations in the literature, analogously to (2.38), are not valid unless we have conjugate symmetry about $\omega = 0$; $t(\omega) = t^*(-\omega)$. Of course, a similar symmetry $t(\delta) = t^*(-\delta)$ is not generally valid. The minimum phase condition of the transmission coefficient is treated thoroughly in Chapter 4.

Here we will only examine the impact of (2.38) on the reconstruction of t. We note that the modulus of t can be found from the reflectivity $R = |r|^2$ when the grating is lossless. Since the phase of t can be computed from $|t|$, we conclude that t is uniquely determined from R, and that the reverse reflection coefficient r_2 is uniquely determined from r_1 by (2.35). Finally, we remark that the logarithmic Hilbert transform relation is generally not valid for the reflection coefficient (see Section 5.1).

2.4.2 Properties of the transformation $q(z) \leftrightarrow r(\delta)$

As we have seen in Section 2.3 we can calculate the complex reflection spectrum from any grating structure $q(z)$. As we will see in Chapter 3, it is also possible to perform the inverse calculation; one can obtain the grating structure $q(z)$ associated with a certain, realizable complex reflection spectrum. The bidirectional transformation $q(z) \leftrightarrow r(\delta)$ is therefore in some sense analogous to the Fourier transforms. Indeed, it is stated in Section 2.2.1 that in the weak grating limit the transformation is essentially equal to a Fourier transform (when ignoring the scaling factors and the complex conjugation in (2.22)). For general gratings, some of the properties of the Fourier transform break down since the transformations no longer are linear. The nonlinearity is readily seen as $|r| < 1$ while $|q|$ has no theoretical limit. Nevertheless, many of the common properties of the Fourier transform remain valid. In this section we will summarize the most important properties. The properties that are not obvious are proved in [22] in a slightly different form.

1. Symmetry relations

$$q(z) \text{ is real} \Leftrightarrow r(\delta) = r^*(-\delta), \ t(\delta) = t^*(-\delta) \tag{2.39}$$
$$q(z) \text{ is imaginary} \Leftrightarrow r(\delta) = -r^*(-\delta), \ t(\delta) = t^*(-\delta)$$
$$q(z) = q^*(-z) \Leftrightarrow r(\delta)/t(\delta) \text{ is real}$$
$$q(z) = -q^*(-z) \Leftrightarrow r(\delta)/t(\delta) \text{ is imaginary}$$
$$q(z) = -q(-z) \Leftrightarrow r(\delta)/t(\delta) = -r(-\delta)/t(-\delta), \ t(\delta) = t^*(-\delta)$$
$$q(z) = q(-z) \Leftrightarrow r(\delta)/t(\delta) = r(-\delta)/t(-\delta), \ t(\delta) = t^*(-\delta)$$

2. Global phase shift (θ_0 is a real constant)

$$q(z) \rightarrow q(z)\exp(i\theta_0) \Leftrightarrow r(\delta) \rightarrow r(\delta)\exp(-i\theta_0), \ t(\delta) \text{ is invariant} \tag{2.40}$$

3. Scaling (a is a real constant)

$$q(z) \rightarrow aq(az) \Leftrightarrow r(\delta) \rightarrow r(\delta/a), \ t(\delta) \rightarrow t(\delta/a) \tag{2.41}$$

4. Translation (z_0 is a real constant)

$$q(z) \rightarrow q(z - z_0) \Leftrightarrow r(\delta) \rightarrow r(\delta)\exp(i2\delta z_0), \ t(\delta) \text{ is invariant} \tag{2.42}$$

5. Frequency shift

$$r(\delta) \rightarrow r(\delta - \delta_0), \ t(\delta) \rightarrow t(\delta - \delta_0) \Leftrightarrow q(z) \rightarrow q(z)\exp(i2\delta_0 z) \tag{2.43}$$

6. Physical inversion

$$q(z) \rightarrow -q^*(-z) \Leftrightarrow r(\delta)/t(\delta) \rightarrow -r^*(\delta)/t^*(\delta), \ t(\delta) \text{ is invariant} \tag{2.44}$$

Note that physical inversion means that $D_{11}(z) \rightarrow D_{11}(-z)$ in (2.10) which in turn implies $q(z) \rightarrow -q^*(-z)$ by (2.10) and (2.13). Also note that δ is assumed to be real.

Chapter 3

Grating synthesis

The synthesis problem of a fiber grating amounts to finding the complex coupling co-efficient $q(z)$ that corresponds or approximates a desired reflection response $r(\delta)$. The simplest approach is to use the approximate Fourier relation (2.22) that results from the first order Born approximation. This method is of course only suitable for weak gratings. For high-reflectivity gratings, one can find the coupling coefficient using classical inverse scattering techniques. Song and Shin [27] demonstrated how one can design corrugated gratings by solving two coupled integral equations that is called the Gel'fand-Levitan-Marchenko (GLM) equations. Their approach is exact but the reflection coefficient must be a rational function. Later, Frangos and Jaggard proposed two different numerical approaches [28, 29] to solve the GLM equations without the rational limitation on $r(\delta)$. Similarly, Peral *et al.* [30] proposed an iterative, numerical method to solve the GLM equations in order to design fiber gratings. Their algorithm is equivalent to the last algorithm by Frangos and Jaggard [29]. The iterative solution to the GLM equations is compared with an optimizing Genetic Algorithm (GA) for the synthesis in the next section. Different trade-offs in the design process is facilitated by the GA algorithm, but since the GA method is so slow, it has not been extensively used later in this work. In 1999, Feced *et al.* [21] adopted the so-called layer-peeling algorithm for the synthesis of fiber gratings. This method is fast and accurate, and in Section 3.2 we simplify it, and compare it to an algorithm proposed by Poladian [31], which turns out to be a variant of the layer-peeling algorithm. The layer-peeling algorithm is general and extremely simple; in fact it is as simple as the forward problem of finding the spectrum from the coupling coefficient. In order to show its generality it has been applied to a similar synthesis problem, namely to design optical thin-film filters (Section 3.3).

Note that the sign convention on the implicit time dependence in Section 3.1 does not correspond to the sign convention in Chapter 2.

3.1 A genetic algorithm for the inverse problem in synthesis of fiber gratings

Authors: Johannes Skaar and Knut Magne Risvik

A Genetic Algorithm for the Inverse Problem in Synthesis of Fiber Gratings

Johannes Skaar and Knut Magne Risvik

Abstract— A new method for synthesis of fiber gratings with advanced characteristics is proposed. By combining the Runge–Kutta method for calculating the reflection spectrum of a fiber grating and a genetic algorithm, we obtain a promising method for the synthesis. Compared to other methods, the proposed method facilitates the task of weighting the different requirements to the filter spectrum. In addition, the method is general, and would thus be useful for other inverse problems.

Index Terms— Fiber Bragg gratings, genetic algorithms, synthesis.

I. INTRODUCTION

A classical problem in applied physics and engineering fields is the inverse problem, such as for instance the synthesis of a system, for which the analysis method is known. An example of such a synthesis is to determine a fiber grating index modulation profile corresponding to a given reflection spectrum. This is not a trivial problem, and a variety of synthesis algorithms has been proposed [1]–[3].

For weak gratings, the synthesis problem of fiber gratings reduces to an inverse Fourier transform of the reflection coefficient. This is known as the first-order Born approximation, and applies only for gratings for which the reflectivity is small. For synthesis of corrugated waveguide filters with higher reflectivity, the Fourier transform technique has been extended by Winick and Roman [1], yielding a better approximation. An exact solution of this inverse scattering problem was found by Song and Shin [2], who solved the coupled Gel'fand–Levitan–Marchenko (GLM) integral equations that appear in quantum mechanics. Their method is exact, but is restricted to reflection coefficients that can be expressed as a rational function. An iterative solution to the GLM equations was found by Peral *et al.* [3], yielding smoother coupling coefficients than the exact method. Their algorithm is converging relatively fast, and gives satisfying results even for high reflectivity gratings. However, when specifying ideal filter responses, it is desirable to have a weighting mechanism, which makes it easier to weight the different requirements. For example, when synthesizing an optical bandpass filter, one may be interested in weighting linear phase more than sharp peaks, because the dispersion may be a more critical

parameter. The iterative GLM method does not support such a mechanism in a satisfactory way.

In this paper we present a new approach to the solution of inverse problems, in particular the problem of synthesizing waveguide gratings. The coupling coefficient is sampled, and the N samples are applied as inputs to a "black box," which calculates the reflection spectrum. The output of the "black box" is an error value to be minimized in order to achieve the aimed reflection spectrum. Thus, the synthesis problem is reduced to a minimization of a nonlinear, hidden function of N variables. This optimization problem is solved using a genetic algorithm [4], i.e., an algorithm that follows the same principle as the evolution process of nature.

The outline of this paper is as follows: Section II contains a short description of Genetic Algorithms, and in Section III and IV the theoretical approach and the synthesis algorithm are presented. Section V contains numerical results and comparisons to alternative synthesis methods, and finally the main conclusions are drawn in Section VI.

II. GENETIC ALGORITHM PRELIMINARIES

Genetic algorithms (GA's) are probabilistic parallel search algorithms based on natural selection. GA's were designed to efficiently search large and poorly understood search spaces where expert knowledge was limited or inaccessible. The basic principles of GA were first laid down by Holland [5], and are well described in [4].

In nature, individuals in a population compete with each other for resources such as food, water and shelter. In addition, members of the same species often compete to attract a mate. Those individuals most successful in surviving and attracting mates will have relative large numbers of offsprings. Poorly performing individuals will produce few or even no offspring at all.

Genetic algorithms use a direct analogy of natural behavior. A population of "individuals" is created, each individual representing a possible solution to a given problem. Each individual is ranked after its "fitness," which is a measure of how well the solution complies with the requirements. A new generation is made from the current generation by creating offsprings from a pair of individuals. The more fit individuals have a higher chance of finding a mate and reproducing. By favoring the mating of the more fit individuals, we explore the more promising areas of the search space.

Solutions or individuals are encoded as a string of values (Fig. 1). This is a direct analogy to genes as described in biology. When reproduction occurs between two individuals,
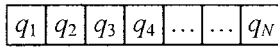
Fig. 1.   Sample string of values.
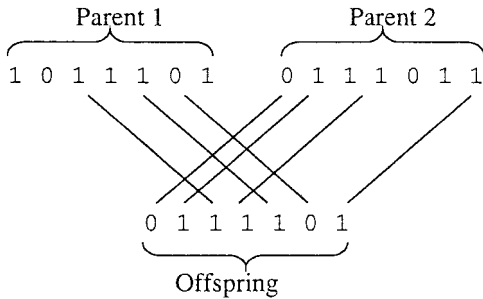
Fig. 2.   Crossover operation.
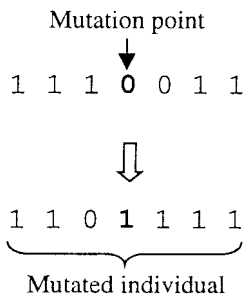
Fig. 3.   Mutation operation.

the two genes are combined. Sometimes an error occurs in the reproduction, in which case the new individual has mutated.

The two basic operations on individual (encoded as a string of values) are crossover and mutation (Figs. 2 and 3). For simplicity, we use binary encoded individuals to show the basic operations.

- *Crossover:* A new individual is created. Each element in the new string of values is taken randomly from one of the parents of the new individual.
- *Mutation:* An existing individual is modified. One element in the string is altered randomly.

Genetic algorithms fall into a category of methods for optimizing nonlinear functions of several variables. Beasley *et al.* [6] compare GA to other methods and discuss the theory and applications of GA.

III. ANALYSIS METHOD

The Bragg scattering of waves in a waveguide occurs when the refractive index is varying in the longitudinal direction z. We assume that the refractive index is varying as a quasi-sinusoidal function

$$n(z) = n_0 + \Delta n(z) \cos\left(\frac{2\pi}{\Lambda} z + \theta(z)\right) \tag{1}$$

where the functions $\Delta n(z)$ and $\theta(z)$ are slowly varying compared to the grating period Λ. If the fiber is in single mode operation, it supports only the fundamental mode, which has two components propagating in opposite directions. In the corrugated region, the forward propagating wave v_1 and the

backward propagating wave v_2 are related by the coupled mode equations [7]

$$\frac{dv_1(z; \delta)}{dz} = -i\delta v_1 + q(z)v_2$$
$$\frac{dv_2(z; \delta)}{dz} = +i\delta v_2 + q^*(z)v_1. \tag{2}$$

In (2), v_1 and v_2 are the complex amplitude envelopes of the waves, obtained by removal of the spatial dependence $\exp(\pm i\pi z/\Lambda)$. $q(z)$ is defined as the complex coupling co-efficient

$$q(z) = \frac{-i\pi}{2n_0\Lambda} \Delta n(z) \exp[-i\theta(z)] \tag{3}$$

and δ is the phase shift per unit length compared to the Bragg wavelength $\lambda_b = 2n_0\Lambda$.

$$\delta = \beta - \beta_b = \frac{2\pi n_0}{\lambda} - \frac{\pi}{\Lambda}. \tag{4}$$

We further define the local reflection coefficient as

$$\rho(z; \delta) = \frac{v_2(z; \delta)}{v_1(z; \delta)}. \tag{5}$$

By calculating $d\rho/dz$, and substituting dv_1/dz and dv_2/dz from the coupled mode equation (2), we get the well-known Riccati equation

$$\frac{d\rho}{dz} = 2i\delta\rho - q(z)\rho^2 + q^*(z). \tag{6}$$

This differential equation can be numerically solved for the reflection coefficient $r(\delta) = \rho(0, \delta)$ at the beginning of the grating of length L by using the Runge–Kutta 4th order and the boundary condition $\rho(L, \delta) = 0$. When the number of samples of $q(z)$ is small, it is necessary to include an interpolation routine to increase the number of samples in order to reduce the error in the Runge–Kutta algorithm. Such an algorithm is implemented in C++, yielding an efficient reflection spectrum calculation algorithm. The computation of a spectrum takes about 10–100 ms for a "normal" grating on a Pentium 150 MHz PC. "Normal" means that the number of samples of $q(z)$ after interpolation and the number of samples of $r(\delta)$ is both about 50–100.

IV. SYNTHESIS USING A GENETIC ALGORITHM

The objective is now to find a coupling coefficient $q(z)$ that produces a reflection coefficient as close as possible to the target spectrum. Since there is no general, exact solution to this problem when L is finite, we will try to utilize a GA to evolve solutions. To rank the solutions, we need to calculate an error for a given solution. The error value will be used as the fitness value for the GA. Given a sample input vector q_j, we can find the error using the following steps:

1) calculate the reflection spectrum for the input vector using the method described above (Runge–Kutta);
2) using a predefined error function, calculate the error of the calculated spectrum related to the target spectrum.

The error function is a measurement of the distance between the calculated reflection spectrum and the target reflection spectrum. It tells the GA how to weight the different parts of the spectrum. Therefore, it is important that the error function is designed according to the filter requirements, especially when the target filter spectrum is unrealizable. An example of an error function is

$$d\{R_{\mathrm{calc}}, R_{\mathrm{target}}\} = \sum_j (R^p_{\mathrm{target}, j} - R^p_{\mathrm{calc}, j})^2 \qquad (7)$$

where $R_{\mathrm{calc}, j}$ and $R_{\mathrm{target}, j}$ denote the jth value of the calculated reflectivity spectrum and the target reflectivity spectrum $R = |r|^2$, respectively. Another more general error function is obtained by introducing a weighting coefficient in the d_p-metric frequently used in functional analysis [8]

$$d_p\{R_{\mathrm{calc}}, R_{\mathrm{target}}\} = \left[\sum_j (c_j |R_{\mathrm{target}, j} - R_{\mathrm{calc}, j}|)^p \right]^{1/p}. \qquad (8)$$

For $p = 1$, we simply obtain the weighted sum of errors, for $p = 2$ we get a weighted Euclidean metric, and in the limit $p \to \infty$, (8) reduces to

$$d_\infty\{R_{\mathrm{calc}}, R_{\mathrm{target}}\} = \max_j (c_j |R_{\mathrm{target}, j} - R_{\mathrm{calc}, j}|). \qquad (9)$$

Thus, p is a parameter that describes how the large errors in the spectrum are weighted compared to the small errors.

For some applications, the phase response $\varphi = \arg(r)$ or the dispersion $D \propto d^2\varphi/d\lambda^2$ is critical as well. Suitable error functions may for example be

$$d = b \cdot d_{p_1}\{R_{\mathrm{calc}}, R_{\mathrm{target}}\} + (1 - b) \cdot d_{p_2}\{\varphi_{\mathrm{calc}}, \varphi_{\mathrm{target}}\} \qquad (10)$$

$$d = b \cdot d_{p_1}\{R_{\mathrm{calc}}, R_{\mathrm{target}}\} + (1 - b) \cdot d_{p_2}\{D_{\mathrm{calc}}, D_{\mathrm{target}}\} \qquad (11)$$

where $d_p\{\cdot, \cdot\}$ is given in (8) and $b \in [0, 1]$ decides how the reflectivity spectrum are weighted compared to the phase response or the dispersion.

Now, utilizing this measurement of error, we apply a GA to the problem. The process of solving the optimization problem by a GA can be illustrated using the pipeline in Fig. 4.

The individuals are represented as vectors of N input samples along with the calculated error, that is as pairs (d, q_j). To create random individuals we produce vectors of size N of random values. Since we have some domain knowledge of our problem, we can put a threshold on the random values. We have used two different threshold functions.

1) Rectangular Threshold: The random vector values should reside in a range $q_{\mathrm{max}}, q_{\mathrm{max}}]$ where q_{max} is the maximum achievable coupling coefficient. By investigating the coupled mode equations, we have found that by limiting q to real values, we will get a symmetric $r(\delta)$.
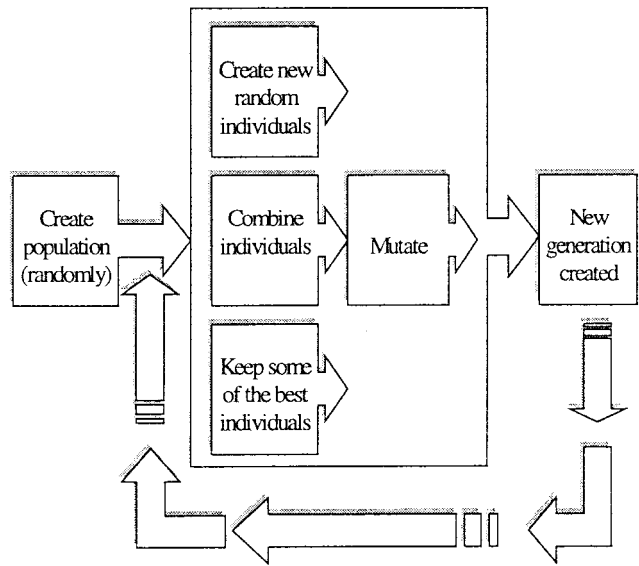
Fig. 4. GA pipeline.

2) Half-Hamming Threshold: Letting the vector elements take random values within the right half of a Hamming window scaled by a factor q_{max}. Such a constraint will prefer a minimum phase solution. This is because the coupling coefficient will be largest for small z, which means that the effective reflection point will be close to the reference point for $r(\delta)$, $z = 0$.

When creating a new generation, we will always keep a certain percentage of the best individuals from the last generations unaltered. We also combine individuals from the last generation to create new offsprings, and create some new (random) individuals.

When selecting the individuals for crossover, each individual has a probability to be used in a crossover that is related to the fitness of that individual. That is, a very fit individual is more likely to be used in a crossover than a poorly fit individual. After a crossover is performed, there is a slight possibility that the newly created offspring will be mutated. That is, for some of the newly created offsprings, we introduce a random value in the string of values.

V. NUMERICAL EXAMPLES AND DISCUSSION

A. Bandpass Filter

An interesting application of the synthesis algorithm is to synthesize a fiber optic bandpass filter. The target bandpass filter is characterized by

$$|r_{\mathrm{target}}(\delta)| = \begin{cases} 1, & |\delta| < a \\ 0, & |\delta| > a \end{cases} \qquad (12)$$

where $2a$ refers to the width of the filter. Note that the filter is bandpass in reflection, i.e., $|\delta| < a$ corresponds to the pass band, which in this case should be 0.2 nm wide. We have applied (12) as input to our implemented algorithm using the error function (7) with $p = 0.75$. Since we will compare our results to a minimum phase solution from the iterative GLM algorithm, a half Hamming threshold has been
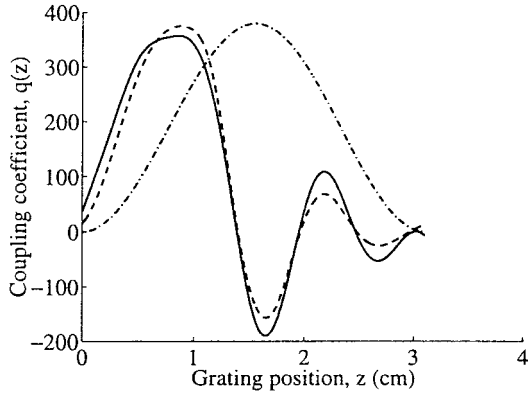
Fig. 5. The coupling coefficient of the genetic bandpass filter, (solid curve), the causal GLM bandpass filter (dashed curve), and the raised cosine filter (dashed-dotted curve).

utilized in the GA. The maximum coupling coefficient is set to 400 m^{-1}, corresponding to a maximum index modulation of 2×10^{-4}. The resulting coupling coefficient is shown in Fig. 5, and is compared to a raised cosine design. Also shown in Fig. 5 is the resulting coupling coefficient from the iterative GLM algorithm [3] using a nonlinear minimum phase of $r(\delta)$ ("causal") and 12 iterations.

The grating lengths are 3.1 cm, and the corresponding reflection spectra are shown in Fig. 6. The skirt steepness of the genetic bandpass filter is somewhat higher than for the raised cosine filter and for the GLM filter, while the side lobes are less for both the GLM filter and the raised cosine grating. In order to suppress the side lobes of the GLM filter, the resulting coupling coefficient is multiplied by a half Hamming window, i.e., a window function for which the top value matches the start position of the grating ($z = 0$). Due to the truncation of the coupling coefficient, it is necessary to multiply this intermediate coupling coefficient by a constant to achieve the desired reflectivity of 99%.

By using our algorithm, it is not necessary to multiply the coupling coefficient by a window function or a final constant. However, the choice of an error function is very important, because it determines to what extent low side lobes or low pass band ripple is preferred.

B. Low-Dispersion Bandpass Filter

For a bandpass filter with low dispersion, the target spectrum is given by (12) provided the phase response is linear, or equivalently $D_{\text{target}} = 0$. We choose a rectangular threshold with the same $q_{\max}$ as before, and the error function (11) with $p_1 = 2$ and $c_j = 1$ for the amplitude part, i.e., non-weighted Euclidean metric. Furthermore, we want to optimize the grating for the worst case dispersion inside the pass band. Therefore, we set $p_2 = \infty$ and

$$c_j = \begin{cases} 1, & j \in PB \\ 0, & j \notin PB \end{cases} \qquad (13)$$

for the dispersion part, where PB denotes the j values corresponding to samples within the passband. Hence, we
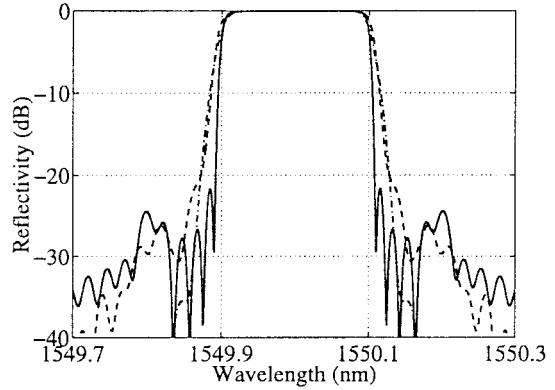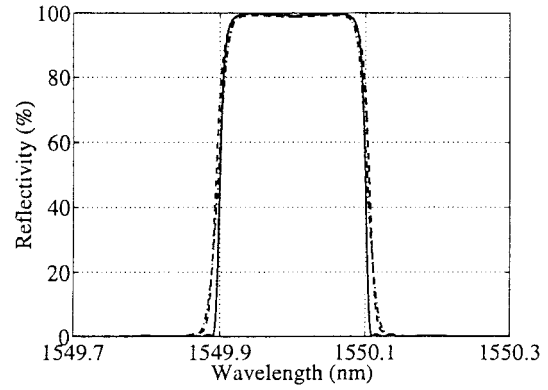
Fig. 6. Calculated reflection spectrum for the genetic bandpass filter (solid curve), the causal GLM bandpass filter (dashed curve), and the raised cosine filter (dashed-dotted curve).
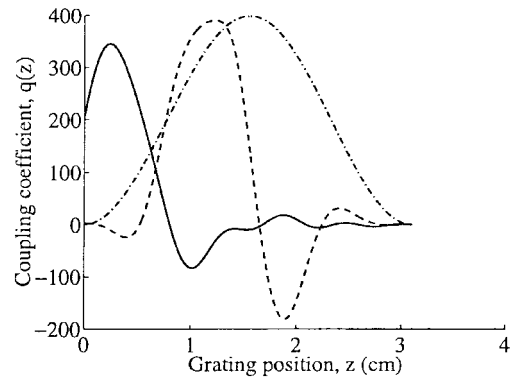
Fig. 7. The coupling coefficient of the genetic low-dispersion bandpass filter, (solid curve), the noncausal GLM bandpass filter (dashed curve), and the raised cosine filter (dashed-dotted curve).

obtain the error function

$$d = b \cdot d_2 \{R_{\text{calc}}, R_{\text{target}}\} + (1 - b) \cdot \max_{j \in PB} |D_{\text{calc},j}|. \qquad (14)$$

The parameter b is chosen so that the weighting between the dispersion and the amplitude response is approximately equal (the value depends on the dispersion unit). The resulting coupling coefficient and reflectivity spectrum is given in Figs. 7 and 8, and is compared to a linear phase GLM solution ("noncausal") and a raised cosine design.

Fig. 9 shows the in-band dispersion of the three filters. The worst case dispersion inside the pass band are 300, 2900, and
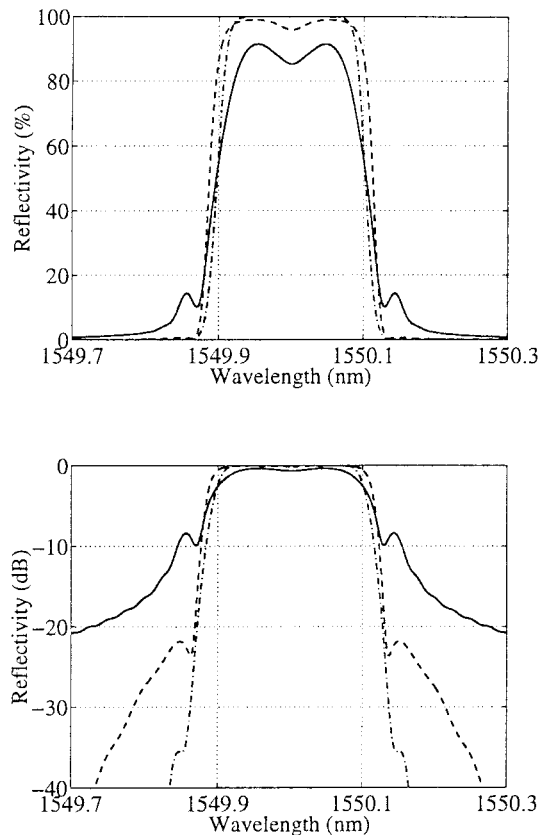
Fig. 8. Calculated reflection spectrum for the low-dispersion genetic bandpass filter (solid curve), the noncausal GLM bandpass filter (dashed curve), and the raised cosine filter (dashed-dotted curve).
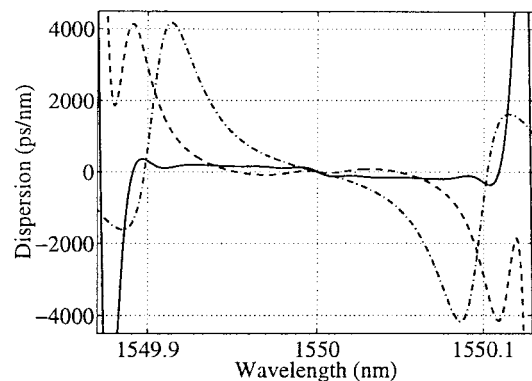
Fig. 9. In-band dispersion for the low-dispersion genetic bandpass filter (solid curve), the noncausal GLM bandpass filter (dashed curve), and the raised cosine filter (dashed-dotted curve).

4200 ps/nm for the genetic, the "noncausal" GLM, and the raised cosine gratings, respectively. On the other hand, the reflectivity spectrum is less square-like for the genetic filter than for the two other. This shows that the grating has been optimized for low dispersion compared to the other gratings.

Such an optimization procedure, for any kind of parameter, is not trivial when using the iterative GLM algorithm, or when using simpler designs as, for example, raised cosine apodization.

The main drawback with our method is the running time. For the problems described above, acceptable solutions were found

after 10 min, and the results given below were found after approximately two hours using a Pentium 150 MHz PC. For comparison, the running time of the iterative GLM method is about a minute. However, Genetic Algorithms exploit a natural parallel form, which makes it ideal for parallel implementation. Parallel algorithms are essential for solving complex problems in a reasonable amount of time. Our proposed method has a great potential for scaling to problems beyond what is possible to solve using conventional methods. GA's can be used to solve the majority of inverse problems, and are not only limited to the fields of fiber grating synthesis.

It is also worth mentioning that the resulting index modulation profiles from the synthesis algorithm can be written into fibers by using for example the method described by Storøy *et al.* [9] and Asseh *et al.* [10].

VI. CONCLUSION

A novel method for synthesizing fiber gratings is proposed. The algorithm is made by combining the Runge–Kutta analysis method and a genetic algorithm, which is analogous to the evolution process in nature. The numerical examples presented show that the method gives results that are comparable or better than other design methods. In addition, the proposed method greatly reduces the problem of weighting the different requirements to the filter response of a fiber grating.

REFERENCES

[1] K. A. Winick and J. E. Roman, "Design of corrugated waveguide filters by Fourier transform techniques," *IEEE J. Quantum Electron.,* vol. 26, pp. 1918–1929, 1990.
[2] G. H. Song and S. Y. Shin, "Design of corrugated waveguide filters by the Gel'Fand–Levitan–Mar.enko inverse-scattering method," *J. Opt. Soc. Amer.,* vol. 2, pp. 1905–1915, 1985.
[3] E. Peral, J. Capmany, and J. Marti, "Iterative solution to the Gel'Fand–Levitan–Mar.enko coupled equations and application to synthesis of fiber gratings," *IEEE J. Quantum Electron.,* vol. 32, pp. 2078–2084, Dec. 1996.
[4] Z. Michalewicz, *Genetic Algorithms + Data Structures = Evolution Programs.* New York: Springer-Verlag, 1992.
[5] J. H. Holland, *Adaption in Natural and Artificial Systems.* Cambridge, MA: The M.I.T. Press, 1975.
[6] D. Beasley, D. R. Bull, and R. R. Martin, *An Overview of Genetic Algorithms: Part 1, Fundamentals,* http://www.mcs.drexel.edu/ shartley/MCS770/index.html.
[7] D. Marcuse, *Theory of Dielectric Optical Waveguides.* San Diego, CA: Academic, 1991.
[8] E. Kreyszig, *Introductory Functional Analysis with Applications.* New York: Wiley, 1989.
[9] H. Storøy, H. E. Engan, B. Sahlgren, and R. Stubbe, "Position weighting of fiber Bragg gratings for bandpass filtering," *Opt. Lett.,* vol. 22, pp. 784–786, 1997.
[10] A. Asseh, H. Storøy, B. E. Sahlgren, S. Sandgren, and R. Stubbe, "A writing teqnique for long fiber Bragg gratings with complex reflectivity profiles," *J. Lightwave Technol.,* vol. 15, pp. 1419–1424, 1997.

Johannes Skaar, photograph and biography not available at the time of publication.

Knut Magne Risvik, photograph and biography not available at the time of publication.

3.2 On the synthesis of fiber Bragg gratings by layer peeling

Authors: Johannes Skaar, Ligang Wang, and Turan Erdogan.

On the Synthesis of Fiber Bragg Gratings by Layer Peeling

Johannes Skaar

Department of Physical Electronics, Norwegian University of Science and Technology (NTNU),

N-7491 Trondheim, Norway

Ligang Wang and Turan Erdogan

The Institute of Optics, University of Rochester, Rochester, NY 14627

Abstract

Two methods for grating synthesis which have appeared in the literature recently are compared directly. In particular, we point out the similarity between the two — both algorithms are based on propagation of the fields through the structure with simultaneous evaluation of the coupling coefficient according to simple causality arguments (layer-peeling algorithms). The first published method [1] (here called the discrete layer-peeling algorithm) is reformulated in a simpler, more efficient way and it is shown that its implementation can be made exact. For mathematical comparison, a derivation of the second method [2] (here called the continuous layer-peeling algorithm) is presented. The methods are compared both mathematically and numerically. We find that the discrete layer-peeling algorithm is significantly faster and can be more stable than its continuous counterpart, whereas the continuous algorithm offers some advantages in flexibility.

1. Introduction

The synthesis of fiber Bragg gratings has attracted many researchers in the field of fiber optics recently [1-6]. The problem amounts to finding the grating structure (grating amplitude and phase) from a specified, complex spectrum. Synthesis is useful both as a design tool and for characterization of already fabricated gratings with complex profiles. It has been a common view that the synthesis problem is complicated, especially compared to the well-known direct problem of computing the reflection spectrum from a grating structure. In a recent article [2], Poladian points out that the synthesis problem actually is as simple as the direct problem; one can find the grating structure from the reflection spectrum simply by propagating the fields along the grating structure, while simultaneously evaluating the grating strength using a simple causality argument. In fact this result has been appreciated in a number of other fields of physics, and this layer-peeling (sometimes called "differential inverse scattering") approach has been used to analyze such systems as transmission lines, vibrating strings, layered acoustic media, and particle scattering in quantum mechanics [7,8].

The purpose of this paper is to first simplify the discrete layer-peeling (DLP) synthesis method proposed by Feced et. al. [1] to improve its clarity and efficiency, and then compare this method with the continuous method described by Poladian [2] (referred to here as CLP for continuous layer peeling). We point out that the continuous method essentially makes use of the same principle as the discrete method. Both are based on the following procedure [8]: by causality, the coupling coefficient at the front end of the grating is determined only by the leading edge of the impulse response, since at the very beginning of the impulse response light does not have time to propagate more deeply into the grating and hence "sees" only the first layer. After computing the value of the coupling coefficient in the first layer, the fields are propagated to the next layer of the grating. This propagation is essentially the direct (forward) calculation and can be accomplished by numerical integration of the coupled-mode equations or by the transfer matrix method described below. Now one is in the same situation as at the beginning, since the effect of the first layer is "peeled off." The process is continued to the back of the grating, so that the entire grating structure is reconstructed. Note that the layer thickness must be chosen sufficiently small that the (complex) coupling coefficient can be approximated as constant throughout the layer.

While the principle behind the DLP and CLP methods is the same, the implementation of the two methods differs. The DLP model is based on a discretization of the grating model itself; i.e., the grating is approximated as a series of discrete, complex reflectors. Once this approximation is made, though, the reconstruction or synthesis algorithm can be made exact. In the CLP method the coupling process is treated continuously, but discretization is introduced in the actual computation of the coupling coefficient and the propagation of the fields. This qualitative comparison is described more precisely and in mathematical terms below. Differences in the implementations of the two methods lead to differences in the numerical performance. As illustrated in the examples below, we find that the discrete layer-peeling algorithm is significantly faster and often more stable than its continuous counterpart, whereas the continuous algorithm can be more flexible. For example, in contrast to the DLP method, the CLP method allows the layer thickness to be varied for a given frequency bandwidth.

The remainder of this paper is organized as follows. In Section 2 we reformulate the discrete layer-peeling algorithm reported in [1], showing that a "moving reference frame" simplifies the algorithm and improves its performance. In Section 3 a derivation is provided for the continuous layer-peeling algorithm, since this has not been published yet, and it is necessary for a clear comparison between the two methods. In Section 4 we compare the two methods mathematically, showing that they are equivalent in certain limits and how they differ in others. Also, several numerical examples are provided to demonstrate the relative performance of the two methods. Finally, in Section 5 we summarize and draw conclusions.

26

2. Discrete Layer Peeling

In this section we describe the layer-peeling method for synthesis of gratings from an inherently discrete model [1]. It was first developed by geophysicists like Goupillaud and Robinson, and was extended and generalized by Bruckstein et. al. (see refs [7,8] for excellent reviews).

The starting point for the discretization is the well-known transfer matrix T of a Bragg grating, which connects the fields at the point $z + \Delta$ with the fields at z,

$$
\begin{bmatrix} u(z+\Delta,\delta) \\ v(z+\Delta,\delta) \end{bmatrix} = \begin{bmatrix} \cosh(\gamma\Delta) + i\dfrac{\delta}{\gamma}\sinh(\gamma\Delta) & \dfrac{q}{\gamma}\sinh(\gamma\Delta) \\ \dfrac{q^*}{\gamma}\sinh(\gamma\Delta) & \cosh(\gamma\Delta) - i\dfrac{\delta}{\gamma}\sinh(\gamma\Delta) \end{bmatrix} \begin{bmatrix} u(z,\delta) \\ v(z,\delta) \end{bmatrix}
\tag{1}
$$

Here $u(z,\delta)$ and $v(z,\delta)$ are the slowly varying amplitudes of the forward and backward propagating fields, respectively, and $\gamma^2 = |q|^2 - \delta^2$, where $q = q(z)$ is the coupling coefficient and $\delta = \beta - \beta_B$ is the wavenumber detuning compared to a Bragg design wavenumber β_B. The implicit harmonic time dependence is assumed to be $\exp(-i\omega t)$, and the spatial dependence $\exp(\pm i\beta_B z)$ has been removed from the fields. We refer to (1) as the piecewise uniform model since the grating is considered uniform in the interval $[z, z+\Delta]$. A further discretization approximation involves replacement of the matrix T by the product of two transfer matrixes $T_\Delta T_\rho$, one of them (T_ρ) describing a discrete reflector, and the other (T_Δ) describing the pure propagation of the fields [1], or

$$
T_\rho = \left(1 - |\rho|^2\right)^{-1/2} \begin{bmatrix} 1 & -\rho^* \\ -\rho & 1 \end{bmatrix}
\tag{2}
$$

$$
T_\Delta = \begin{bmatrix} \exp(i\delta\Delta) & 0 \\ 0 & \exp(-i\delta\Delta) \end{bmatrix}
\tag{3}
$$

where the discrete, complex reflection coefficient is given by

$$
\rho = -\tanh(|q|\Delta)\frac{q^*}{|q|}.
\tag{4}
$$

27
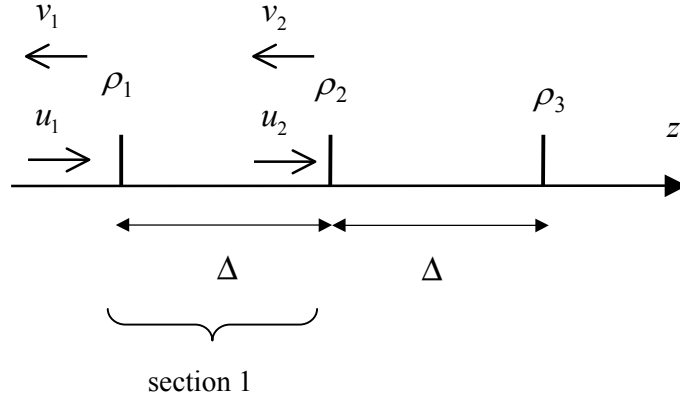
Fig. 1: The discrete model of a fiber grating; the forward (u_j) and backward (v_j) propagating fields associated with each layer are indicated on the drawing.

The transfer matrix T_ρ can be obtained from T by letting all coupling take place at a single point in (1); i.e., $|q| \to \infty$, while the product $q\Delta$ remains constant. It can also be written directly since it merely describes the standard transfer matrix of a discrete reflector with ρ and $-\rho^*$ the reflection coefficients from the left and right, respectively, and $\left(1-|\rho|^2\right)^{1/2}$ the transmission coefficient for both directions.

The discrete model of the entire grating is thus a series of N discrete, complex reflectors with a distance Δ between all reflectors. From a realizable complex reflection spectrum $r_1(\delta)$ we wish to reconstruct the complex reflector amplitudes ρ_j, $j = 1, 2, ..., N$. Define the forward and backward propagating fields before the jth section as $u_j(\delta)$ and $v_j(\delta)$, see Fig. 1. The fields before the first section are then given by

$$\begin{bmatrix} u_1(\delta) \\ v_1(\delta) \end{bmatrix} = \begin{bmatrix} 1 \\ r_1(\delta) \end{bmatrix}. \tag{5}$$

The causality argument illustrates how to find the complex amplitude of the first reflector. We note that the impulse response of the reflector stack for time $t = 0$ is independent of the reflectors ρ_j for $j \geq 2$ because light does not have sufficient time to propagate to and from the second and higher reflectors. Thus, when looking at the impulse response of the stack for $t = 0$, we obtain the same response as if only the first reflector were present. Therefore, we can compute ρ_1 from the inverse Fourier transform of $r_1(\delta) = v_1(\delta)/u_1(\delta)$ evaluated at time $t = 0$. Since we then know ρ_1, we can use $T_\Delta T_{\rho_1}$ to transfer the fields to the next section. At

28

this point we find ourselves in the same situation as with the first reflector, so in effect the first layer is "peeled off." This procedure can be repeated until the entire series of reflectors is determined. The coupling coefficient function $q(z)$ is then determined from Eq. (4).

Using (2) and (3) it is straightforward to show that the task of transferring the fields by the transfer matrix product $T_\Delta T_{\rho_1}$ can be described in terms of the local reflectivities as

$$r_2(\delta) = \exp(-i2\delta\Delta)\frac{r_1(\delta) - \rho_1}{1 - \rho_1^* r_1(\delta)}, \tag{6}$$

where $r_j(\delta) = v_j(\delta)/u_j(\delta)$. It is interesting to note that (6) is equivalent to a recursion formula proposed by Schur for testing the boundedness of an analytic function outside the unit circle of the complex plane [8].

To obtain an explicit expression for the determination of ρ_1 by the inverse Fourier transform, we note that the spectrum $r_1(\delta)$ can be written as a discrete-time Fourier transform (Fourier series) of the impulse response $h_1(\tau)$,

$$r_1(\delta) = \sum_{\tau=0}^{\infty} h_1(\tau)\exp(i\delta\,\tau 2\Delta), \tag{7}$$

because the impulse response is discrete with the sample period 2Δ, which is equal to the "round-trip" propagation length of one layer. We have defined $\tau = t/2\Delta$ as the discrete time variable with t as the normalized time. Since the impulse response for $\tau = 0$ is the same as if only the first reflector were present, we can see that ρ_1 is simply the zeroth Fourier coefficient of the series (7), or

$$\rho_1 = h_1(0) = \frac{\Delta}{\pi}\int_{-\pi/2\Delta}^{\pi/2\Delta} r_1(\delta)d\delta. \tag{8}$$

Thus far the model is based on inherently discrete functions that describe the grating structure. For numerical implementation, the spectral dependence must also be discrete, and hence the calculation of ρ_1 by the inverse Fourier transform of $r_1(\delta)$ can be achieved by the discrete Fourier transform

$$\rho_1 = \frac{1}{M}\sum_{m=1}^{M} r_1(m) \tag{9}$$

where $r_1(m)$ denotes a discrete version of the spectrum $r_1(\delta)$ in the range $|\delta| \le \pi/2\Delta$, and $M \ge N$ is the number of wavelengths in the spectrum. Note that Eqs. (7)–(9) are valid for all

layers j by substituting $1 \rightarrow j$ in the subscripts, because the reference plane is transferred to the actual layer through (6).

The desired impulse response $h_1(\tau)$ must be nonzero for $\tau \geq 0$, and if necessary, it should therefore be apodized to reduce the Gibbs phenomenon, and shifted so that it starts at $\tau = 0$ [1]. The apodizing-windowing procedure reduces the undesirable oscillations in the spectrum due to the finite length of the desired impulse response that is represented in the computer. Note that M, the number of wavelengths in the discrete spectrum, which is equal to the number of points in the impulse response, should be greater than or equal to the number of layers N. The number N is chosen from the desired grating length or detuning range, or is chosen such that we obtain a desired accuracy in the realized spectrum.

The discrete layer-peeling algorithm may be summarized in the following simple steps:
i)   Start with a physically realizable reflection coefficient $r_1(\delta)$ (see Appendix).
ii) Compute ρ_1 from Eq. (9).
iii) Propagate the fields using the transfer matrixes (2)–(4) or the equivalent expression (6).
iv) Repeat step ii) until the entire grating structure is determined.

A count of the number of operations shows that the running time is of the same order $O(MN)$ as the conventional approach for computing the direct problem, i.e., computing the spectrum $r_1(\delta)$ from the reflector amplitudes ρ_j using the transfer-matrix. We also note that the inverse problem actually is as simple as the forward problem.

A difference between the approach described here and that of Feced [1] is that we move the reference plane as we propagate through the structure (or peel off the layers). The reference plane in [1] is always located at $z = 0$, and consequently it is necessary to take into account the propagation of the fields back and forth from $z = 0$ to the layer being reconstructed. While this approach certainly works, it unnecessarily increases the computation time and the clarity of the presentation.

We conclude this section by discussing the implications of choosing the frequency domain vs. the time domain for implementation of the layer-peeling algorithm. In a similar fashion to that chosen by Feced [1], we implement the algorithm in the frequency domain. The main disadvantage with this choice is that, strictly speaking, the synthesis algorithm is not exact unless we have perfect spectral resolution ($M \rightarrow \infty$). However, this is not a fundamental limitation of the DLP method, because the algorithm can be made exact by transforming it into the time domain [7]. By an inverse Fourier transform of the discrete transfer-matrix relation, we find

$$\begin{bmatrix} u_{j+1}(t+\Delta) \\ v_{j+1}(t-\Delta) \end{bmatrix} = \left(1 - |\rho_j|^2\right)^{-1/2} \begin{bmatrix} 1 & -\rho_j^* \\ -\rho_j & 1 \end{bmatrix} \begin{bmatrix} u_j(t) \\ v_j(t) \end{bmatrix},$$ (10)

where $u_j(t)$ and $v_j(t)$ are the inverse Fourier transforms of the fields $u_j(\delta)$ and $u_j(\delta)$, respectively. Since the reference plane for the fields $u_j(t)$ and $v_j(t)$ is fixed at $z = 0$, the local reflectivities are simply

$$\rho_j = \left.\frac{v_j}{u_j}\right|_{t=j\Delta}.$$ (11)

The vector $u_1(t)$ is initialized to the unit impulse function, and $v_1(t)$ is set equal to the desired impulse response in agreement with (5). From Eqs. (10) and (11) we can then determine the local reflectivities *exactly* from the impulse response (by $O(N^2)$ operations), and we therefore expect better accuracy than with the frequency-domain DLP implementation. However, for the frequency-domain approach, if the number of spectral points M is set significantly larger than N, for example $M=2N$, the performance in most practical situations is about the same as for the time-domain implementation. Finally, we note that only the first N points of the impulse response are needed to reconstruct the grating up to layer N. In principle, this requirement applies frequency-domain DLP also, but since errors associated with the utilization of band-limited reflection spectra are repeatedly propagated and thereby exacerbated by Eq. (6), the accuracy of the frequency-domain DLP procedure improves when we increase the number of points in the impulse response (i.e., increase the spectral resolution).

3. Continuous Layer Peeling

The continuous layer-peeling (CLP) method was first developed by Bruckstein et. al. and Corones et. al. [8,9]. In this section, we summarize the main principles of the method for synthesis of Bragg gratings, particularly as they relate to the discrete layer-peeling method. The synthesis relation resulting from the causality argument is derived, and it is shown that the method introduced in [2] is clearly a version of the continuous layer-peeling method.

The continuous model for coupling of counter-propagating modes in a grating is described by the familiar coupled-mode equations,

$$\frac{d}{dz}u(z,\delta) = +i\delta\, u(z,\delta) + q(z)v(z,\delta)$$

$$\frac{d}{dz}v(z,\delta) = -i\delta\, v(z,\delta) + q^*(z)u(z,\delta) \tag{12}$$

where all of the parameters are defined in the previous section. The two coupled equations can be combined into a single Riccati equation for the local reflectivity $r(z,\delta) = v(z,\delta)/u(z,\delta)$ by computing $dr(z,\delta)/dz$ and substituting the derivatives from (12),

$$\frac{d}{dz}r(z,\delta) = -2i\delta\, r(z,\delta) - q(z)r(z,\delta)^2 + q^*(z). \tag{13}$$

Eq. (13) can be solved numerically by Runge-Kutta integration methods. Thus the model itself is not inherently discrete (like a series of localized reflectors); nevertheless some form of discretization must be introduced in order to numerically solve the coupled-mode or Riccati equations to propagate the fields.

As indicated previously, inverse scattering relies heavily on causality, so in order to find a relation analogous to (8) we must also consider the time domain in the description of propagation in the grating, or

$$\frac{\partial u(z,t)}{\partial z} = -\frac{\partial u(z,t)}{\partial t} + q(z)v(z,t)$$

$$\frac{\partial v(z,t)}{\partial z} = +\frac{\partial v(z,t)}{\partial t} + q^*(z)u(z,t) \tag{14}$$

where Eqs. (14) are obtained by inverse Fourier transform of Eqs. (12). Note that the time t here is normalized such that the velocity of the waves equals unity. Now, we imagine that the grating is probed by a wave with a leading impulse. The grating is assumed to be dark at $t = 0$, so by causality the fields must vanish for $t < z$ and have the form [8]

$$u(z,t) = \delta(t-z) + H(t-z)\tilde{u}(z,t)$$

$$v(z,t) = H(t-z)\tilde{v}(z,t) \tag{15}$$

where $\tilde{u}$, $\tilde{v}$ are some functions describing the fields in the grating, $H(t-z)$ denotes the unit step function that is 0 for $t < z$ and 1 for $t \geq z$, and $\delta(t-z)$ is the Dirac delta function. By substituting (15) into the second of equations (14), and equating the coefficients of $\delta(t-z)$ on both sides, we obtain

32

$$q^*(z) = -2\tilde{v}(z, t = z^+) = -2v(z, t = z^+). \tag{16}$$

By the initial value theorem for the unilateral Fourier transform (Laplace transform) [10], we have $v(z, t = 0^+) = -\lim_{\delta \to \infty} i\delta\, v(z, \delta)$, and therefore $v(z, t = z^+) = -\lim_{\delta \to \infty} i\delta\, v(z, \delta) \exp(-i\delta z)$ from the shift property of the Fourier transform. Hence we can write

$$q^*(z) = \lim_{\delta \to \infty} 2i\delta\, v(z, \delta) \exp(-i\delta z) = \lim_{\delta \to \infty} 2i\delta\, r(z, \delta), \tag{17}$$

where the last equality results from the fact that $u(z, \delta) \to \exp(i\delta z)$ as $\delta \to \infty$ according to (15). By using the initial value theorem once again, we can see that the complex conjugate of the coupling coefficient is equal to the leading edge of the impulse response multiplied by a factor of –2, or

$$q^*(z) = -1/\pi \int_{-\infty}^{\infty} r(z, \delta) \exp(-i\delta 0^+) d\delta. \tag{18}$$

In [2] this relation is incorrectly written as $q^*(z) = -1/\pi \int_{-\infty}^{\infty} r(z, \delta) d\delta$, after translation to our convention for the coupled-mode equations. However, because the impulse response is discontinuous at $t = 0$, the Fourier integral evaluated at $t = 0$ is given by the average of the impulse response at $t = 0^-$ and $t = 0^+$. Therefore, one should either multiply the synthesis relation in [2] by a factor of 2, or be careful to write the relation explicitly in the form (18). This problem does not occur in the discrete layer-peeling algorithm because there we choose the spectrum $r_j(\delta)$ to be the discrete-time Fourier transform of the *discrete* impulse response (see discussion in Section 4).

The continuous layer-peeling algorithm is thus performed by following these simple steps:
i) Start with a physically realizable reflection coefficient $r(0, \delta)$ (see Appendix).
ii) Compute $q(z)$ for the present z value from (18) or

$$q^*(z) = -2/\pi \int_{-\infty}^{\infty} r(z, \delta) d\delta. \tag{19}$$

   The integral may be evaluated using standard numerical integration routines, such as Simpson's rule.
iii) Propagate the fields using the transfer matrix relation (1), or by integration of (13) using a backward difference scheme.
iv) Repeat step ii) until the entire grating structure is determined.

33

The primary sources of error in the continuous layer-peeling procedure are the evaluation of the synthesis integral (19) and the propagation of the fields.

4. Comparison and Numerical Properties

In this section we first consider the similarities and differences between the two methods from a fundamental, mathematical standpoint. Then we compare the numerical performance using several realistic examples.

First, we expect that the two methods should be equivalent in the limit where the discretization step (layer thickness for matrix multiplication) approaches zero. By letting $\Delta \to 0$ in (4), we obtain $\rho \to -q^*\Delta$. Substituting this result into (8) gives

$$q^*(j\Delta) = -\frac{1}{\pi} \int_{-\pi/2\Delta}^{\pi/2\Delta} r_j(\delta)d\delta \tag{20}$$

for the jth layer. In the limit of small Δ, we obtain the relation (19) (divided by 2). However, we must be careful at this point, because the spectra $r_j(\delta)$ and $r(j\Delta,\delta)$ are not exactly equivalent to one another. For a fixed position given by $z = j\Delta$ the spectrum $r(j\Delta,\delta)$ is the Fourier transform of a continuous impulse response, whereas $r_j(\delta)$ is a Fourier series with a discrete impulse response as its coefficients. While the determination of the impulse response using $r(j\Delta,\delta)$ requires a factor of 2 to fix the "wrong" convergence of the inverse Fourier integral at $t = 0$, the determination of the Fourier coefficient (8) from $r_j(\delta)$ does not. With this subtle difference taken into account, relations (19) and (20) are consequently equivalent in the limit $\Delta \to 0$.

Owing to the nonequivalence between $r_j(\delta)$ and $r(j\Delta,\delta)$, the target spectra $r_1(\delta)$ and $r(0,\delta)$, the starting physical realizable spectrum for DLP and CLP respectively, should ideally be specified in different ways. The discrete model spectrum $r_1(\delta)$ should equal a discrete-time Fourier transform of a causal, discrete impulse response, whereas the continuous model spectrum $r(0,\delta)$ should equal the Fourier transform of a causal, continuous impulse response. Therefore, if one starts with a true grating spectrum in both DLP and CLP (reconstruction problems), the DLP will give wrong result for the coupling coefficient of the first section, whereas the CLP will give the right answer. Similarly, the situation will be reversed in synthesis problems where one starts with a spectrum that is a discrete Fourier transform of a discrete impulse response. Usually, this does not impose any problems as long as the grating

starts smoothly at the front end. If this is not the case, one could fix the algorithm at the first layer by including an extra factor of 2 in (9) for reconstruction problems, and exclude the extra factor of 2 in (19) for synthesis problems.

To make the equivalence between the two methods clearer, it is also instructive to derive the synthesis relation (8) from a more physical standpoint than that of the derivation in Section 2. As above, we assume the grating is comprised of a series of N discrete reflectors separated by equal distance of Δ. Also, the scattering is assumed to happen at the beginning of each layer. At the beginning of the $(j+1)$st layer, $r(z = j\Delta, \delta)$ is the corresponding local reflectivity associated with the grating beyond that layer. Recall that the reference plane is shifted from $z = 0$ to $z = j\Delta$, and the associated definition of zero time is also shifted to the layer of interest.

The reflection of a *single* layer between z and $z + \Delta$ is simply that of a discrete reflector at $z = j\Delta$ followed by a free propagation of distance of Δ. Thus, according to Eq. (2), the reflection from this layer only is ρ_j. Note that this single-layer reflection is independent of frequency, which is a direct result of the discretization of the coupling process. Based on causality, at time $t = 0^+$ the impulse response contains a contribution only from the reflector at $z = j\Delta$. Therefore we can write

$$\int_{-\pi/2\Delta}^{\pi/2\Delta} \rho_j \exp(-i\delta\tau)d\delta\Big|_{\tau=0^+} = \int_{-\pi/2\Delta}^{\pi/2\Delta} r(z,\delta)\exp(-i\delta\tau)d\delta\Big|_{\tau=0^+} . \tag{21}$$

The limits on the integral arise because the discrete grating model produces a periodic spectrum with periodicity of $\delta = \pi/\Delta$. Consequently, only a single period of the spectrum should be considered.

Next, we note that since ρ_j is independent of the detuning δ, the integral on the left may be evaluated so that Eq. (21) becomes

$$\rho_j \frac{\pi}{\Delta} = \int_{-\pi/2\Delta}^{\pi/2\Delta} r(z,\delta)\exp(-i\delta\tau)d\delta\Big|_{\tau=0^+} . \tag{22}$$

According to the definition of ρ_j in Eq. (4), this expression may be written in terms of the coupling coefficient as

$$-\frac{q^*(z)}{|q(z)|}\tanh(|q(z)|\Delta)\frac{\pi}{\Delta} = \int_{-\pi/2\Delta}^{\pi/2\Delta} r(z,\delta)\exp(-i\delta\tau)d\delta\Big|_{\tau=0^+} . \tag{23}$$

Eq. (23) is the integral form of the synthesis relation for the discrete layer peeling (DLP) method, analogous to Eq. (8). By taking the limit as $\Delta \to 0,$ on both sides of Eq. (23), the synthesis relation (18) for the continuous layer peeling (CLP) method is readily obtained:

$$q*(z) = -\frac{1}{\pi} \int r(z,\delta) \exp(-i\delta 0^+) d\delta. \tag{24}$$

Although simple, this analysis makes it clear that the CLP method is essentially identical to the DLP method in the limiting case of infinitesimally thick layers, or $\Delta \to 0$.

For the first numerical comparison example, we consider a dispersionless band-pass filter. We take the ideal spectrum to be a flat-top, nearly rectangular pass-band filter described by the "super-gaussian" function

$$r(\delta) = \sqrt{R} \exp\left[-(\delta/\delta_{PB})^{20}\right], \tag{25}$$

where the maximum reflectivity is $R = 0.90$ and the width is determined by $\delta_{PB} = 19.2$ cm^{-1}, which corresponds to a pass-band full width at half maximum (FWHM) of 37.84 cm^{-1} in wavenumber, or 1 nm in wavelength at a center wavelength of 1550 nm. We choose the detuning window (frequency range) to be 157 cm^{-1}, which corresponds to a wavelength window of about 4 nm. This choice determines the layer thickness, since for the DLP method the layer thickness Δ_{DLP} and detuning window δ_W must be related by

$$\Delta_{\mathrm{DLP}} = \frac{\pi}{\delta_w}. \tag{26}$$

Thus $\Delta_{\mathrm{DLP}} = 0.02$ cm. Furthermore, we choose the length of the grating to be $L = 10$ cm, which therefore determines the number of layers $N = L/\Delta_{\mathrm{DLP}}$; in this case $N = 500$. Finally, we choose the number of wavelengths $M = 1000$. For both methods, the actual target spectrum is obtained as the discrete Fourier transform of the impulse response associated with (25), windowed to be causal and apodized by a Hanning function. Ideally, for comparison we would like to choose the same parameters for the CLP method. However, for this choice of parameters we find that the CLP method does not converge on a reasonable solution. In fact this behavior appears to be a general result (at least for some structures) — the CLP method does not yield a reasonable structure for layer thickness roughly greater than or equal to that dictated by the DLP method (through (26)). Therefore, for the CLP simulation we must choose a smaller layer thickness. We pick 0.01 cm, and keep all other parameters equal. We

note that this ability is actually an inherent advantage of the CLP method — the layer thickness can be adjusted independently of δ_W, as long as it is not made too large. Unfortunately, the smaller layer thickness does not enable a totally fair comparison, so we also include for a third case a DLP simulation with the same layer thickness (0.01 cm), but because of the constraint in (26) we must increase the frequency range to 314 cm^{-1}, and we double the number of wavelengths ($M = 2000$) in order to keep the frequency sampling resolution constant. To summarize, the three cases considered for the first example are denoted (by layer thickness) as "DLP 0.02 cm," "CLP 0.01 cm," and "DLP 0.01 cm."
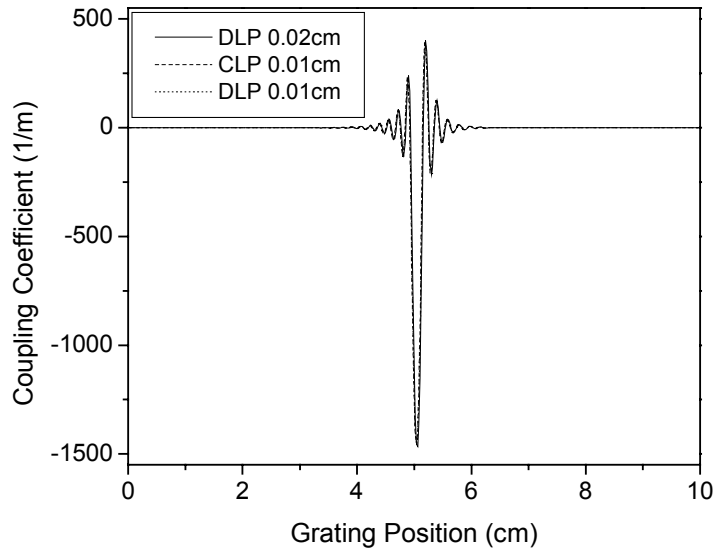
Fig. 2: Plots of the (real) coupling coefficient reconstructed from a nearly ideal, flat-top, dispersionless reflection spectrum using both DLP and CLP methods and different sets of parameters.

The three calculations for this example had associated processor run times of 0.66 sec, 25.26 sec, and 2.25 sec, for the "DLP 0.02 cm," "CLP 0.01 cm," and "DLP 0.01 cm" cases, respectively. These were implemented using the program MATLAB on a 550 MHz Pentium III computer. The DLP method is at least an order of magnitude faster than the CLP method. In Fig. 2 we plot the coupling coefficient (which is real for this example) determined for each of the three cases described above. On this plot it is very difficult to distinguish the three curves. The main difference is a slight lateral shift in the position of the profile with respect to the spatial window. In Fig. 3(a) we show the calculated reflectivity spectra for the three cases. Note that all spectra in this figure are computed using the "exact" transfer matrix method described by Eq. (1). Fig. 3(b) shows the group delay curves associated with the power spectra in 3(a). Again all are nearly indistinguishable, except for a slight difference in the absolute delay, which is expected given the lateral shifts seen in Fig. 2. From the power reflectivity curves, we observe that the layer thickness is important in determining how well

the spectrum of the reconstructed grating approximates the target spectrum. For the direct comparison of the DLP and CLP methods with the same layer thickness (0.01 cm), the DLP method synthesizes an excellent approximation to the target spectrum for reflectivities down to about −40 dB, whereas the CLP method is able to match the spectrum down to about −50 dB. However, sidelobes produced by the CLP method do not fall off quite as rapidly as those produced by the DLP method.
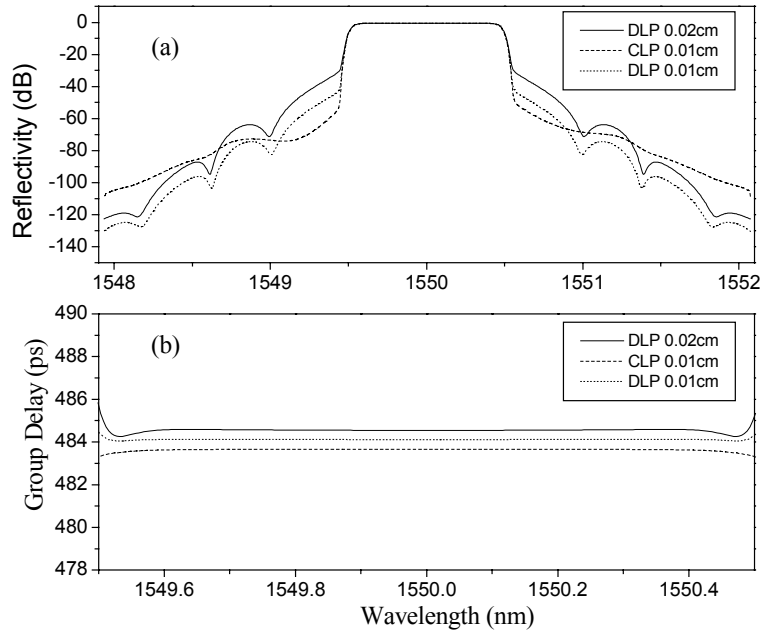
Fig. 3: Plots of the (a) reflectivity spectra, and (b) group delay curves associated with the reconstructed gratings in Fig. 2. All spectra are computed using the "exact" transfer matrix described by Eq. (1).

In Section 2 we make the claim that except for the approximation resulting from the grating coupling model itself (the discretized transfer matrix model), the DLP method can be made *exact*. This claim is now verified numerically, although we use the frequency domain implementation of the DLP, so here it is "exact" only within the error resulting from the finite spectral resolution limitation discussed in Sec. 2. In Fig. 4 we plot the reflection spectrum for the example above, but only for the case "DLP 0.02 cm." The dashed line is from Fig. 3(a), and the solid line is computed from the same coupling coefficient, but for the forward problem calculation we use the discretized matrix (2)–(4) instead of the "exact" matrix (1). Here we obtain an excellent approximation to the target spectrum for reflectivities down to about −170 dB. Of course this result is not necessarily physically significant, since for strong gratings the actual spectrum is usually more accurately predicted by the piecewise uniform ("exact") matrix calculation, but it shows that the method is exceptionally self-consistent — it

does an almost perfect job of reproducing the desired spectrum within the limits of the discretized-matrix approximation.
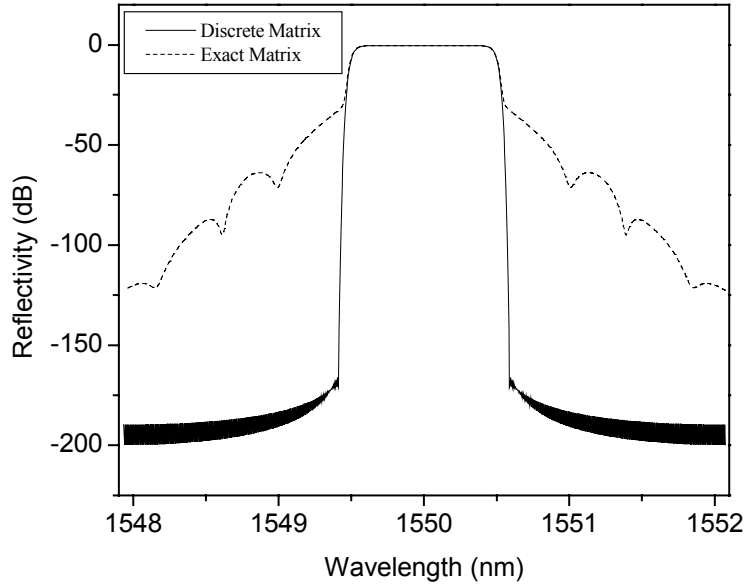
Fig. 4: Reflection spectra for the case "DLP 0.02 cm" in Fig. 2 computed using the discrete and the "exact" transfer matrixes.

For a second example, we consider for the target reflection spectrum a simple gaussian function with a quadratic phase (non-zero dispersion) of the form

$$r(\delta) = \sqrt{R} \exp\left[-(\delta/\delta_{PB})^2\right] \exp\left[-i\beta_2 L_F (c\delta/n)^2/2\right], \qquad (27)$$

where the maximum reflectivity is $R = 0.95$ and the width is determined by $\delta_{PB} = 12.3$ cm^{-1}, which corresponds to a pass-band full width at half maximum (FWHM) of 20.4 cm^{-1} in wavenumber, or 0.54 nm in wavelength at a center wavelength of 1550 nm. The dispersion is described by the product of the β_2 parameter (second derivative of the propagation constant with respect to frequency) and a characteristic length L_F for an optical fiber. Here we assume $\beta_2 = -21.7$ ps^2/km ($D = 17$ ps/nm-km) and $L_F = 30$ km, so that the grating is capable of compensating the dispersion of a standard (non-dispersion-shifted) fiber over a length of 30 km. The detuning window and layer thicknesses are the same as in the first example. The length of the grating is chosen to be $L = 12$ cm, which determines the number of layers $N = 600$. For this example the number of wavelengths is $M = 1200$. As in the example above, to present the fairest comparison we consider three cases: DLP with equal layer thickness to CLP, DLP with equal detuning window to CLP, and the CLP method.
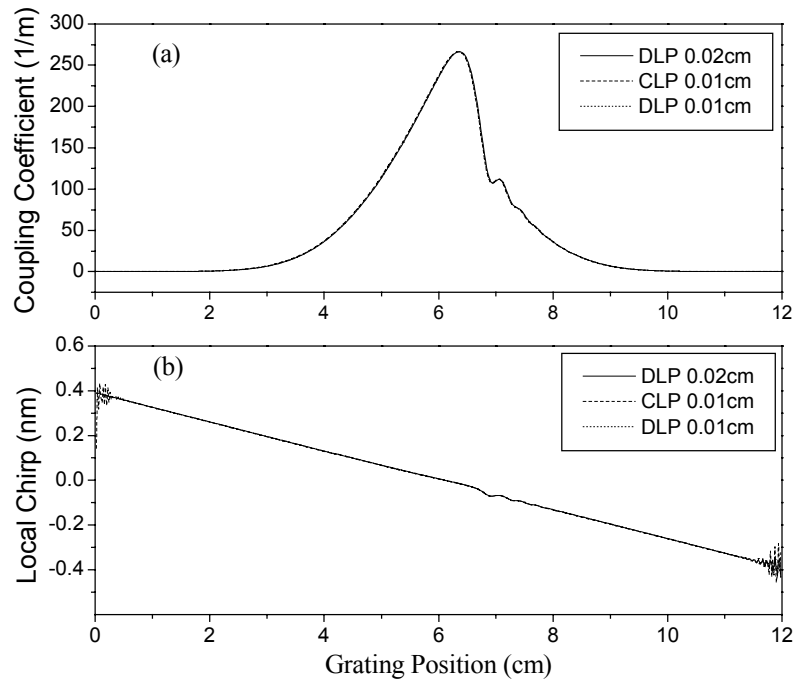
Fig. 5: Plots of the (a) magnitude of the coupling coefficient, and (b) relative chirp of the grating period with respect to a nominal period (arbitrarily defined to be at the middle of the grating), for gratings reconstructed from a constant-dispersion, gaussian-shaped reflection spectrum using both DLP and CLP methods and different sets of parameters.

The three calculations for the second example had associated processor run times of 0.93 sec, 35.92 sec, and 3.29 sec, for the "DLP 0.02 cm," "CLP 0.01 cm," and "DLP 0.01 cm" cases, respectively. The relative run times among the three cases for this example are almost identical to those for the first example. The coupling coefficient profiles are plotted in Figs. 5(a) and (b), where 5(a) shows the magnitude of the coupling coefficient and 5(b) shows the relative chirp of the grating period with respect to a nominal period (arbitrarily defined to be at the middle of the grating). Again the curves are nearly indistinguishable. In Fig. 6 we plot the spectra associated with the reconstructed gratings. For this example there is almost no difference among the spectra, indicating that for relatively smooth functions both methods work equally well for practical applications.
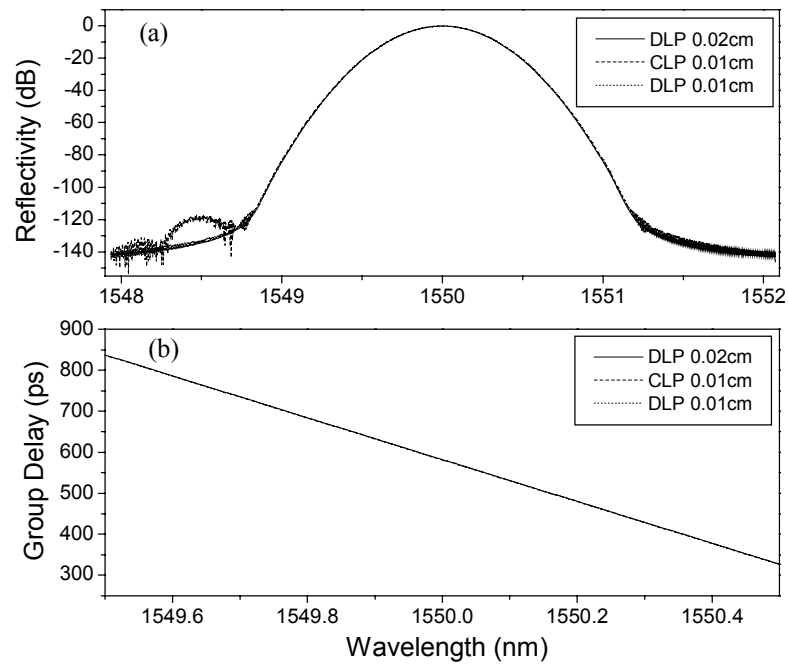
Fig. 6: Plots of the (a) reflectivity spectra, and (b) group delay curves associated with the reconstructed gratings in Fig. 5. All spectra are computed using the "exact" transfer matrix described by Eq. (1).

5. Conclusion

We have reformulated the discrete layer-peeling method for the synthesis of fiber gratings and showed how the discrete grating model can be reconstructed exactly from its spectrum, since the only approximation in this method is that resulting from the discretization of the mode coupling itself. The continuous layer-peeling method for grating reconstruction has been derived and it has been compared both mathematically and numerically to the discrete method. We show that the methods are based on the same principle, and that the continuous method is essentially equivalent to the discrete method in the limit of infinitesimally thin layers.

A numerical comparison reveals several interesting facts and apparent trends. First, we find that the DLP method is significantly faster than the CLP method, due in large part to the absence of any calculation of special (hyperbolic) functions for wave propagation and to the sufficiency of simple summations instead of more sophisticated numerical integration routines. Both of these simplifications result from the discretized approximation to the transfer matrix, and they come at a price — the DLP method is fundamentally limited by the degree of approximation associated with the simplified matrix calculation. The CLP method has the advantage that it allows for a variable layer thickness for a given choice of the spectral window. However, we find empirically that the method is not able to produce reasonable results for layer thicknesses similar to or greater than the thickness required for the DLP method. Thus CLP seems to inherently require smaller layer thickness than the DLP method, a characteristic which, while compounding its computation-time disadvantage, does allow it to yield somewhat better results for difficult structures (like those with rapidly varying coupling coefficients). When both methods are implemented with equal layer thicknesses (but a significantly larger frequency window and identical frequency resolution used for the DLP method), we still find about an order of magnitude improvement in the computation time for the DLP method over the CLP method. In this case the accuracy is similar for the two methods. Decreasing the layer thickness in the CLP method so that it is much smaller than the thickness dictated by the DLP method (i.e., for thicknesses down to even just a couple of grating periods), does not appear to provide much improvement in the accuracy with which the reproduced spectrum matches the target spectrum.

Appendix: Spectrum Realizability

When using the layer-peeling algorithm for synthesis of actual filters, the desired reflection spectrum is not necessarily realizable for a series of N reflectors or a grating of length L. To obtain a realizable reflection spectrum, we can use the (apodizing-)windowing procedure that is common in digital finite-impulse-response (FIR) filter design. This procedure was used by Feced for the synthesis of practical fiber gratings using the layer-peeling algorithm [1]. It consists of forcing the impulse response to be zero outside of a certain window, apodizing the windowed impulse response to cause the tails to approach zero more smoothly, and then shifting the whole response so that it starts at $t = 0$. This new impulse response is referred to as the "target impulse response," and we note that it has a finite duration. Strictly speaking, the (complex) reflection spectrum of any real fiber grating structure contains poles, and consequently the associated impulse response has infinite duration. In other words, even the target impulse response is not exactly realizable — the impulse response of the realized grating contains tails that extend beyond the windowed target impulse response, and these tails have nothing to do with the tails that were windowed. The realized tails cause undesirable fluctuations in the realized reflection spectrum, but as the examples in Feced's paper indicate [1], the influence of the tails is small for most practical filters with N>>1 and $\left| \rho_j \right| << 1$.

This windowing procedure is not necessarily optimal for the synthesis of finite length gratings as the following example demonstrates. Suppose one desires to synthesize a grating of length L with reflection spectrum $r(\delta)$, and assume that $r(\delta)$ happens to be identical to the reflection spectrum of a certain shorter grating , but of course this coincidence is not known in advance. Then, by using the windowing procedure, one gets a target spectrum $r_1(\delta)$ that is approximately realizable for a grating of length L. By applying the layer-peeling algorithm to this spectrum, one ends up with a grating of length L with a spectrum that approximates the desired function $r(\delta)$. Since the spectrum could have been realized *exactly* using a shorter grating, we would have been better off shortening the starting grating length than attempting to window the starting impulse response. Thus it should be clear that adjusting the windowing is not necessarily the best way in all cases to achieve the simplest structure to match a desired reflection spectrum. Nevertheless, it is a straightforward approach and often yields good results in practice.

It should also be noted that for the case of a discrete grating model, the realizable filter functions can be identified exactly. For N reflectors, the class of realizable filters is Nth order rational functions of $z^{-1} = \exp(i2\delta\Delta)$ with rather strict conditions on the coefficients [11]. However, these conditions are difficult to handle, and it is not a trivial problem to find the allowed coefficients that give the best fit to a desired response.

References

1. R. Feced, M. N. Zervas, and M. A. Muriel, "An efficient inverse scattering algorithm for the design of nonuniform fibre Bragg gratings," J. Quantum El., vol. 35, pp. 1105-1115, 1999.
2. L. Poladian, "Simple grating synthesis algorithm," Opt. Lett., vol. 25, pp. 787-789, 2000.
3. E. Brinkmeyer, "Simple algorithm for reconstructing fiber gratings from reflectometric data," Opt. Lett., vol. 20, pp. 810–812, 1995.
4. E. Peral, J. Capmany, and J. Marti, "Iterative solution to the Gel'Fand-Levitan-Marchenko coupled equations and application to the synthesis of fiber gratings," IEEE J. Quantum Electron., vol. 32, pp. 2078–2084, 1996.
5. M. A. Muriel, J. Azana, and A. Carballar, "Fiber grating synthesis by use of time-frequency representations," Opt. Lett., vol. 23, pp. 1526–1528, 1998.
6. J. Skaar and K. M. Risvik, "A genetic algorithm for the inverse problem in synthesis of fiber gratings," J. Lightwave Tech., vol. 16, pp. 1928–1932, 1998.
7. A. M. Bruckstein and T. Kailath, "Inverse scattering for discrete transmission-line models," SIAM Rev., vol. 29, pp. 359-389, 1987.
8. A. M. Bruckstein, B.C. Levy, and T. Kailath, "Differential methods in inverse scattering," SIAM J. Appl. Math. vol. 45, pp. 312-335, 1995.
9. J. P. Corones, M. E. Davison, and R. J. Krueger, "Direct and inverse scattering in the time domain via invariant imbedding equations," J. Acoust. Soc. Amer., 74, pp. 1535-1541, 1983.
10. A. Papoulis, *The Fourier integral and its applications*, (McGraw-Hill, New York, 1962).
11. E. M. Dowling and Duncan L. MacFarlane, "Lightwave lattice filters for optically multiplexed communication systems," J. Lightwave Tech., vol. 12, pp. 471-486, 1994.

3.3 Synthesis of thick optical thin-film filters using a layer-peeling inverse scattering algorithm

Authors: Johannes Skaar and Turan Erdogan

Synthesis of thick optical thin-film filters using a layer-peeling inverse scattering algorithm

Johannes Skaar

Department of Physical Electronics, Norwegian University of Science and Technology

N-7491 Trondheim, Norway

Turan Erdogan

The Institute of Optics, University of Rochester

Rochester, New York 14627, USA

We present an efficient and accurate method for synthesis of optical thin-film structures. The method is based on a differential inverse scattering algorithm and considers therefore both the phase and amplitude reflectance data. We apply the algorithm to the synthesis of filters with arbritrary index layers and two-material filters consisting of only high and low index layers. The layered structure is approximated by a stack of discrete reflectors with equal distance between all reflectors. This mirror stack is in turn determined from the desired, complex reflection spectrum by a layer-peeling inverse scattering algorithm. The complexity of the design algorithm is about the same as the forward problem of computing the spectrum from a known structure.

1. Introduction

Optical thin-film structures consisting of alternating layers of high- and low-index dielectric materials are vital components for many applications, including architecture, energy management, automobiles, scientific instruments, data storage, and display devices [1]. In addition to their use as high-reflection mirrors and anti-reflection coatings, thin-film structures form the basis for optical filters with sophisticated complex responses (reflection and transmission). In particular, thin-film filters enable tailorable dispersion for ultra-short pulse lasers [2] and extremely thick films are now a key technology for wavelength-division-multiplexed (WDM) fiber-optic communication systems. Thin-film filters with hundreds of layers have become possible to fabricate [3] and hence the ability to synthesize structures with increasingly demanding filter characteristics is a critical tool.

The calculation of the optical characteristics of a particular structure, i.e., the forward problem, is straightforward, whereas the calculation of a structure associated with specified optical characteristics, the inverse problem, is signficantly more difficult. Many approaches to the inverse problem for thin-film design can be classified into two main categories: numerical refinement and thin-film synthesis [1,4]. Both rely heavily on optimization algorithms, and hence tend to be based on a reasonable starting guess at the final structure. In this paper, we propose a new method for the synthesis of multilayer optical filters based on a specified complex reflection spectrum. The method is a direct approach analogously to the Fourier transform method [5]. However, in contrast to the Fourier method, the layer-peeling inverse scattering method is exact, i.e. the layers are exactly determined from the associated spectrum. The inverse scattering algorithm is based on direct inversion of the transfer matrix model after the following principle: Consider the desired impulse response which is determined by an inverse Fourier transform of the desired spectrum. At the leading edge of the impulse response, the light "sees" only the first layer because at the very beginning of the impulse response the light does not have time to propagate more deeply into the structure. By this causality argument one can determine the first reflector and hence the first transfer matrix. Then one can use the transfer matrix to propagate the fields to the next layer. Now one is in the same situation as at the beginning, since the effect of the first layer is "peeled off". The process is continued to the back of the filter.

With this method, any thin-film filter structure can be reconstructed from the associated complex reflection spectrum. For synthesis problems, however, the desired reflection spectrum does not necessarily have to be realizable for a thin-film filter since the required Fresnel reflectivities might be complex. To come around this problem, we first synthesize a mirror stack consisting of discrete, complex reflectors, and then approximate the stack by an inhomogeneous layer filter or a two-index thin-film filter. The remainder of this paper is organized as follows: In section 2 we give the basic principles behind the layer-peeling inverse scattering synthesis algorithm. In section 3 we first consider the easiest problem, namely to synthesize filters consisting of layers with arbitrary refractive indexes. Although this class of filters might be realizable in practice, at least in the future, for practical reasons it is often desireable to design filters consisting of only two different refractive indices, high (n_h) and low (n_l). Two-material structures could be

achivied by transforming the arbritrary index layers using the standard Herpin equivalent-index concept [6]. In this paper however, we compute the two-material filters directly from the discrete reflectors, and this procedure is described in section 3. In section 4, we present numerical examples of filters in both categories.

2. The layer-peeling inverse-scattering algorithm

In this section, we review the basic principles behind the differential inverse scattering algorithm. It was first developed by geophysicists for the recognition of layered-earth media from scattering data. A thorough analysis and comparison to other algorithms can be found in Bruckstein [7,8]. Whereas Bruckstein used the algorithm only for real reflectors, we extend the algorithm to consider complex reflectors. This is done to enable synthesis of asymmetric filter characteristics, which require quasi-periodical structures.

We state the inverse scattering problem as follows. We assume a stack of N discrete, complex reflectors with distance d between all reflectors. From the corresponding complex reflection spectrum $r(k)$ we wish to reconstruct the complex reflector amplitudes ρ_j, $j = 1,2,...,N$, where $k = 2\pi/\lambda$ is the vacuum wave number. This inverse scattering problem is inherently discrete in nature, and may be solved exactly by the layer-peeling algorithm. The running time of this algorithm is of the same order $O(N^2)$ as the conventional approach for computing the forward problem, i.e., computing the spectrum $r(k)$ from the reflector amplitudes ρ_j using the transfer-matrix method [9].
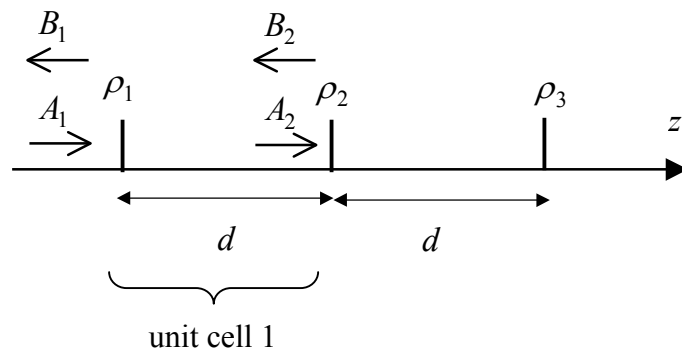
Fig. 1: The stack of discrete reflectors. The distance between the reflectors is d, and the complex fields before the jth section is A_j and B_j.

For a physical picture of how the layer-peeling algorithm works, we imagine that the filter is probed by a delta-function pulse. Thus the forward and backward propagating fields before the first section, A_1 and B_1 respectively, are

$$\begin{bmatrix} A_1(k) \\ B_1(k) \end{bmatrix} = \begin{bmatrix} 1 \\ r(k) \end{bmatrix}. \tag{1}$$

Each "unit cell" of the reflector stack is composed of the discrete localized reflector followed by a pure propagation section, as illustrated in Fig. 1. The jth unit cell is therefore described by the transfer matrix product $T_d T_{\rho,j}$, where

$$T_d = \begin{bmatrix} \exp(ikd) & 0 \\ 0 & \exp(-ikd) \end{bmatrix} \tag{2}$$

is the standard propagation matrix, and

$$T_{\rho,j} = \left(1 - \left|\rho_j\right|^2\right)^{-1/2} \begin{bmatrix} 1 & -\rho_j^* \\ -\rho_j & 1 \end{bmatrix} \tag{3}$$

describes a pure, discrete reflector. The discrete reflector is generally complex, with ρ_j and $-\rho_j^*$ the reflection coefficientsfrom the left and right, respectively, and $\left(1 - \left|\rho_j\right|^2\right)^{1/2}$ the transmission coefficient for both directions. If we manage to determine the first reflector, we can use $T_d T_{\rho,1}$ to transfer the fields to the next section. We then find ourselves in the same situation as with the first reflector, so in effect the first layer is "peeled off". This procedure can be repeated until the entire stack is determined.

In order to find the complex amplitude of the first reflector, we note that the impulse response of the reflector stack for time $t < 2d/c$ is independent of the reflectors ρ_j for $j \geq 2$ because light does not have sufficient time to propagate to and from the second and higher reflectors. Thus, when looking at the impulse response of the stack for $t < 2d/c$, we obtain the same response as if reflector 1 was alone. Therefore, we can compute ρ_1 as

the inverse Fourier transform of $r(k) = B_1(k)/A_1(k)$ evaluated at time $t = 0$. More precisely, because $r(k)$ is periodic with period π/d, we find

$$\rho_1 = \frac{d}{\pi} \int_{period} \frac{B_1(k)}{A_1(k)} dk \qquad \text{or} \qquad \rho_1 = \frac{1}{M} \sum_{m=1}^{M} \left. \frac{B_1}{A_1} \right|_m , \tag{4}$$

where m denotes the sample number of the ratio B_1/A_1 and $M \geq N$ is the number of spectral points, in one spectral period. We must ensure that M is chosen to be sufficiently large to represent the target $r(k)$ with a desired accuracy. Strictly speaking, we must have $M = \infty$ to make the layer-peeling algorithm truly exact. However, in practical situations, it turns out that M does not have to be considerably greater than N. For the examples in this paper, we used $M = N$. A way of getting the layer-peeling procedure strictly exact is to transform it to the time domain, and represent the intermediate results (fields) as time domain responses [7,8].

We can summarize the algorithm in the following simple steps:
i)   Start with a physically realizable reflection coefficient $r(k)$ (see the remark below).
ii) Compute ρ_1 from eq. (4)
iii) Transform the fields using the transfer matrixes, or by using the equvivalent Schur recursion expression

$$\frac{B_2(k)}{A_2(k)} = \exp(-i2kd) \frac{\dfrac{B_1(k)}{A_1(k)} - \rho_1}{1 - \rho_1^* \dfrac{B_1(k)}{A_1(k)}} \tag{5}$$

   Eq. (5) results from the transfer matrix muliplication and is similar to a recursion formula proposed by Schur for testing the boundedness of an analytic function outside the unit circle of the complex plane [8].
iv) Return to ii until the entire filter is determined.

When using the layer-peeling algorithm for synthesis of actual filters, the desired reflection spectrum $r(k)$ is not neseccarily realizable, even for a stack of complex reflectors. To obtain a realizable reflection spectrum, we use the windowing procedure

that is common in digital FIR filter design [10]. The same procedure was used by Feced et al. for the synthesis of fiber Bragg gratings using a layer-peeling algorithm [11]. First we compute the inverse Fourier transform of the desired spectrum to obtain the impulse response. This response is then forced to be causal and realizable by multiplying it by a window function, and shifting it so that it is nonzero only for times $t \geq 0$. The window function should be smooth in order to reduce the Gibbs phenomenon. The realizable $r(k)$ is finally obtained by Fourier transform of the windowed impulse response. Note that the target impulse response has a finite duration. Strictly speaking, the impulse response of any stack consisting of two or more mirrors must have infinite duration, so the target response is not exactly realizable for a stack of N reflectors. Thus there is always an unwanted tail in the realized impulse response. The realized tails cause undesirable fluctuations in the realized reflection spectrum, but as the examples below and the examples in ref. [11] indicate, the influence of the tail is small for most practical filters with $N \gg 1$ and $|\rho_j| \ll 1$.

3. Design of thin-film structures

In this section we show how to convert the stack of complex, discrete reflectors into a physical filter. If we were designing a corrugated filter, e.g., a fiber Bragg grating, this procedure would be very simple: comparison to Feced [11] shows that the samples of the complex coupling coefficient of the grating are related to the discrete reflection coefficients by the relation

$$q_j = -\frac{1}{d} \frac{\rho_j^*}{|\rho_j|} \operatorname{arctanh}|\rho_j|. \tag{6}$$

In this paper however, our goal is a layered thin-film filter. For simplicity, we neglect all kinds of loss in the structure. First, we consider the simplest problem, namely to find a layered structure with arbitrary indexes. The indexes n_j must satisfy $n_l \leq n_j \leq n_h$, where n_l and n_h is the lowest and highest realizable indexes, respectively. From the Fresnel reflection coefficients it is straighforward to obtain index jumps that realize real ρ_j provided

$$\left|\rho_j\right| < \left(n_h - n_l\right)/\left(n_h + n_l\right). \tag{7}$$

The refractive index profile must be held between the limits n_l and n_h. If the required index of the jth layer becomes too small or too large, one can simply insert a section corresponding to a round-trip phase shift of π to reverse the index jump. The phase of ρ_j must be realized by deviating the positions of the index jumps compared to the positions of the discrete reflectors. This is clearly an approximation as the induced phase response will be frequency dependent (linear phase) whereas the discrete reflectors are independent of frequency. However, this approximation is apparently good for bandwidths that are much less than the center frequency, $\Delta k << k_0$ which usually is true for the usable bandwidth of thin-film filters.

In practice, it is often more desireable to design two-material thin-film filters consisting of only high (n_h) and low (n_l) refractive index layers. Such filters can be designed from the corresponding inhomogenous layers above by the standard Herpin equvivalent-index concept [6]. In this work however, we present another, more direct approach of obtaining the layer thicknesses from the desired stack of discrete reflectors. By using the transfer matrixes, we show that a symmetrically defined Bragg period (see Fig. 2) can be approximately represented by a discrete reflection coefficient.
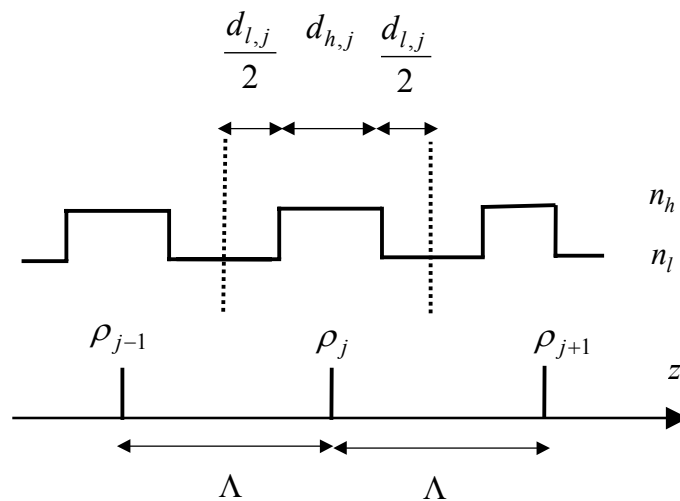
Fig. 2: Refractive index profile of the thin-film filter. The symmetrically defined Bragg period, or "unit cell," is the region between the dashed vertical lines. The discrete reflectors ρ_j are indicated below the profile.

We assume that the grating is perfectly matched to the surrounding media (the refractive indexes of the surrounding media are assumed to be n_l). Furthermore, we define $d_{h,j}$ and $d_{l,j}$ as the thicknesses, and $\phi_{h,j} = k n_h d_{h,j}$ and $\phi_{l,j} = k n_l d_{l,j}$ as the phase shifts in the high- and low-index layers, respectively, all in the jth symmetrically defined Bragg period or "unit cell" (see Fig. 2). Using a standard transfer-matrix method, we find the complex reflection coefficients of each "unit cell" to be [9]

$$ r_j = \frac{-2ir\sin\varphi_{h,j}}{\exp\left[-i\left(\varphi_{l,j}+\varphi_{h,j}\right)\right]-r^2\exp\left[-i\left(\varphi_{l,j}-\varphi_{h,j}\right)\right]} \quad . \tag{8}$$

where the parameter $r = (n_h - n_l)/(n_h + n_l)$ denotes the Fresnel reflectivity at each index step. Eq. (8) results from a transfer matrix multiplication of the two index-step matrices inserted between the appropriate propagation matrices. Now, we want to represent the above reflectors with discrete, complex reflectors to be able to apply a layer-peeling synthesis algorithm. To force the reflection coefficient (8) to be independent of wavelength, we must make an approximation. Therefore we define the amplitude of the wavelength-independent discrete reflector to be

$$ \left|\rho_j\right| = \left|r_j\right|_{\lambda=\lambda_B} = \left.\frac{2r\sin\varphi_{h,j}}{\left(1+r^4-2r^2\cos\left(2\varphi_{h,j}\right)\right)^{1/2}}\right|_{\lambda=\lambda_B}, \tag{9}$$

where λ_B denotes a design Bragg wavelength and we have assumed $0 \le \varphi_h \le \pi$. The phase of the reflection associated with the jth unit cell at λ_B is

$$ \varphi_{r,j} = \arg r_j\big|_{\lambda=\lambda_B} = \left.\arctan\frac{\sin\left(\varphi_{l,j}+\varphi_{h,j}\right)-r^2\sin\left(\varphi_{l,j}-\varphi_{h,j}\right)}{\cos\left(\varphi_{l,j}+\varphi_{h,j}\right)-r^2\cos\left(\varphi_{l,j}-\varphi_{h,j}\right)}\right|_{\lambda=\lambda_B}, \tag{10}$$

where we have ignored the phase shift due to the factor $-i$ in (8) since it is the same for all unit cells. We account for the variation in the phase shifts $\varphi_{r,j}$ resulting from variation in the layer thicknesses by assigning a phase factors to the discrete reflection coefficients

ρ_j, such that $\rho_j = |\rho_j| \exp(i\varphi_j)$. That is, we let the distance between the discrete reflectors be constant, and account for chirp due to variation in the layer thicknesses using φ_j. The phase difference between reflections from two neighboring reflectors must equal the phase difference between reflections from two neighboring unit cells, so that

$$\varphi_j - \varphi_{j-1} + 2\pi = \varphi_{r,j} - \varphi_{r,j-1} + \varphi_{h,j-1} + \varphi_{l,j-1} + \varphi_{h,j} + \varphi_{l,j} . \tag{11}$$

Here we have moved the reflection reference planes of the unit cells j and $j-1$ to the same position, namely to the middle of unit cell $j-1$. This transformation, which is done to enable comparison of the phases, yields the last four terms in (11) (see Fig. 2). The same transformation is performed on the left-hand side, but the round-trip propagation phase between reflector j and $j-1$ is simply set to 2π since the distances between all neighboring reflectors is the same and since we will require $\varphi_j - \varphi_{j-1} = 0$ if the right-hand side is 2π.

Now that we have modeled the thin-film filter as a stack of discrete, complex reflectors ρ_j with identical distances between all reflectors, then once the discrete reflectors ρ_i are found by use of the layer-peeling method, the layer phase shifts can be computed from (11) and through inversion of (9) and (10): From the known $|\rho_j|$ and φ_j, eq. (9) gives $\varphi_{h,j}$ for all j. After substituting (10) into (11) the only remaining unknowns are $\varphi_{l,j}$ and $\varphi_{l,j-1}$. Thus the inversion is initiated by picking an arbitrary value for $\varphi_{l,1}$. Then (11) gives $\varphi_{l,2}$; the rest of the $\varphi_{l,j}$ are determined by repeated application of (11). The equation solving is conveniently performed by numerical optimization packages. However, for most practical situations the Fresnel reflectivity of each interface is small, or $r \ll 1$, so that eqs. (9) through (11) may be approximated by the relations

$$|\rho_j| = 2r \sin\varphi_{h,j} \tag{12}$$

and

$$\varphi_{h,j} + \varphi_{l,j} = \pi + (\varphi_j - \varphi_{j-1})/2. \tag{13}$$

In fact, this approximation can be justified even if the Fresnel reflectivity is relatively large since the approximation that the reflection coefficient of each unit cell is independent of wavelength, implicit in eqs. (9) and (10), is usually more significant. Therefore, equations (12) and (13) are sufficient to compute the layer phases from the synthesized stack of discrete reflectors. Finally, we obtain the layer thicknesses from the definitions $\phi_{h,j} = k_B n_h d_{h,j}$ and $\phi_{l,j} = k_B n_l d_{l,j}$, where k_B denotes the design Bragg wave number.

4. Numerical examples

As a numerical example, we first apply the synthesis algorithm to design dispersionless square filters with high reflectivities. Such filters are potentially important for the Wavelength Division Multiplexed (WDM) communications technology of the future. The target filter is a square filter with maximum reflectivity of 99.9%, no dispersion, and a bandwidth of 0.13 μm. In order to make the target filter causal and realizable the impulse response is apodized using a Kaiser$_{10}$ window [10], and shifted so that it starts at time $t = 0$. We take the number of reflectors to be 150. We have synthesized both an inhomogenous layer filter (fig. 3), and a thin-film filter consisting of high- and low-index layers (two-material filter, fig. 4). In the latter case the indexes of the materials are set to 1.5 and 2.0, which are close to the indexes of the standard dielectric materials SiO_2 and Ta_2O_5, respectively. The total thicknesses of the resulting filters are 39 μm and 52 μm, respectively. The filter performances have been computed by an exact transfer matrix method, and are shown in Figs. 5 and 6. In Fig. 5, the reflectivity spectra for the two filters are compared. We observe a small ripple of $4 \cdot 10^{-4}$ in the pass band for both filters. The side lobe level is -24dB and -19dB for the inhomogenous-layer filter and the two-material filter, respectively. As can be observed in Fig. 6, the ripple or deviation of the group delay dispersion is roughly 20 fs^2 and 50 fs^2 inside the pass band for the inhomogenous layer filter and the two-material filter, respectively.

Next, we show an example of synthesis of a dispersion compensating bandpass filter. This type of filter has become important in ultra-fast laser physics [2]. The target dispersion for this example is 275 fs^2, that is the group delay is linear as a function of wave number. The dispersion is specified after the windowing process. The number of

layers is set to 200. The maximum reflectivity and the indexes of the materials are the same as in the previous example. The result of the synthesis is shown in Figs. 7 through 10. As expected, the performance of the filters is about the same as their non-dispersive counterparts, but the group delay dispersion is nearly constant as a function of wave number in the reflection band. While we choose a linear group delay for the sample dispersion response, the power of the layer-peeling method is its ability to synthesize an arbitrary group delay spectrum based on the known dispersive properties of the system that requires compensation.

One of the main advantages of the layer-peeling algorithm compared to the conventional optimization methods is the efficiency: Because the running time is of the same order as the forward transfer matrix calculation of the spectrum, we can design extremely thick filters very fast. The two calculations in this paper had associated run times of less than 0.2sec using the program MATLAB on a 300MHz Pentium computer. In addition, it is evident from the examples that the layer-peeling method is particularly suitable for designing filters when the entire spectrum is relevant to the designer, not only a small bandwidth. For example, one observes that the spectra of the designed filters match well to the goal spectrum in both the reflection (pass) band and also the stop band. The disadvantage is clearly that one cannot weight different trade-offs in the same way as with optimization methods. However, if a certain parameter is critical, as for example the group delay dispersion, one can use numerical refinement techniques to optimize for that parameter with the layer-peeling design as a starting point.

5. Conclusion

We have proposed a method for synthesis of thin-film filters using a layer-peeling inverse scattering algorithm. This method is particularly useful for designing filters with many film layers, and has the advantage that no knowledge of a reasonable starting guess at the final structure is necessary. The method has been used for designing filters consisting of arbitrary index layers and for designing two-material thin-film filters. The running time of the synthesis algorithm is about the same as the running time of the conventional transfer matrix method for computing the spectrum from a known structure.
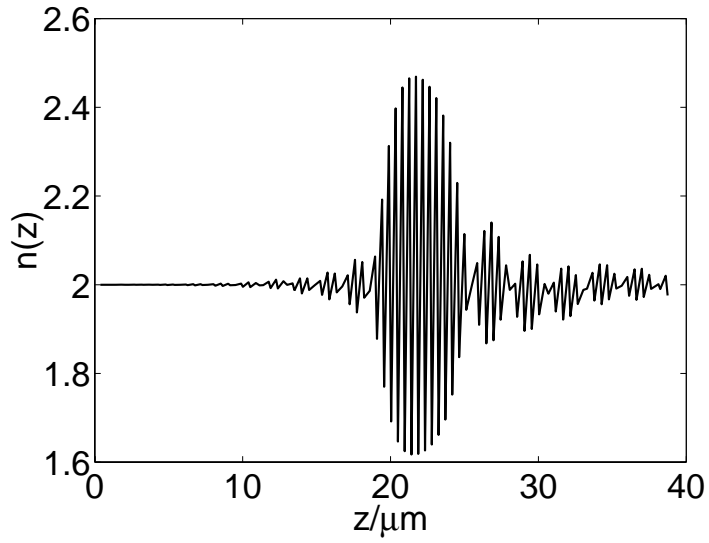
Fig. 3: The refractive index profile of the inhomogenous layer non-dispersive bandpass filter.
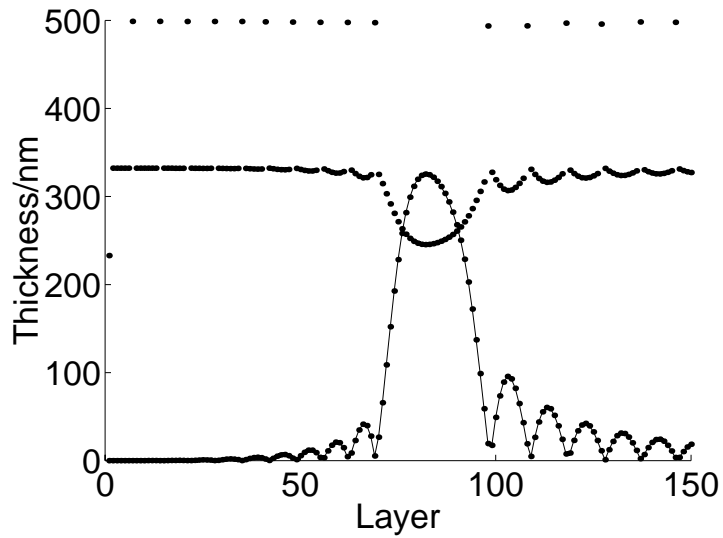
Fig. 4: Layer thicknesses of the two-material non-dispersive bandpass filter. The dots represent the thicknesses of the low-index layers ($d_{l,j}$) whereas the lined-through dots are 5 times the thicknesses of the high-index layers ($d_{h,j}$).
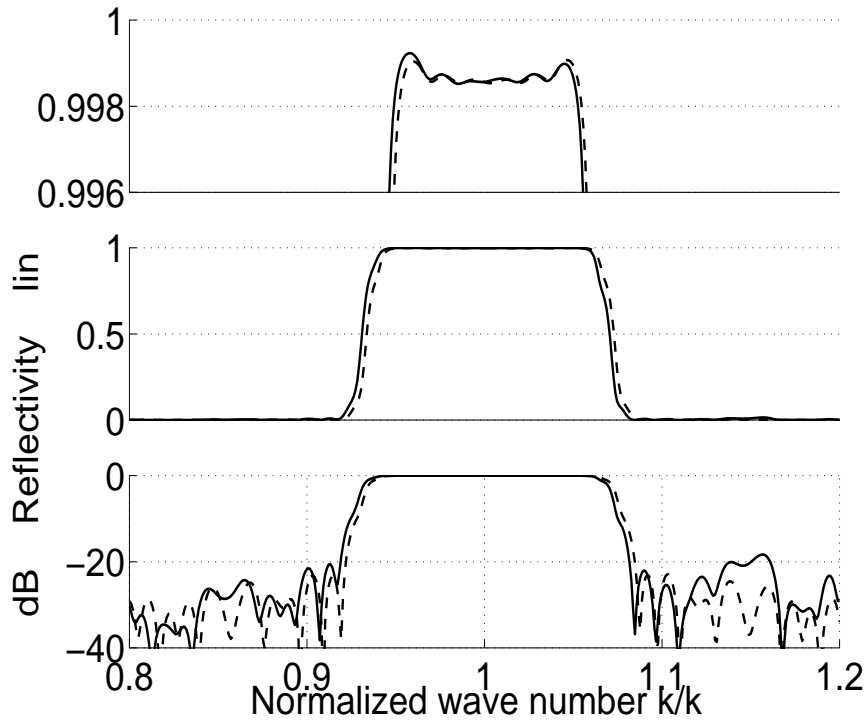
Fig. 5: Reflectivity of the non-dispersive bandpass filter. The dashed line is the spectrum of the inhomogenous layer filter, whereas the solid line represents the spectrum of the two-material filter. The spectra are shown in both linear and logarithmic scales.
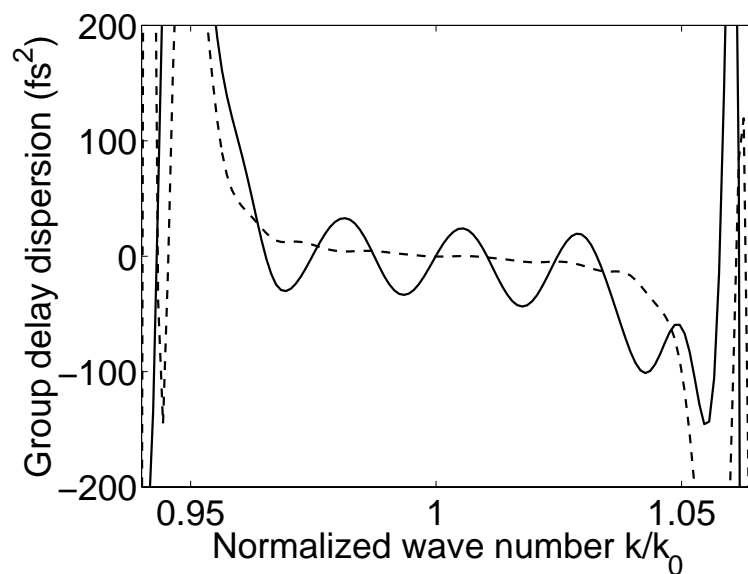
Fig. 6: Group delay dispersion for the "non-dispersive" bandpass filters. The dashed line is the dispersion spectrum of the inhomogenous-layer filter, whereas the solid line represents the dispersion of the two-material filter.
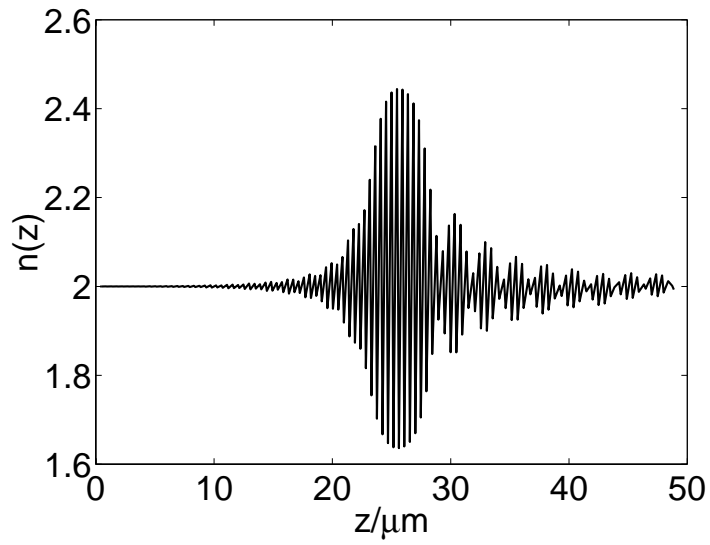
Fig. 7: The refractive index profile of the inhomogenous layer dispersive bandpass filter.
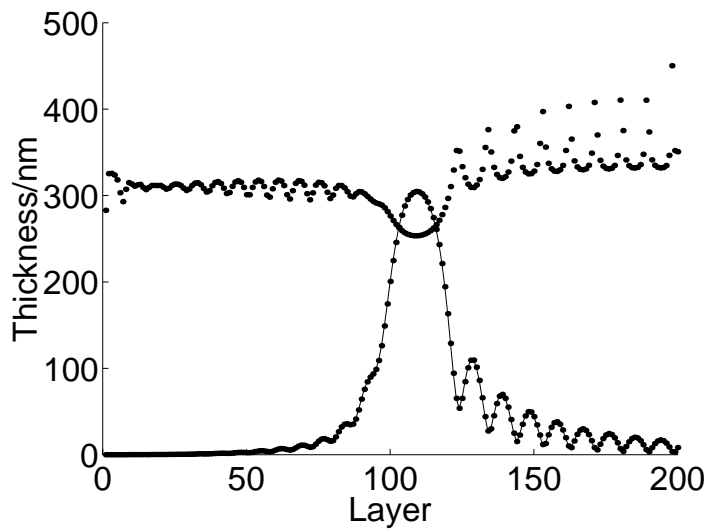
Fig. 8: Layer thicknesses of the two-material dispersive bandpass filter. The dots represent the thicknesses of the low-index layers ($d_{l,j}$) whereas the lined-through dots are 5 times the thicknesses of the high-index layers ($d_{h,j}$).
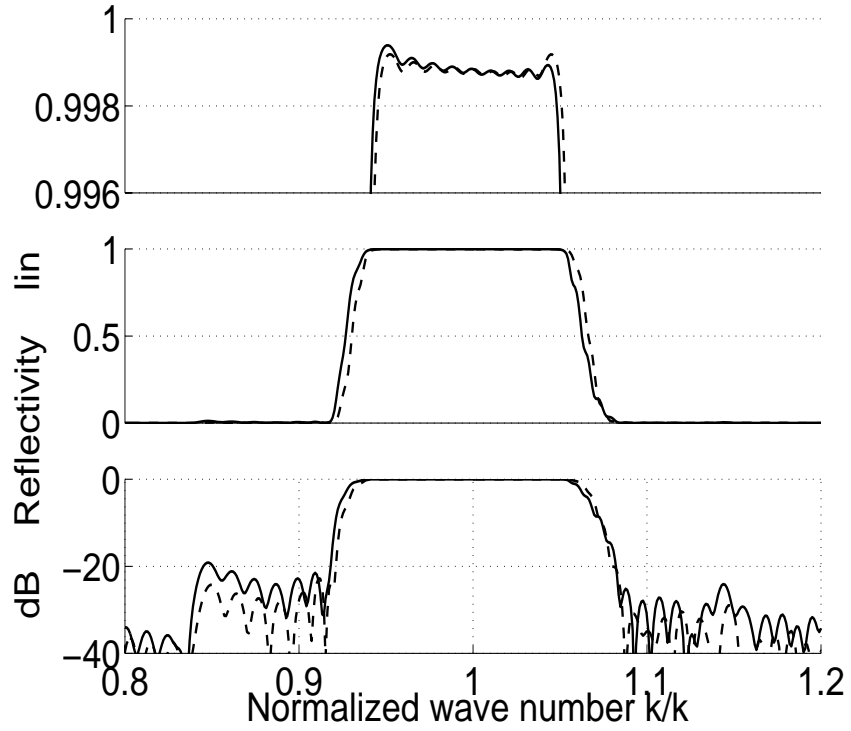
Fig. 9: Reflectivity of the dispersive bandpass filter. The dashed line is the spectrum of the inhomogenous layer filter, whereas the solid line represents the spectrum of the two-material filter. The spectra are given in both linear and logarithmic scales.
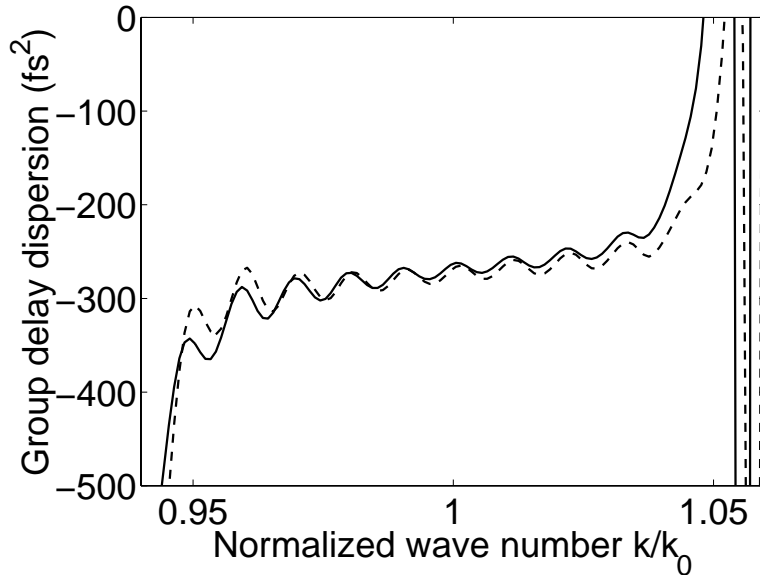
Fig. 10: Group delay dispersion of the dispersive bandpass filters. The dashed line is the dispersion spectrum of the inhomogenous layer filter, whereas the solid line represents the dispersion of the two-material filter.

References

1. J. A. Dobrowolski, "Numerical methods for optical thin films," Opt. and Photon. News, 24-33 (June 1997).

2. N. Matuschek, F.X. Kärtner, and U. Keller, "Analytical design of douple-chirped mirrors with custom-tailored dispersion characteristics," IEEE J. Quant. El. **35**, 129-137 (1999).

3. S. R. A. Dods, Z. Zhang, and M. Ogura, "Highly dispersive mirror in Ta_2O_5/SiO_2 for femtosecond lasers designed by inverse spectral theory," Appl. Opt. **38**, 4711-4719 (1999).

4. See for example commercial thin-film design software on the internet: http://www.qis.net/~bnichols/opticsnotes/thincad.htm.

5. J. A. Dobrowolski and D. Lowe, "Optical thin film synthesis program based on the use of Fourier transforms," Appl. Opt. **17**, 3039-3050 (1978).

6. J. A. Dobrowolski and S. H. C. Piotrowski, "Refractive index as a variable in the numerical design of optical thin-film systems," Appl. Opt. **21**, 1502-1511 (1997).

7. A.M. Bruckstein and T. Kailath, "Inverse scattering for discrete transmission-line models," SIAM Rev. **29**, 359-389 (1987).

8. A.M. Bruckstein, B.C. Levy, and T. Kailath, "Differential methods in inverse scattering," SIAM J. Appl. Math. **45**, 312-335 (1995).

9. H. A. Macleod, Thin-fim optical filters (Bristol: Adam Hilger, 1985).

10. J. G. Proakis, *Digital signal processing,* (Prentice Hall, 1996).

11. R. Feced, M.N. Zervas, and M.A. Muriel, "An efficient inverse scattering algorithm for the design of nonuniform fibre Bragg gratings," J. Quant. El. **35**, 1105-1115 (1999).

Chapter 4

Synthesis of fiber gratings for use in transmission

This chapter is devoted to a related subject to that of the previous chapter. A method for synthesis of gratings with desired complex transmission coefficients is developed. Because the transmission coefficient of a fiber grating satisfies the minimum phase condition, only a limited bandwidth is considered for the synthesis. Then the minimum phase condition can be fulfilled due to the behavior of the transmission coefficient outside that bandwidth.

The first paper contains a general method for synthesis of minimum phase functions with a desired, complex response inside a finite bandwidth window. Dependent on the required asymptotic behavior, one gets two different variants of the method. The transfer functions resulting from the method in this paper is not necessarily passive, and consequently, a modification is required when designing practical filters without gain. In the next paper, we apply the general design method to fiber gratings and show how one can obtain passive filters. Practical gratings are designed, and the performance of the designs are discussed. For an introduction to the field, consult the introductions in the respective papers.

4.1 Synthesis of limited bandwidth minimum phase filters

Author: Johannes Skaar

Synthesis of limited bandwidth minimum phase filters

Johannes Skaar

Department of Physical Electronics, Norwegian University of Science and Technology, N-7491 Trondheim, Norway

Abstract.   A method for designing minimum phase or minimum delay filters with an arbitrary complex transfer function inside a finite frequency interval is proposed. The method is based on a result of Krein and Nudel'man [Problemy Peredachi Informatsii 11, 37-60 1975]. The filters are divided into two classes, depending on their asymptotic behavior for large frequencies. For filters with asymptotic value different from zero, a straightforward and completely general synthesis method is proposed yielding good numerical results. A similar method is shown to be suitable for a limited class of filters whose responses are required to approach zero in a certain sense.

1. Introduction

Several physical filter configurations yield so-called minimum phase transfer functions. By minimum phase transfer functions, we essentially mean transfer functions that are zero-free in the lower half of the complex ω plane. The minimum phase characteristic is often a fundamental property of the physical configuration itself, rather than a desired or designed response. Examples of such configurations are transmission lines [1] or optical transmission filters, e.g. optical thin-film filters or fiber Bragg gratings that work in transmission [2, 3, 4, 5]. One important property of such transfer functions is that the amplitude and phase responses are uniquely related. Thus there are fundamental constraints that strongly limit what is possible to realize. On the other hand, in some applications it is desirable to realize a certain complex transfer function inside a relevant bandwidth without changing the overall filter configuration. Since it is in general impossible to realize an arbitrary minimum phase transfer function $H = H(\omega)$ for all frequencies, we will limit our bandwidth of consideration to a finite interval, say $\Omega = (\omega_1, \omega_2)$, where $0 \leq \omega_1 < \omega_2 < \infty$. This means that we want to obtain a desired minimum phase transfer function $H(\omega)$ for $\omega \in \Omega$, but we do not care what $H(\omega)$ is for $\omega \notin \Omega$. If we do not restrict ourselves to minimum phase transfer functions, the solution to this continuation problem is unique and can be found by the Carleman formula [6]. A condition for existence has been given by Krein and Nudel'man [7, 8]; it is rather strict, and in addition, the transfer function solution might have a large energy. Therefore, Krein and Nudel'man also solved the similar problem of finding a minimum

norm solution to the problem, given a desired precision on Ω. If we do restrict ourselves to minimum phase filters, the solution to the continuation problem will of course still be unique, but the existence condition will be stricter, as the continuation into the lower half-plane must be zero-free. Therefore, we will consider the problem of finding a transfer function H, which approximates a desired response for $\omega \in \Omega$, and satisfies the minimum phase condition due to its behavior outside Ω.

This paper is organized as follows: In section 2, we make the minimum phase condition precise, and divide the most common physical filters into two classes, depending on their asymptotic behavior as $\omega \to \infty$. Moreover, we state the synthesis problems for those classes, and propose corresponding solution methods. In section 3, a numerical solution algorithm is described and examples are given.

2. Synthesis of minimum phase systems

A linear system is characterized by an impulse response $h(t)$, which we assume can be written as

$$h(t) = a\delta(t) + h_{L^2}(t), \tag{1}$$

where a is a real constant and $h_{L^2} \in \hat{L}^2(0, \infty)$. $\hat{L}^2(0, \infty)$ denotes the real Hilbert space consisting of all real-valued functions in the complex Hilbert space $L^2(0, \infty)$. We write h in this form because we will include transfer functions of linear transmission systems where the transfer function approaches a constant (for example 1) as $\omega \to \infty$. The number a is determined by the type of the filter. The transfer function is defined as the Fourier transform of h,

$$H(\omega) = (\mathcal{F}h)(\omega) = \int_0^\infty h(t) \exp(-i\omega t) \mathrm{d}t, \tag{2}$$

where $\mathcal{F}$ is the Fourier transform operator. Similarly, we define H_{L^2} as the Fourier transform of h_{L^2}, $H_{L^2} = \mathcal{F}h_{L^2}$, so

$$H(\omega) = H_{L^2}(\omega) + a. \tag{3}$$

The lower limit in (2) is set to zero due to causality, i.e. $h_{L^2}(t) = 0$ for $t < 0$. Consequently, the real and imaginary part of $H_{L^2}(\omega) = H(\omega) - a$ form a Hilbert transform pair by the Titchmarsh theorem [9]. However, we are interested in the connection between the modulus and phase of H. In general, there is no such unique relation owing to zeros of H in the lower half-plane [10]. But for an important class of filters, there are no zeros of the transfer function in the closed lower half-plane, and we can derive relations between the modulus and phase. This filter class is called minimum phase (shift) functions. The form of the relations may differ, depending on the asymptotic behavior of H as $\omega \to \infty$. In addition, there is a variety of equivalent relations for the same class of filters [10, 11, 12]. Here, we will use the original Hilbert transforms to connect the modulus and phase. We must therefore form a function $G = G(\omega)$ with its real and imaginary parts derived from the modulus and phase of H. G must satisfy the Titchmarsh theorem, that is: (i) it must be square integrable along

the real axis, (ii) it must be analytic in the lower half-plane, and (iii) there must be a uniform bound $k < \infty$ such that

$$\int_{-\infty}^{\infty} |G(x+iy)|^2 dx \leq k \qquad \text{for } y < 0. \tag{4}$$

The hypotheses (i) through (iii) are equivalent to the condition that G belongs to the Hardy space H^2 of the lower half-plane [13]. Since the asymptotic behavior is dependent on the value of a, we must treat two cases separately.

2.1. Filter class with $a \neq 0$

First we assume that $a \neq 0$. This is the case for example for typical transmission filters where the input signal is going straight through the filter outside a certain pass band. The number a is determined by the asymptotic value of H. For this class, consider

$$G(\omega) = \log H(\omega)/a. \tag{5}$$

Because H is a minimum phase function, it is zero-free in the closed lower half-plane. Then G is analytic in the lower half-plane. Provided that $|H(\omega)| \geq \epsilon$ for a certain $\epsilon > 0$ in the closed lower half-plane, the function G satisfies the integrability condition (4). Then, the Titchmarsh theorem is applicable for G, which means that the real and imaginary parts of G form a Hilbert transform pair. The modulus and phase of H are therefore uniquely related by means of a logarithmic Hilbert transform [12].

We recall that our problem is to find a minimum phase transfer function $H(\omega) = H_{L^2}(\omega) + a$ approximating a desired response in Ω. From the above discussion it seems plausible that this problem can be reduced to the problem of finding another transfer function $G = \log H/a$ approximating a function F in Ω. Since we would like the transfer function H to be as close as possible to a outside Ω, we optimize for least norm of G. This problem has been studied by Krein and Nudel'man [7, 8], and we adopt their problem formulation:

Given a desired response $F \in L^2(\omega_1, \omega_2)$ and a number ϵ, $(0 < \epsilon \leq \|F\|)$, find a $g \in \hat{L}^2(0, \infty)$ having least norm $\|g\|$, and such that

$$\int_{\omega_1}^{\omega_2} |F(\omega) - G(\omega)|^2 d\omega \leq \epsilon^2, \tag{6}$$

where $G = \mathcal{F}g \in L^2(-\infty, \infty)$.

The minimum phase transfer function H is then given by

$$H(\omega) = a \exp[G(\omega)]. \tag{7}$$

H satisfies the Hermitian property $H(-\omega) = \overline{H(\omega)}$, and in the Appendix we show that $H - a$ belongs to L^2 and satisfies the Titchmarsh theorem $(H_{L^2} \in H^2)$ if F satisfies the Lipschitz condition and vanishes as $\omega \to \omega_1$ and $\omega \to \omega_2$. Moreover, H is zero-free in the closed lower half-plane, and it is therefore realizable as a transfer function of the minimum phase transfer function class with $a \neq 0$. The condition that the goal function F must vanish at the endpoints is not a further constraint as it can be fulfilled by extending the interval Ω with a smooth termination of F.

The problem above has a unique solution, and can be solved by finding the function g from the integral equation [7, 8]

$$\mu g(t) + \int_0^\infty \left[\frac{\sin \omega_2(t-s)}{\pi(t-s)} - \frac{\sin \omega_1(t-s)}{\pi(t-s)} \right] g(s)\mathrm{d}s = f(t), \qquad 0 \le t < \infty \tag{8}$$

where

$$f(t) = \mathrm{Re}\ \frac{1}{\pi} \int_{\omega_1}^{\omega_2} F(\omega) \exp(i\omega t)\mathrm{d}\omega, \tag{9}$$

and $\mu = \mu(\epsilon)$ is some positive function of ϵ. This function is defined in [7, 8]; it is dependent on F and is decreasing monotonically to zero as $\epsilon \downarrow 0$. In the next section, we solve (8) numerically by extrapolating to the negative semiaxis, and transforming to the frequency domain.

2.2. Filter class with $a = 0$

When $a = 0$, we have $H = H_{L^2} \in L^2(-\infty, \infty)$. The asymptotic condition must in this case be treated with care, as $|\log H| \to \infty$. One common, possible asymptotic form of $\log |H|$ is [12]

$$\log |H| \to -(n+1) \log |\omega| + A \qquad \omega \to \pm\infty, \tag{10}$$

along the real axis, where $n \ge 0$ and A is a real constant. For integer n, this asymptotic form may arise when the nth derivative of h has a jump at the origin, while the lower order derivatives are zero. If $\log H$ is differentiable and $|H|$ has the asymptotic form (10), we can construct the function

$$G(\omega) = i\frac{\mathrm{d}\log H}{\mathrm{d}\omega} = \frac{i}{H}\frac{\mathrm{d}H}{\mathrm{d}\omega} \tag{11}$$

with asymptotic form

$$\mathrm{Im}\ G \to -\frac{n+1}{\omega} \qquad \omega \to \pm\infty. \tag{12}$$

Now, the idea is to use Krein-Nudel'man to synthesize a function G. Then, by integration of (11), it turns out that we may obtain a function $H \in H^2$ that is zero-free in the closed lower half-plane. Note that this time, we have assumed the specific asymptotic condition (10), and not every $g \in \hat{L}^2(0, \infty)$ will correspond to a $G = \mathcal{F}g$ satisfying (12). Therefore, the results of Krein and Nudel'man are not always directly applicable to this case. To come around this problem, we can modify the synthesized G from Krein and Nudel'man for $|\omega|$ larger than a certain ω_B to obtain the asymptotic behavior (12) along the real axis. We must ensure that the new function is analytic in the lower half-plane, so we are only modifying the imaginary part of G to satisfy (12), and adjusting the real part accordingly,

$$\mathrm{Im}\ \tilde{G} = \mathrm{Im}\ G + \Delta, \qquad \mathrm{Re}\ \tilde{G} = -\mathcal{H}\mathrm{Im}\ \tilde{G}. \tag{13}$$

In (13), $\Delta \in L^2$ is the required modification function that is zero for $|\omega| < \omega_B$, and $\mathcal{H}$ denotes the Hilbert transform. The error we have introduced in this procedure is ‡

$$\text{Re } \tilde{G}(\omega) - \text{Re } G(\omega) = -(\mathcal{H}\Delta)(\omega) = \frac{1}{\pi} \int_{|\omega'|>\omega_B} \frac{\Delta(\omega')\mathrm{d}\omega'}{\omega - \omega'}, \tag{14}$$

and can therefore be made arbitrarily small in Ω by choosing ω_B large enough. Finally, we compute the minimum phase transfer function by using $\tilde{G}$ in (11). In practice, we integrate along the real axis choosing the origin as the starting point, and adjust a suitable multiplicative integration constant of H to satisfy the desired amplitude response in Ω. The integral $\int_0^\omega -i\tilde{G}(\omega')\mathrm{d}\omega'$ is well-defined for any point ω in the closed lower half-plane. Moreover, the integral as a function of ω is clearly analytic in the lower half-plane, and hence its real and imaginary parts are harmonic conjugate functions. Since $\log|H|$ gets the asymptotic behavior (10), it follows that $H \in L^2$, and also that

$$\int_{-\infty}^{\infty} \frac{\log|H(\omega)|}{1+\omega^2}\mathrm{d}\omega > -\infty. \tag{15}$$

Therefore, H must belong to H^2 [13]. In addition, since the integral $\int_0^\omega -i\tilde{G}(\omega')\mathrm{d}\omega'$ is finite for finite ω in the closed lower half-plane, H is zero-free there. The Hermitian property of $\tilde{G}$ translates into the same property of H, $H(-\omega) = \overline{H(\omega)}$. The function H is therefore realizable as a minimum phase transfer function of the class with $a = 0$. Note that in this case, it is not necessary to restrict the goal function F to be continuous or Lipschitz because any function $\tilde{G} \in H^2$ with the right asymptotic behavior (12) yields by (11) a function H in L^2. Also note that we have no control of the energy of $H - a = H$ in this case, the filter is rather optimized for small energy of G.

3. Numerical algorithm and examples

In this section, we solve the integral equation (8) numerically and apply the algorithm to the synthesis of different minimum phase filters. To the best of the author's knowledge, the integral equation of Krein-Nudel'man has not been solved numerically previously. First, we must transform equation (8) in a way that is suitable for discretization and numerical implementation. By extrapolating (8) to the whole t-axis and Fourier transforming, we see that the extrapolated solution g_e is an entire function with the representation [8]

$$g_e(t) = \frac{1}{2\pi} \int_{\hat{\Omega}} G_e(\omega) \exp(i\omega t)\mathrm{d}\omega, \qquad \hat{\Omega} = (-\omega_2, -\omega_1) \cup (\omega_1, \omega_2) \tag{16}$$

where

$$\mu G_e(\omega) + G(\omega) = F(\omega), \qquad \omega \in \Omega. \tag{17}$$

‡ Physically, this error corresponds to an error in the group delay or the derivative of the phase response.

This is realized from the fact that the integral terms in (8) correspond to the transmission of a signal $g(t)$ through an ideal filter with pass band Ω. G is the causal version of G_e, that is

$$G(\omega) = \int_0^\infty \exp(-i\omega t)g_e(t)\mathrm{d}t = \frac{1}{2\pi}\int_0^\infty \exp(-i\omega t)\int_{\hat{\Omega}}\exp(i\omega' t)G_e(\omega')\mathrm{d}\omega'\mathrm{d}t \qquad (18)$$

We can therefore connect G and G_e through the following Hilbert transform relation

$$G(\omega) = \frac{1}{2}G_e(\omega) - \frac{1}{2\pi i}\int_{\hat{\Omega}}\frac{G_e(\omega')\mathrm{d}\omega'}{\omega' - \omega}, \qquad \omega \in \Omega. \qquad (19)$$

The integral is taken in the principal value sense. Note that (19) can be extrapolated to the entire ω axis provided that $G_e(\omega)$ is set equal to zero outside $\hat{\Omega}$. By substituting the expression above into (17), we obtain [8]

$$\left(\mu + \frac{1}{2}\right)G_e(\omega) - \frac{1}{2\pi i}\int_{\hat{\Omega}}\frac{G_e(\omega')\mathrm{d}\omega'}{\omega' - \omega} = F(\omega), \qquad \omega \in \Omega. \qquad (20)$$

Our goal is to solve (20) and then substitute the resulting G_e into (19) yielding the solution G. In fact, an explicit solution to (20) is given in [8], see (A.2) in the present document. However, this expression is not suitable for numerical calculations due to the fast oscillating exponential expressions. Therefore, we will instead discretize (20) directly. The truncated Hilbert integral operator in (20) is linear so its discrete counterpart can be represented as a matrix. Therefore, the equation can be solved numerically by a simple matrix inversion. Once G_e is found, G can be calculated from (19) using a discrete Hilbert transform.

By representing G_e and F as vectors of samples in the interval Ω, the discrete approximation of (20) becomes

$$\left(\mu + \frac{1}{2}\right)\mathbf{G}_e - \frac{1}{2i}\left(\mathbf{H}_-\overline{\mathbf{G}}_e + \mathbf{H}\mathbf{G}_e\right) = \mathbf{F}, \qquad (21)$$

where $\mathbf{H}_-\overline{\mathbf{G}}_e$ and $\mathbf{H}\mathbf{G}_e$ corresponds to the Hilbert transform integral of G_e in $(-\omega_2, -\omega_1)$ and (ω_1, ω_2), respectively. First, we will treat the case when ω_1 is considerably larger than zero, that is when the term $\mathbf{H}_-\overline{\mathbf{G}}_e$ is negligible. Later, we will show how to deal with the problem when ω_1 is or is near to zero.

The matrix $\mathbf{H}$ corresponds to integration of a singular integrand. The most common way to perform such a Hilbert transform numerically is to use Fast Fourier Transforms (FFT). Therefore, we can use the expression for the discrete Fourier transform to obtain the matrix $\mathbf{H}$. By comparing (18) and (19) we obtain the relation

$$-\frac{1}{2\pi i}\int_\Omega\frac{G_e(\omega')\mathrm{d}\omega'}{\omega' - \omega} = \frac{1}{2\pi}\int_{-\infty}^\infty \exp(-i\omega t)\left(u(t) - \frac{1}{2}\right)\int_\Omega\exp(i\omega' t)G_e(\omega')\mathrm{d}\omega'\mathrm{d}t \qquad (22)$$

where $u(t)$ is the unit step function. The discrete counterpart of (22) is

$$(\mathbf{H}\mathbf{G}_e)(m) = \frac{i}{N}\sum_{n=1}^N\sum_{k=-\frac{N-1}{2}}^{\frac{N-1}{2}}\mathrm{sgn}(k)G_e(n)\exp[i2\pi k(n-m)/N], \qquad (23)$$

where

$$\text{sgn}(k) = \begin{cases} -1 & \text{for } k < 0 \\ 0 & \text{for } k = 0 \\ 1 & \text{for } k > 0 \end{cases} . \tag{24}$$

In (23) $m \in \{1, 2, \ldots, N\}$, and we have for simplicity assumed that N is an odd number. When discretizing (22), G_e becomes periodical, so in order to limit the resulting errors, we imagine that $\mathbf{G}_e$ is padded with so many zeros that the contribution from the repeated spectra is eliminated. In practice, this means that the number N is increased from the number of samples of F, and that we are only using a certain inner square of the Hilbert transform matrix $\mathbf{H}$ below. That is we effectively pad $\mathbf{G}_e$ with N_z zeros on each side by setting the Hilbert transform matrix in (21) equal to

$$(\mathbf{H})(m, n) = \frac{i}{N} \sum_{k=-\frac{N-1}{2}}^{\frac{N-1}{2}} \text{sgn}(k) \exp[i2\pi k(n-m)/N] \tag{25}$$

$$\text{for } m, n \in \{N_z, N_z + 1, \ldots, N_z + N_F\},$$

where N_F is the number of samples of F and $N = N_F + 2N_z$. It is convenient to use the number N_z that corresponds to the extra bandwidth for which we want to calculate $G(\omega)$ on each side of Ω. Now, we can solve (21) by inverting the matrix $(2\mu+1)\mathbf{I} - \mathbf{H}/i$, which has the dimension $N_F \times N_F$. The (discrete) Hilbert transform is energy conserving, $\|\mathbf{u}\| = \|\mathbf{v}\|$ in the l^2-norm, for any Hilbert transform pair $\{\mathbf{u}, \mathbf{v}\}$ with zero mean value. Thus the truncated Hilbert operator (25) will satisfy

$$\|\mathbf{H}\|/(2\mu + 1) < 1, \qquad \mu > 0. \tag{26}$$

Therefore, the matrix $(2\mu+1)\mathbf{I} - \mathbf{H}/i$ is guaranteed invertible [14]. Once we have found $\mathbf{G}_e$, $\mathbf{G}$ is computed from a discrete Hilbert transform of a zeropadded version of $\mathbf{G}_e$, according to (19). To sum up, the algorithm goes as the following:

(i) Pick a $\mu > 0$.

(ii) Solve (21) for the desired F by matrix inversion.

(iii) Calculate $\mathbf{G}$ by a Hilbert transform of $\mathbf{G_e}$ padded with zeros outside Ω (discrete version of (19)).

(iv) Compute ϵ as the rms error of the elements of $\mathbf{F} - \mathbf{G}$ (discrete version of (6)).

(v) If ϵ is not small enough, pick a smaller μ and return to ii.

As the chosen μ is getting smaller, the error ϵ is decreasing and $\|\mathbf{G}\|$ is growing. Usually, this means that the transfer function is getting more difficult to realize. At a certain point, the error is not decreasing further due to finite bandwidth in the calculations. This bandwidth can be increased by increasing N_z in (25) and padding $\mathbf{G}_e$ with more zeros in step iii. Finally, it is not possible to get any less error due to the quantization errors in the computer.

The Hilbert transform in step iii is computed using FFT, so the algorithm scales with the total bandwidth as $\mathcal{O}(N_z \log N_z)$. Note that the computation time of (25)

scales only linearly with N_z. Owing to the matrix inversion involved, we also observe that the algorithm scales with the resolution in Ω as $\mathcal{O}(N_F^3)$.

When $\omega_1 = 0$, we can use the same procedure as the one described above simply by redefining Ω to the interval $(-\omega_2, \omega_2)$. If ω_1 is near zero however, we must take the term $\mathbf{H\_\overline{G}}_e$ into account. This term is trivial, since it corresponds to a simple integration of a non-singular integrand. The integrand is found from the Hermitian property of G_e, and the integration may for example be performed using the trapezoidal formula. By splitting (21) into the real and imaginary parts, it is possible to invert the equations in a similar way as we did in the situation above.

3.1. Reconstruction of a Hilbert transform pair

In the first example, we define a Hilbert transform pair $\{u, v\}$ by

$$u(\omega) = \begin{cases} (\omega - \omega_0)/2\omega_w & \text{for } |\omega - \omega_0| < \omega_w \\ 0 & \text{for } |\omega - \omega_0| \geq \omega_w \end{cases}, \tag{27}$$

where $2\omega_w$ is the window size of Ω, and ω_0 is the middle frequency. For simplicity we assume that $\omega_0 >> \omega_w$ so the negative frequencies can be ignored in (20) or (21). The function v is found from a Hilbert transform of u defined in (27). Now, we set $G = u + iv$ and apply $F = G$ for $\omega \in \Omega$ to the algorithm to see how well the function G is reconstructed outside Ω. The results are showed in figure 1. We observe that the produced solution for $\mu = 1$ has less norm than the original, as expected. For μ less than about 0.1, the reconstructed and original G is virtually identical. In figure 2 the dependence of the rms error is shown for 10 different values of μ. The figure shows the expected behavior; the error decreases with decreasing μ until a certain point where the finite bandwidth and/or quantization error is dominating. The bandwidth in the simulation is $14\omega_w$. By increasing this bandwidth, it is possible to get considerably less rms error.

3.2. All-pass filter with cubic phase response, $a = 1$

First, we will try to design a minimum phase filter of the category with $a = 1$. This category corresponds to typical transmission filters, e.g. optical transmission filters. The logarithm of the transfer function shall be as near as possible to

$$F(\omega) = 0 - i \left(\frac{\omega - \omega_0}{\omega_w}\right)^3 \tag{28}$$

in Ω, that is for $|\omega - \omega_0| < \omega_w$. Note that F is defined for negative frequencies by the Hermitian relation $F(-\omega) = \overline{F(\omega)}$. Again, we assume that $\omega_0 >> \omega_w$ so that the negative frequencies can be ignored in (20) or (21). Eq. (28) corresponds to a filter with a flat pass band of unity transmission and a cubic phase response. $F(\omega)$ is not approaching zero at the edges of Ω, and we should therefore extend Ω with a smooth termination of $F(\omega)$. However, according to the discussion in the Appendix, this procedure is sufficient but not necessary, and in numerical calculations we might
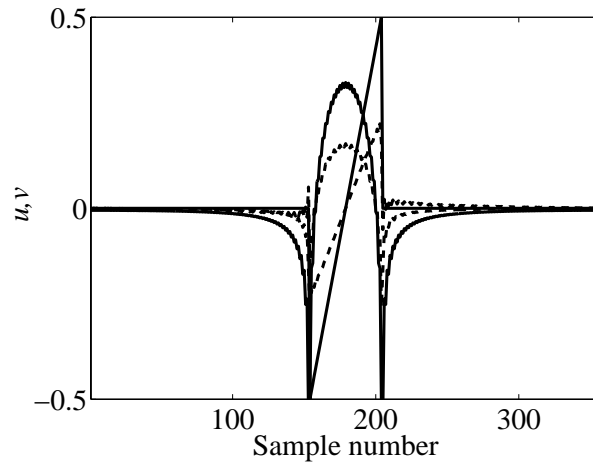
Figure 1. Real and imaginary part of the original G (solid curves) and reconstructed G (dashed curves) using $\mu = 1$. The reconstructed G for μ less than about 0.1 is virtually identical to the original.
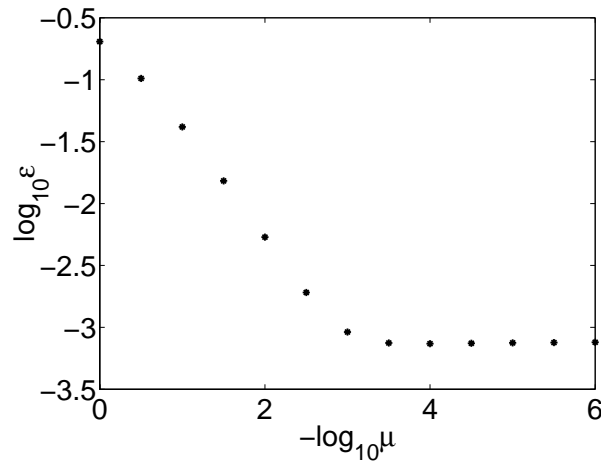
Figure 2. Rms error inside Ω for different values of μ.

omit it. If the produced transfer function has no singularities, then it was acceptable to use the discontinuous F.

By applying the expression for F to our algorithm we get the responses given in figure 3 and 4. The results are shown for $\mu = 10^{-3}$ and a simulation bandwidth of $40\omega_w$. The corresponding rms error is approximately 0.06, and we observe a small ripple in the amplitude response in Ω. This ripple/error will decrease if μ is decreased, but $\|G\|$ will increase correspondingly, making the filter harder to realize.

3.3. Filter with flat pass band and quadratic group delay response, $a = 0$

We will also try to design a similar filter as the above, but of the category with $a = 0$. For a flat pass band and a quadratic group delay response (cubic phase response as
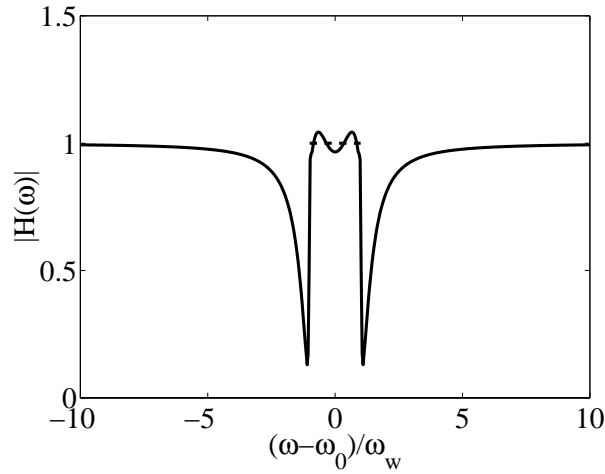
Figure 3. Amplitude response $|H(\omega)|$ of the designed filter with cubic phase response and flat pass band. The asymptotic value $a = 1$. The dashed curve shows the desired response as defined within a limited range.
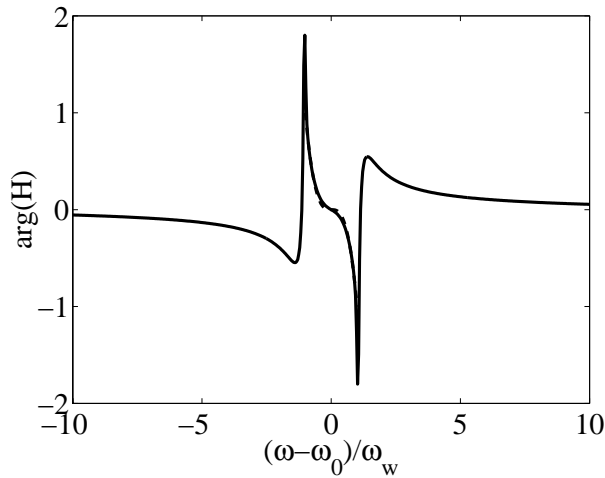
Figure 4. Phase response $\arg H(\omega)$ of the designed filter with cubic phase response and flat pass band. The dashed curve shows the desired response.

above), the goal function F must according to (11) be set to

$$F(\omega) = i0 - \left(\frac{\omega - \omega_0}{\omega_w}\right)^2 \tag{29}$$

for $|\omega - \omega_0| < \omega_w$. By applying (29) to the algorithm, we obtain G. In this case, G turns out to have approximately the right asymptotic behavior, so only a small Δ is required. The resulting spectra for $\mu = 10^{-4}$ are shown in figure 5 and 6, and shows relatively small errors. The rms error is approximately 0.09 in Ω.

If we would like to design a filter of the class $a = 0$ with a similar goal function as (29), but with opposite sign, the resulting asymptotic behavior would be far from the desired. Although the modification method described in Section 2 would fix this
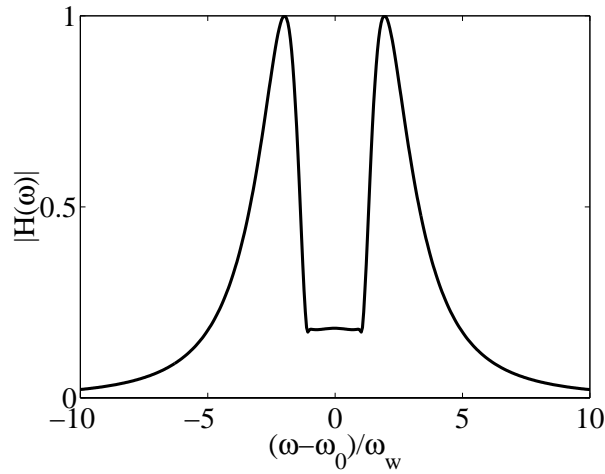
Figure 5. Amplitude response $|H(\omega)|$ of the designed filter with quadratic group delay and flat pass band. The asymptotic value $a = 0$.
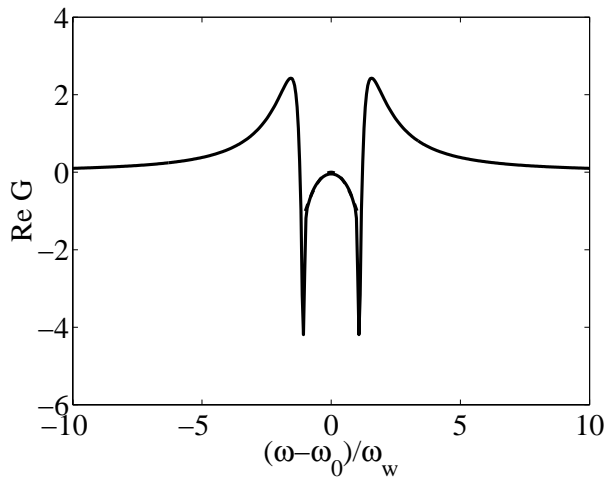
Figure 6. Re $\tilde{G}$, the derivative of the negative phase response, that is the negative group delay of the designed filter ($a = 0$). The dashed curve shows the desired response.

behavior, this synthesis method is not always appropriate in practice, as the filter energy may be very large in such cases. Note that this disadvantage only applies for the filters of the $a = 0$ class.

4. Conclusion

We have proposed a method for synthesis of minimum phase filters with desired complex transfer functions inside a limited bandwidth window. The method is general and straightforward in the case of asymptotic value $a \neq 0$. For $a = 0$, the method is suitable for a restricted class of filter responses. A numerical solution technique is given and applied for the synthesis of specific filters of both classes.

Acknowledgments

Appendix A.

A minimum phase transfer function of the class with $a \neq 0$ is found from the transfer function G by the formula

$$H(\omega) = a \exp[G(\omega)]. \tag{A.1}$$

The function G is the solution of Krein-Nudel'man's problem of finding a transfer function (in H^2) approximating a desired $F \in L^2(\omega_1, \omega_2)$ with a certain precision parameter μ. Here we will show that the function $H_{L^2}(\omega) = H(\omega) - a$, where H is given in (A.1), satisfies the Titchmarsh theorem, $H_{L^2} \in H^2$, if F satisfies the Lipschitz condition [9] and vanishes as $\omega \to \omega_1$ and $\omega \to \omega_2$. This condition is sufficient but not necessary.

First we must ensure that $H_{L^2} \in L^2(-\infty, \infty)$. We recall that $G \in L^2(-\infty, \infty)$, and that G essentially is a Hilbert transform of a function G_e of finite support (19). Define $\tilde{\Omega}$ as $\tilde{\Omega} = (-\omega_2 - \epsilon, -\omega_1 + \epsilon) \cup (\omega_1 - \epsilon, \omega_2 + \epsilon)$ for a small $\epsilon > 0$. Then, G is bounded for real $\omega \notin \tilde{\Omega}$. So provided that G does not have singularities in $\tilde{\Omega}$, H_{L_2} must belong to $L^2(-\infty, \infty)$. To analyze the behavior in $\tilde{\Omega}$, we need information on the form of G_e. As in ref. [8], we assume with no loss of generality that $\Omega = (0, 1)$, that is $\tilde{\Omega} = (-1 - \epsilon, 1 + \epsilon)$. Krein and Nudel'man gives a formula for G_e in this case which can be written as

$$G_e(\omega) = \frac{1 + 1/2\mu}{1 + \mu} F(\omega) + iB \exp\left[iA \ln \frac{1 + \omega}{1 - \omega}\right] \int_{-1}^{1} \frac{F(\nu)}{\nu - \omega} \exp\left[-iA \ln \frac{1 + \nu}{1 - \nu}\right] d\nu, \tag{A.2}$$
$$-1 < \omega < 1.$$

In (A.2) A and B are real constants that depend on μ, and F is defined for negative ω by the Hermitian relation $F(-\omega) = \overline{F(\omega)}$. Now we take a truncated Hilbert transform of (A.2) on the interval $(-1, 1)$ and look for singularities. If we assume that F approaches zero as $\omega \to \pm 1$ and satisfies the Lipschitz condition of order α, the Hilbert transform of the first term in (A.2) will be bounded [9]. The Hilbert transform of the second term needs a more thorough examination around $\omega = \pm 1$. We note that the integral in (A.2) equals the Hilbert transform of a function $F(\nu) \exp\left[-iA \ln \frac{1+\nu}{1-\nu}\right]$. It is straightforward to show that this product adopts the Lipschitz property from $F(\nu)$, and consequently the Hilbert transform of this expression will be bounded and also satisfy the Lipschitz condition of order α. Therefore, we consider the integral

$$I(\omega) = \int_{-1}^{1} B(x) \exp\left[iA \ln \frac{1 + x}{1 - x}\right] \frac{dx}{\omega - x}, \tag{A.3}$$

where $B(x)$ is a bounded Lipschitz function. Eq. (A.3) can be transformed by the substitution $\xi = \ln[(1+x)/(1-x)]$ to

$$I(\omega) = \int_{-\infty}^{\infty} \frac{2\beta(\xi)e^{\xi}e^{iA\xi}\mathrm{d}\xi}{(e^{\xi}+1)[(e^{\xi}+1)\omega - e^{\xi}+1]} = \int_{-\infty}^{\infty} \frac{2\beta(\xi)e^{\xi}e^{iA\xi}\mathrm{d}\xi}{(e^{\xi}+1)[2+\epsilon+\epsilon e^{\xi}]}, \tag{A.4}$$

where $\beta(\xi) = B((e^{\xi}-1)/(e^{\xi}+1))$ and we have set $\omega = 1+\epsilon$, $\epsilon > 0$ in the last expression. We observe that $\beta(\xi)$ is bounded and that $\beta(\xi) \to B(\pm 1)$ as $\xi \to \pm\infty$. The integral from $-\infty$ to 0 is therefore bounded, so we consider only the integral

$$\left| \int_{0}^{\infty} \frac{2\beta(\xi)(e^{\xi}+1-1)e^{iA\xi}\mathrm{d}\xi}{(e^{\xi}+1)[2+\epsilon+\epsilon e^{\xi}]} \right|$$

$$\leq \left| \int_{0}^{\infty} \frac{2\beta(\xi)e^{iA\xi}\mathrm{d}\xi}{(e^{\xi}+1)[2+\epsilon+\epsilon e^{\xi}]} \right| + \left| \int_{0}^{\ln 1/\epsilon} \frac{2\beta(\xi)e^{iA\xi}\mathrm{d}\xi}{2+\epsilon+\epsilon e^{\xi}} \right| + \left| \int_{\ln 1/\epsilon}^{\infty} \frac{2\beta(\xi)e^{iA\xi}\mathrm{d}\xi}{2+\epsilon+\epsilon e^{\xi}} \right|, \tag{A.5}$$

We realize that the first and the last integral in the right-hand side of (A.5) are bounded as $\epsilon \downarrow 0$, and the other satisfies

$$\left| \int_{0}^{\ln 1/\epsilon} \frac{(2+\epsilon+\epsilon e^{\xi}-\epsilon-\epsilon e^{\xi})\beta(\xi)e^{iA\xi}\mathrm{d}\xi}{2+\epsilon+\epsilon e^{\xi}} \right|$$

$$\leq \left| \int_{0}^{\ln 1/\epsilon} \beta(\xi)e^{iA\xi}\mathrm{d}\xi \right| + \int_{0}^{\ln 1/\epsilon} \frac{(\epsilon+\epsilon e^{\xi})\,|\beta(\xi)|\,\mathrm{d}\xi}{2}, \tag{A.6}$$

where the last integral is clearly bounded. The first integral is also bounded as can be realized by setting $\beta(\xi) = \beta(\infty) + \beta(\xi) - \beta(\infty)$ and noting that $|\beta(\xi) - \beta(\infty)| = |B(\omega) - B(1)| \leq C|(e^{\xi}-1)/(e^{\xi}+1) - 1|^{\alpha} < 2Ce^{-\alpha\xi}$ by the Lipschitz condition on B, where C is a constant and $0 < \alpha < 1$. Hence $I(\omega)$ is bounded as $\omega \downarrow 1$. Next we make the substitution $\epsilon \to -\epsilon$ into (A.4), and split the integral into four parts

$$I(1-\epsilon) = \int_{-\infty}^{\infty} \frac{2\beta(\xi)e^{\xi}e^{iA\xi}\mathrm{d}\xi}{(e^{\xi}+1)[2-\epsilon-\epsilon e^{\xi}]} = \int_{-\infty}^{0} + \int_{0}^{\ln 1/\epsilon} + \int_{\ln 1/\epsilon}^{\ln 3/\epsilon} + \int_{\ln 3/\epsilon}^{\infty}. \tag{A.7}$$

By a similar argument as above, we find that the first, second and fourth integral in the right-hand side of (A.7) are bounded. Using the substitution $\tau = e^{\xi}$ we find that the third integral is (Cauchy principal value)

$$\int_{1/\epsilon}^{3/\epsilon} \frac{u(\tau)}{2-\epsilon-\epsilon\tau}\mathrm{d}\tau, \qquad u(\tau) = 2B\left(\frac{\tau-1}{\tau+1}\right)\gamma(\tau), \qquad \gamma(\tau) = \frac{e^{iA\ln\tau}}{\tau+1}. \tag{A.8}$$

By differentiation of γ and using the Lipschitz condition on B, we get $|u(\tau+\Delta\tau)-u(\tau)| \leq C_1\epsilon^2|\Delta\tau| + C_2\epsilon^{1+2\alpha}|\Delta\tau|^{\alpha}$ for ϵ sufficiently small. Thus the integral in (A.8) is bounded as $\epsilon \downarrow 0$. From the symmetry of (A.3) it is then clear that $I(\omega)$ is bounded as $\omega \to \pm 1$, and we can conclude that G is bounded in $\tilde{\Omega}$. Hence we have shown that both G and H_{L^2} belong to $L^2(-\infty,\infty) \cap L^{\infty}(-\infty,\infty)$.

Finally, we must check the behavior of H_{L^2} in the lower half-plane. Since G is analytic here, H_{L^2} is analytic as well, and approaches zero as $\omega \to \infty$. Like G, it must also satisfy the square integrable condition (4). Hence H_{L^2} satisfies the Titchmarsh theorem, and $H_{L^2} \in H_2$. It is also zero-free in the closed lower half-plane since G is bounded there.

References

[1] Members of the Technical Staff 1982 *Transmission systems for communications* (Bell Telephone Laboratories, New Jersey)

[2] Tikhonravov A V 1993 Some theoretical aspects of thin-film optics and their applications *Appl. Opt.* **32** 5417-5426

[3] Brinkmeyer E 1995 Simple algorithm for reconstructing fiber grating from reflectometric data *Opt. Lett.* **20** 810-812

[4] Poladian L 1997 Group-delay reconstruction for fiber Bragg gratings in reflection and transmission *Opt. Lett.* bf 22 1571-1573

[5] Lenz G, Eggleton B J, Giles C R, Madsen C K, Slusher R E 1998 Dispersive properties of optical filters for WDM systems *IEEE J. Quant. El.* **34** 1390-1402

[6] Aizenberg L 1993 *Carleman's formulas in complex analysis* (Kluwer Academic Publishers, The Netherlands)

[7] Krein M G and Nudel'man P Ya 1973 On some new problems for Hardy class functions and continuous families of functions with double orthogonality *Dokl. Akad. Nauk SSSR* **206** 537-540

[8] Krein M G and Nudel'man P Ya 1975 Approximation of functions by minimum-energy transfer functions of linear systems *Problemy Peredachi Informatsii* **11** 37-60

[9] Titchmarsh, E C 1948, *Introduction to the theory of Fourier integrals* (Oxford University Press, Oxford), Theorem 95 and 106

[10] Klibanov V, Sacks P E, and Tikhonravov A V 1995 The phase retrieval problem *Inv. Probl.* **11** 1-28

[11] Nussenzveig M 1972 *Causality and dispersion relations* (Academic Press, New York)

[12] Papoulis A 1962, Chapter 10 *The Fourier integral and its applications* (McGraw-Hill, New York)

[13] Garnett J B 1981, Chapter 2 *Bounded analytic functions* (Academic Press, New York)

[14] Young N 1988 *An introduction to Hilbert space* (Cambridge University Press, UK) p 73

4.2 Synthesis of fiber Bragg gratings for use in transmission

Author: Johannes Skaar

Synthesis of fiber Bragg gratings for use in transmission

Johannes Skaar

Department of Physical Electronics, Norwegian University
of Science and Technology (NTNU), N-7491 Trondheim,
Norway

johannes.skaar@fysel.ntnu.no

 A method for designing fiber Bragg gratings with desired complex transmission coefficients is proposed. The transmission coefficient of a fiber grating satisfies the minimum phase condition when ignoring the linear phase from the pure propagation. Therefore, only a finite bandwidth is considered for the synthesis. The algorithm is based on a result of Krein and Nudel'man [Problemy Peredachi Informatsii 11, 37-60 1975]. A numerical algorithm is developed and by numerical examples it is demonstrated that it is possible to realize gratings with specified complex transmission responses inside the considered bandwidth. The method is also applicable for thin-film filters. © 2000 Optical Society of America

OCIS codes: 050.2770, 060.2340

1.   Introduction

Fiber Bragg gratings have become very useful components for realizing complex optical filter functions.[1,2] By using inverse scattering design methods an arbitrary complex filter function can be approximated by the reflection spectrum of the grating. Synthesis of such reflection filters consists in determining the grating strength and grating period as a function of position to obtain the desired, complex spectrum.[3] In some applications however, there are several reasons for rather using the fiber grating in transmission. When the grating is operating in transmission the complexity and cost of the system are reduced as it is not required to use a coupler or a circulator. In addition the phase response in transmission is often more robust to imperfections in the grating structure compared to the phase response in reflection.[4] In some applications, as for example Wavelength Division Multiplexing (WDM), one uses the grating both in reflection and transmission at the same time, and it is therefore desirable to get a better understanding of how one can obtain a certain complex transmission coefficient. Unfortunately, it is much harder to realize a given complex filter function in transmission.

The reduced flexibility compared to the reflection spectrum is due to the fact that the transmission coefficient will satisfy the minimum phase condition when ignoring the linear phase associated with the pure propagation through the grating.[5–7] Thus, there is a unique relation between the amplitude and phase response in transmission, which strongly limits what is possible to realize. In addition, the synthesis problem will not be unique as opposed to the situation in reflection. This ambiguity arises because a grating with a given reflection amplitude response will correspond to the same complex transmission coefficient, no matter what the reflection phase response is. For example, if we reverse a fiber grating, the complex transmission coefficient will remain the same, whereas the complex reflection spectrum or grating structure of course are different in the case of an asymmetric grating.

The use of fiber gratings in transmission has been discussed in several papers. Ouellette[8] studied theoretically the use of uniform Bragg gratings for dispersion compensation using the highly dispersive regions near the band edge of the grating. Later, dispersion compensation using uniform gratings was demonstrated both experimentally and numerically by Eggleton et.al.[9] and Litchinitser et.al.[10] The performance of the pulse compression was improved by use of apodized gratings.[10] Furthermore, Hinton[4] analyzed the transmission performance for dispersion compensation near the band edge of a couple of different apodization functions.

Dispersion compensation using fiber gratings in transmission is an example of a situation where one wants a certain amplitude and phase response inside a limited bandwidth. The desired amplitude response is in this case flat, whereas the desired phase response is quadratic in the same area (linear group delay). The purpose of this paper is to find a general method for obtaining a grating profile (apodization and chirp profile or complex coupling coefficient) to approximate any desired complex transmission spectrum. Since it is generally impossible to realize an arbitrary complex transmission coefficient for all frequencies, we limit our bandwidth of consideration to a finite interval, say $\Omega = (\omega_1, \omega_2)$, where $0 < \omega_1 < \omega_2 < \infty$. That is we want to obtain a desired transmission coefficient $H(\omega)$ for $\omega \in \Omega$, leaving the response for $\omega \notin \Omega$ unspecified.[11] By using a fast and simple algorithm, we demonstrate that we can obtain a function $H(\omega)$ which approximates the desired complex spectrum in Ω, and also satisfies the required minimum phase condition due to its behavior outside Ω. The algorithm is based on a theory by Krein and Nudel'man on approximation of $L^2(\omega_1, \omega_2)$ functions by Hardy class functions.[12,13] H may be synthesized as a fiber grating by synthesizing a filter with reflectivity $R(\omega) = 1 - |H(\omega)|^2$ and arbitrary reflection phase response, for example linear phase or minimum/maximum phase.

This paper is organized as follows: In Section 2 the minimum phase condition on the transmission coefficient is reviewed. In Section 3 the synthesis problem is stated, and we apply the theory of Krein and Nudel'man to a derived function of H, and show that the produced transfer function can be made realizable as a transmission coefficient of a fiber grating. In Section 4 the numerical algorithm is described in detail, and it is applied to three examples in Section 5. The first example deals with reconstruction (extrapolation) of a transfer function from data inside a limited bandwidth, and the next two examples present designs of second and third order dispersion compensating filters.

2. Minimum phase and the transmission coefficient of fiber gratings

The transmission coefficient $H(\omega)$ of a fiber grating satisfies the minimum phase condition when ignoring the linear phase response from the pure propagation.[5–7] Mathematically, the minimum phase condition states that all the zeros of H is located in the upper half of the complex ω plane. Physically, the minimum phase condition means that the filter with the given amplitude response has the least possible phase response and group delay for all frequencies. The amplitude and minimum phase response are uniquely related by means of logarithmic Hilbert transform relations. The form of the relations may differ, depending on the asymptotic behavior of H as $\omega \to \infty$. In addition, there is a variety of equivalent relations for the same class of filters.[14–16]

Consider the transfer function $H(\omega)$. If we set the input and output reference planes to the same position, the transmission coefficient will equal the Fourier transform of an impulse response $h(t)$ which vanishes for $t < 0$ (causality)

$$H(\omega) = (\mathcal{F}h)(\omega) = \int_0^\infty h(t)\exp(-i\omega t)dt, \tag{1}$$

where $\mathcal{F}$ is the Fourier transform operator. The impulse response has a Dirac's delta component in the origin

$$h(t) = \delta(t) + h_{L^2}(t). \tag{2}$$

In Eq. (2), h_{L^2} is a real, square integrable function ($h_{L^2} \in L^2(0,\infty)$). Similarly, we define H_{L^2} as the Fourier transform of h_{L^2}, $H_{L^2} = \mathcal{F}h_{L^2}$, so

$$H(\omega) = H_{L^2}(\omega) + 1. \tag{3}$$

We observe that the asymptotic value of the transmission coefficient is

$$H(\omega) \to 1, \qquad \omega \to \infty. \tag{4}$$

Physically, this behavior makes sense since the optical wave is not altered by the passive grating outside a certain bandwidth. Due to the causality ($h_{L^2}(t) = 0$ for $t < 0$) the real and imaginary parts of H_{L^2} form a Hilbert transform pair by the Titchmarsh theorem (see e.g.[17]). The causality condition is also equivalent to the condition that H_{L^2} is analytic in the lower half-plane and $\int_{-\infty}^\infty |H_{L^2}(\omega)|^2 d\omega < c$ for some number c along any line parallel to the real axis, uniformly in the closed lower half-plane.

In order to examine the relation between the amplitude and phase response, we study the function

$$\tilde{H}(\omega) = \ln[H(\omega)]. \tag{5}$$

The transmission coefficient H of a fiber grating is a minimum phase function, and consequently it is zero-free in the closed lower half-plane. Hence $\tilde{H}$ is analytic in the lower half-plane. Moreover, $\int_{-\infty}^\infty |\tilde{H}(\omega)|^2 d\omega < c$ for some number c along any line parallel to the real axis, uniformly in the closed lower half-plane. The integrability is realized from the corresponding integrability of H_{L^2} and because there is an $\epsilon > 0$ such that $|H(\omega)| \geq \epsilon$ uniformly in the closed lower half-plane. Then, the Titchmarsh theorem is applicable for $\tilde{H}$, which

means that the real and imaginary parts of $\tilde{H}$ form a Hilbert transform pair. The modulus and phase of H are therefore uniquely related by means of a logarithmic Hilbert transform

$$\arg H = \mathcal{H}\{\ln |H|\}, \qquad \arg H(\omega) = \frac{1}{\pi} \int_{-\infty}^{\infty} \frac{\ln |H(\omega')|}{\omega' - \omega} d\omega', \tag{6}$$

where $\mathcal{H}$ stands for the Hilbert transform operator, and the integral makes sense by means of the Cauchy principal value. Note that Eq. (6) is not necessarily valid if the asymptotic behavior were $H(\omega) \to 0$ for $\omega \to \infty$. In some of these cases however, a similar relation can be derived, provided that the behavior of $\ln H$ at infinity is sufficiently well controlled.[14, 16] Another solution would be to apply the Hilbert transform to the derivative of $\ln H$.[11]

3. Synthesis method

We recall that our problem is to find a transmission coefficient H that approximates a desired complex function H_{des} in Ω. This problem can now be divided into three parts: First we must find a minimum phase transfer function approximating a desired function in Ω. Then, if necessary, we must modify the resulting filter so that it is passive, $|H(\omega)| \leq 1$ for all real ω, and so that the asymptotic behavior is correct. Finally, we can design a grating with the resulting reflectivity $R(\omega) = 1 - |H(\omega)|^2$.

A first naive approach to the first problem would be to use an extrapolation technique for functions that are analytic in the lower half-plane. In fact, such extrapolation is unique if it exists, and can be found by the Carleman formula.[18] However, the existence condition on the transfer function data inside Ω is rather strict. Of course, the condition will be even stricter when the continuation to the lower half-plane must be zero-free. Therefore, it is more desirable to utilize a result by Krein and Nudel'man on approximation of the goal function given a desired precision. Their formulation is as follows:

Given a function $F \in L^2(\omega_1, \omega_2)$ and a number ϵ, $(0 < \epsilon \leq \|F\|)$, find a real $g \in L^2(0, \infty)$ having least norm $\|g\|$, and such that

$$\int_{\omega_1}^{\omega_2} |F(\omega) - G(\omega)|^2 d\omega \leq \epsilon^2, \tag{7}$$

where $G = \mathcal{F}g \in L^2(-\infty, \infty)$.

The unique solution g to this problem can be found from a certain integral equation,[13] and in Section 3 we show how to find the transfer function G numerically. In the rest of this section we simply assume that we have the solution to Krein-Nudel'man's problem at hand. As follows from the problem formulation, the resulting G will be analytic but not necessarily zero-free in the lower half-plane. A possible remedy is to apply Krein-Nudel'man to a certain branch of $F(\omega) = \ln[G_{des}(\omega)]$, and form the solution

$$H(\omega) = \exp[G(\omega)]. \tag{8}$$

Then H will be zero-free and analytic in the lower half-plane. Moreover, it is shown in ref[11] that $H - 1$ belongs to L^2 and satisfies the Titchmarsh theorem if F satisfies the Lipschitz condition and vanishes as $\omega \to \omega_1$ and $\omega \to \omega_2$. The condition that the goal function F must

vanish at the endpoints is not a further constraint as it can be fulfilled by extending the interval Ω with a smooth termination of F. The Lipschitz condition is certainly satisfied if F is once differentiable. When the problem is discretized, however, none of these conditions is important as the finite number of samples of F always can represent a continuous and differentiable function. By Eq. (8) and Krein-Nudel'man's result, we have now constructed a function with the desired properties.

One important point remains to be treated, namely what if the produced transfer function H is not passive? Indeed, we have no guarantee that $|H(\omega)| \leq 1$ with the method outlined above, so in many cases it is necessary to modify the transfer function. This modification is usually easier if we redefine Eq. (8). As an extra bonus with the following definition, F does not have to satisfy the Lipschitz condition or have to vanish at the endpoints; it is sufficient that $F \in L^2(\omega_1, \omega_2)$.

We will apply Krein-Nudel'man to the function

$$F(\omega) = i\frac{d}{d\omega}\ln[H_{des}(\omega)], \tag{9}$$

yielding a solution G. The corresponding transfer function solution is set equal to

$$H(\omega) = \exp[G_1(\omega)], \tag{10}$$

where G_1 is a modified version of the integral of $-iG$. We modify only the real part of the integral to satisfy Re $G_1 \leq 0$ for all (real) ω and Re $G_1 \to 0$ as $\omega \to \infty$, and adjust the imaginary part accordingly such that Im $G_1 = \mathcal{H}\{\text{Re } G_1\}$. To be more concrete we set the real and imaginary parts of G_1 equal to

$$\text{Re } G_1(\omega) = \begin{cases} \int^\omega \text{Im } G(\omega')d\omega' + C & \text{for } \left|\omega - \frac{\omega_1+\omega_2}{2}\right| \leq \omega_B \\ 0 & \text{for } \left|\omega - \frac{\omega_1+\omega_2}{2}\right| > \omega_B \end{cases}. \tag{11}$$

$$\text{Im } G_1(\omega) = \mathcal{H}\{\text{Re } G_1(\omega)\} \tag{12}$$

Here, ω_B is a bandwidth satisfying $\omega_B >> \omega_2 - \omega_1$ and C is chosen such that Re $G_1(\omega) \leq 0$. This modification procedure introduces an error in the imaginary part of $G_1(\omega)$ in the relevant bandwidth $\Omega = (\omega_1, \omega_2)$, and therefore in the group delay $-d \arg H/d\omega$ of the filter. By (9) it follows that the original, unmodified group delay is Re $G(\omega)$. Define $\omega_\pm = (\omega_1 + \omega_2)/2 \pm \omega_B$ and $G_\pm = \text{Re } G_1(\omega_\pm)$. The group delay error due to the above modification can then be written

$$-\frac{d}{d\omega}\text{Im } G_1(\omega) - \text{Re } G(\omega) = -\frac{d}{d\omega}\mathcal{H}\text{Re } G_1 + \mathcal{H}\text{Im } G = \mathcal{H}\{-\frac{d}{d\omega}\text{Re } G_1 + \text{Im } G\}$$

$$= \frac{1}{\pi}\int_{-\infty}^{\omega_-} \frac{\text{Im } G(\omega')d\omega'}{\omega' - \omega} + \frac{1}{\pi}\int_{\omega_+}^{\infty} \frac{\text{Im } G(\omega')d\omega'}{\omega' - \omega} - \frac{G_-}{\pi(\omega_- - \omega)} + \frac{G_+}{\pi(\omega_+ - \omega)}, \tag{13}$$

where we have interchanged the order of differentiation and Hilbert transformation. Since Im $G(\omega) \to 0$ as $\omega \to \infty$,[11] this error can be made arbitrarily small in Ω by choosing ω_B large enough. The last two terms result from the discontinuous points $\omega_\pm$, and can be

further reduced if $G_1(\omega)$ is made smoother around $\omega_\pm$. By the modification method we conclude that the resulting H satisfies $|H(\omega)| \leq 1$ and has the right asymptotic behavior $H(\omega) \to 1$. Moreover, it is by Eq. (10) zero-free and analytic in the lower half-plane. The analyticity is realized from the fact that the real and imaginary part of G_1 form a Hilbert transform pair, and consequently G_1 is analytic in the lower half-plane. The resulting transfer function H is therefore realizable as a transmission coefficient of a fiber grating (or a thin-film filter[19]). Note that according to Eq. (9), the goal function F contains the group delay and the derivative of the amplitude response. In other words it is the group delay and not the phase response which is matched to the desired response. This corresponds to the common practice of specifying dispersion in terms of group delay. The absolute level of the resulting amplitude response is determined by the bandwidth ω_B and the integration constant C.

From the above discussion we sum up the synthesis method in the following steps:

1. Find the solution G of Krein-Nudel'man's problem using the input function F defined by Eq. (9) and the algorithm described in the next section.

2. Use Eqs. (10) and (11) to determine the transmission coefficient $|H|$. The filter performance can be somewhat improved by smoothing the intermediate response $G_1(\omega)$ around $\omega = \omega_\pm$.

3. Synthesize a fiber grating with reflectivity $R(\omega) = 1 - |H(\omega)|^2$ and for example linear phase response. Fiber grating synthesis is fast and conveniently performed by use of a layer-peeling inverse scattering algorithm.[3,20]

4. Numerical algorithm

In this section, we present a numerical algorithm for solving Krein-Nudel'man's problem. It can be shown that the solution G can be found from the integral equation[11,13]

$$\left(\mu + \frac{1}{2}\right) G_e(\omega) - \frac{1}{2\pi i} \int_{\hat{\Omega}} \frac{G_e(\omega')d\omega'}{\omega' - \omega} = F(\omega), \qquad \omega \in \Omega. \tag{14}$$

where G_e is a noncausal version of G, that is

$$G(\omega) = \frac{1}{2\pi} \int_0^\infty \exp(-i\omega t) \int_{\hat{\Omega}} \exp(i\omega' t) G_e(\omega') d\omega' dt \tag{15}$$

or equivalently

$$G(\omega) = \frac{1}{2} G_e(\omega) - \frac{1}{2\pi i} \int_{\hat{\Omega}} \frac{G_e(\omega')d\omega'}{\omega' - \omega}, \qquad \omega \in \Omega. \tag{16}$$

The integrals in Eqs. (14) and (16) are taken in the principal value sense. The interval of integration is $\hat{\Omega} = (-\omega_2, -\omega_1) \cup (\omega_1, \omega_2)$, but for optical filters, the center frequency is many orders of magnitude larger than the typical bandwidth, and consequently we can ignore the negative frequencies in the Hilbert integral, i.e. set $\hat{\Omega} = \Omega$. Furthermore, $\mu = \mu(\epsilon)$ is some positive function of ϵ; it is dependent on F and is decreasing monotonically to zero as $\epsilon \to 0^+$.[12,13] It is not necessary to have this function at hand; we can instead use μ as the precision parameter.

The truncated Hilbert integral operator in (14) is linear so its discrete counterpart can be represented as a matrix. Therefore, the equation can be solved numerically by a simple matrix inversion. Once G_e is found, G can be calculated from (16). Note that (16) can be extrapolated to the entire ω axis provided that $G_e(\omega)$ is set equal to zero outside $\hat{\Omega}$. By representing G_e and F as vectors of samples in the interval Ω, the discrete approximation of (14) becomes

$$\left(\mu + \frac{1}{2}\right) \mathbf{G}_e - \frac{1}{2i} \mathbf{H} \mathbf{G}_e = \mathbf{F}, \tag{17}$$

where $\mathbf{HG}_e$ corresponds to the Hilbert transform integral of G_e in (ω_1, ω_2). The matrix $\mathbf{H}$ corresponds to integration of a singular integrand. The most common way to perform such a Hilbert transform numerically is to use Fast Fourier Transforms (FFT). Therefore, we can use the expression for the discrete Fourier transform to obtain the matrix $\mathbf{H}$. By comparing (15) and (16) we obtain the relation

$$-\frac{1}{2\pi i} \int_\Omega \frac{G_e(\omega')d\omega'}{\omega' - \omega} = \frac{1}{2\pi} \int_{-\infty}^\infty \exp(-i\omega t)\left(u(t) - \frac{1}{2}\right) \int_\Omega \exp(i\omega' t) G_e(\omega')d\omega' dt \tag{18}$$

where $u(t)$ is the unit step function. The discrete counterpart of (18) is

$$\left(\mathbf{HG}_e\right)(m) = \frac{i}{N} \sum_{n=1}^N \sum_{k=-\frac{N-1}{2}}^{\frac{N-1}{2}} \mathrm{sgn}(k) G_e(n) \exp[i2\pi k(n-m)/N], \tag{19}$$

where

$$\mathrm{sgn}(k) = \begin{cases} -1 & \text{for } k < 0 \\ 0 & \text{for } k = 0 \\ 1 & \text{for } k > 0 \end{cases}. \tag{20}$$

In (19) $m \in \{1, 2, \ldots, N\}$, and we have for simplicity assumed that N is an odd number. When discretizing (18), G_e becomes periodical, so in order to limit the resulting errors, we imagine that $\mathbf{G}_e$ is padded with so many zeros that the contribution from the repeated spectra is eliminated. In practice, this means that the number N is increased from the number of samples of F, and that we are only using a certain inner square of the Hilbert transform matrix $\mathbf{H}$ below. That is we effectively pad $\mathbf{G}_e$ with N_z zeros on each side by setting the Hilbert transform matrix in (17) equal to

$$\begin{aligned} \left(\mathbf{H}\right)(m,n) = \quad & \frac{i}{N} \sum_{k=-\frac{N-1}{2}}^{\frac{N-1}{2}} \mathrm{sgn}(k) \exp[i2\pi k(n-m)/N] \\ & \text{for } m, n \in \{N_z, N_z + 1, \ldots, N_z + N_F\}, \end{aligned} \tag{21}$$

where N_F is the number of samples of F and $N = N_F + 2N_z$. It is convenient to use the number N_z that corresponds to the extra bandwidth for which we want to calculate $G(\omega)$ on each side of Ω. Now, we can solve (17) by inverting the matrix $(2\mu + 1)\mathbf{I} - \mathbf{H}/i$, which has the dimension $N_F \times N_F$. Because the (discrete) Hilbert transform is energy conserving, $\|\mathbf{u}\| = \|\mathbf{v}\|$ for any DC-free Hilbert transform pair $\{\mathbf{u}, \mathbf{v}\}$ in the l^2-norm, the truncated Hilbert operator (21) will satisfy

$$\|\mathbf{H}\|/(2\mu + 1) < 1, \qquad \mu > 0. \tag{22}$$

86

Therefore, the matrix $(2\mu + 1)\mathbf{I} - \mathbf{H}/i$ is guaranteed invertible.[21] Once we have found $\mathbf{G}_e$, $\mathbf{G}$ is computed by a discrete Hilbert transform of a zeropadded version of $\mathbf{G}_e$, according to (16). To sum up, the algorithm goes as the following:

1. Set the precision by picking a $\mu > 0$. Usually, values in the range $[10^{-5}, 10^{-2}]$ are appropriate.

2. Solve (17) for the desired F by matrix inversion.

3. Calculate $\mathbf{G}$ by a Hilbert transform of $\mathbf{G_e}$ padded with zeros outside Ω (discrete version of (16)).

4. Compute ϵ as the rms error of the elements of $\mathbf{F} - \mathbf{G}$ (discrete version of (7)).

As the chosen μ is getting smaller, the error ϵ is decreasing and $\|\mathbf{G}\|$ is growing. Usually, this means that the transmission coefficient H is getting more difficult to realize as a fiber grating. At a certain point, the error is not decreasing further due to finite bandwidth in the calculations. This bandwidth can be increased by increasing N_z in (21) and padding $\mathbf{G}_e$ with more zeros in Step 3. Finally, it is not possible to get any less error due to quantization errors in the computer.

The Hilbert transform in Step 3 is computed using FFT, so the algorithm scales with the total bandwidth as $\mathcal{O}(N_z \log N_z)$. Note that the computation time of (21) scales only linearly with N_z. Owing to the matrix inversion involved, we also observe that the algorithm scales with the resolution in Ω as $\mathcal{O}(N_F^3)$.

5. Examples

A. Reconstruction of a Hilbert transform pair

In the first example, we wish to verify the algorithm given in the last section. We define a Hilbert transform pair $\{u, v\}$ by

$$u(\omega) = \begin{cases} (\omega - \omega_0)/2\omega_w & \text{for } |\omega - \omega_0| < \omega_w, \\ 0 & \text{for } |\omega - \omega_0| \geq \omega_w \end{cases}, \tag{23}$$

where $2\omega_w$ is the bandwidth of Ω, and ω_0 is the middle frequency. The function v is found from a Hilbert transform of u defined in (23). Now, we set $G = u + iv$ and apply $F = G$ for $\omega \in \Omega$ to the algorithm to see how well the function G is reconstructed outside Ω. The results are showed in Fig. 1. We observe that the produced solution for $\mu = 1$ has less norm than the original, as expected. For μ less than about 0.1, the reconstructed and original G are virtually identical. In Fig. 2 the dependence of the rms error is shown for 10 different values of μ. The figure shows the expected behavior; the error decreases with decreasing μ until a certain point where the finite bandwidth and/or quantization are dominating the error. The bandwidth in the simulation is $14\omega_w$. By increasing this bandwidth, it is possible to get considerably less rms error.

We observe that the algorithm is capable of extrapolating the data from within Ω. The method may therefore also be used as a technique for extrapolating a transfer function G or
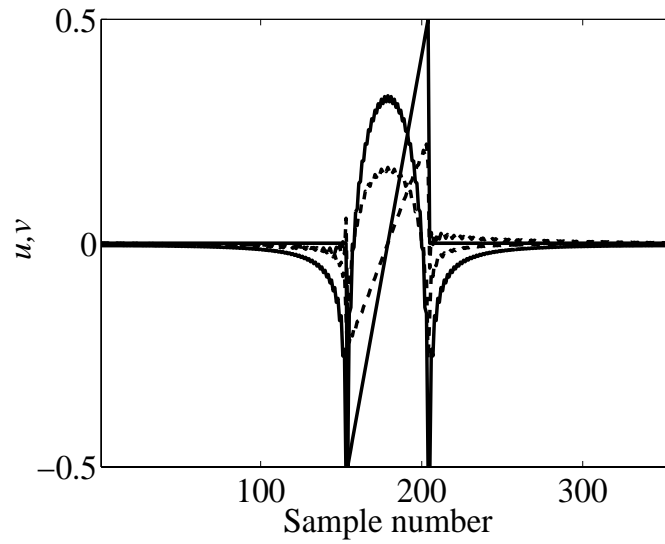
Fig. 1. The original (solid) and reconstructed (dashed) Hilbert transform pair for $\mu = 1$. For μ less than about 0.1, the reconstructed and original functions are virtually identical on this plot.
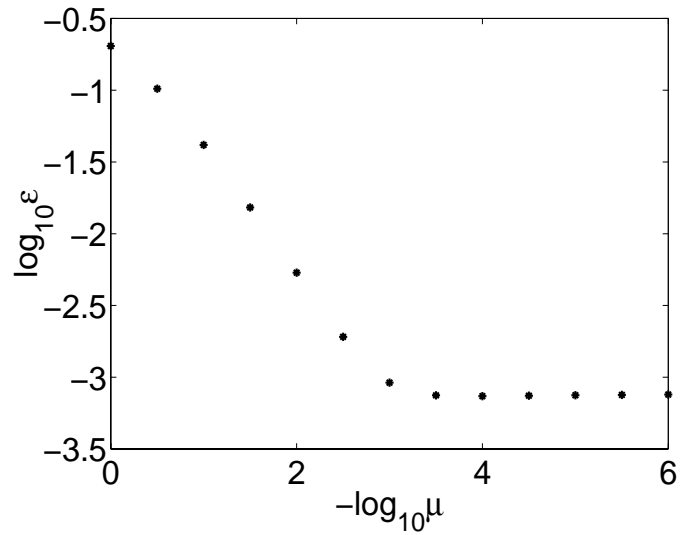
Fig. 2. Rms error of the reconstructed transfer function G inside Ω for different values of μ.
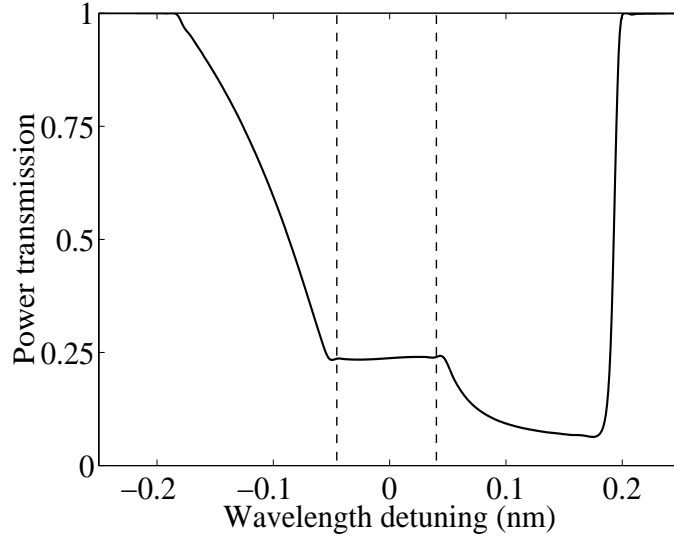
Fig. 3. Power transmission of the fiber grating in example B. The relevant wavelength interval corresponding to frequencies inside Ω is indicated with vertical, dashed lines.

a minimum phase transfer function H from data inside Ω. However, in the case of noise in the data, the extrapolated function far away from Ω might have large errors as the continuation problem clearly is unstable. The algorithm is regularized by the parameter μ which decides how to treat the tradeoff between stability and accuracy. If μ is set to a larger value, the accuracy is decreased, but the stability is increased correspondingly.

B.   Second order dispersion compensation grating

As a first example of actual synthesis of a fiber grating, we try to synthesize a filter with constant amplitude response and linear group delay (i.e. a second order dispersion compensation grating). This example is chosen because it shows both the powerfulness of the method and also the weaknesses. In addition the example indicates how one can modify the filter to optimize for different applications.

According to the specifications, the input function should equal

$$F(\omega) = a(\omega - \omega_0) + i0, \qquad \omega \in \Omega, \tag{24}$$

where a is a number proportional to the dispersion coefficient, and ω_0 is the center frequency. This function is applied as input to the algorithm for solution of Krein-Nudel'man's problem using the precision $\mu = 10^{-3}$ and a total bandwidth of 10 times the bandwidth of Ω. The solution is then modified according to the algorithm presented in Section 3 setting ω_B to twice the bandwidth of Ω. Finally, a layer-peeling algorithm has been applied for the synthesis of a 20cm long fiber grating centered at 1550nm. The bandwidth of Ω was set to 0.09nm. The arbitrary reflection phase response was chosen linear, so that the reflection response is dispersionless. Note that the entire process can be implemented in a single and automatic computer program. The resulting grating transmission spectra are shown in Figs 3 and 4.

89
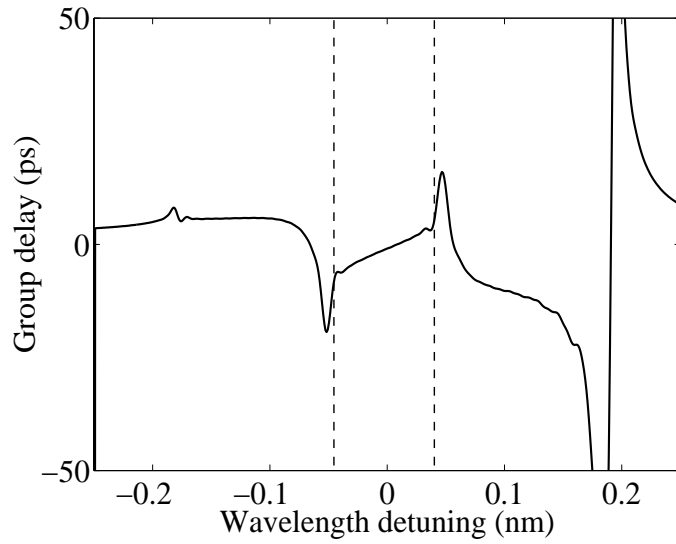
Fig. 4. Transmission group delay of the designed fiber grating in example B. The relevant band Ω is indicated with vertical, dashed lines. Note that the delay offset associated with the pure propagation has been removed because the input and output reference planes coincide.
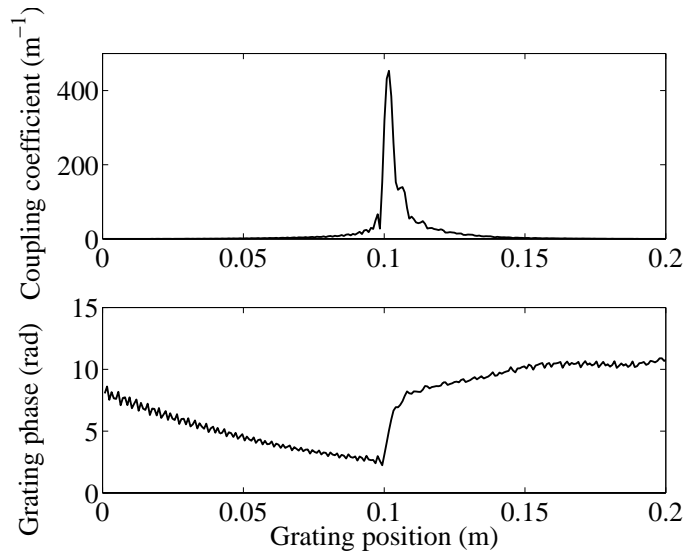
Fig. 5. Magnitude and phase of the complex coupling coefficient of the designed grating (example B).

We observe a flat pass band at 24% transmitivity; the ripple is ±0.03. Moreover, the group delay is nearly linear in the pass band; the deviation is less than 0.5ps compared to a linear response. The dispersion in Ω is roughly 140ps/nm. The designed grating structure (amplitude and phase) is shown in Fig. 5.

One problem with the designed spectrum is clearly that the power transmission in Ω is only 24%. This is a result of the spectrum shape on the left-hand side; it has to grow as ω departs from the edge of Ω. Since the power transmission cannot be greater than unity, this problem arises. It is possible to increase the transmission in Ω by shrinking the bandwidth ω_B on the left-hand side. The resulting performance of the filter will of course be somewhat worse in Ω.

For some applications, it might be desirable to increase the dispersion. If we scale the group delay $\tau_g = -d\arg H/d\omega$ with a factor k, i.e. $\tau_g \to k\tau_g$, the function $\ln(|H|)$ scales by the same factor (see Eq. (6)). Hence, the transmission coefficient changes according to $H \to H^k$. In other words, when $k > 1$ the power transmission will be less for all ω, and the response will be more rapidly varying. The grating is therefore more difficult to realize. Another way of getting larger dispersion is to scale the bandwidth of the designed grating. If the bandwidth is reduced by a factor k, i.e. $(\omega - \omega_0) \to (\omega - \omega_0)/k$, the dispersion $D \propto d^2 \arg H/d\omega^2$ is scaled by a factor k^2. The price one would have to pay is to increase the grating length and decrease the grating strength with the same factor k, i.e. the coupling coefficient $q(z)$ scales according to $q(z) \to 1/k\, q(z/k)$.[22] For example the dispersion of the filter in Figs. 3 and 4 will change to 3500ps/nm if the bandwidth of Ω is reduced by a factor 5. The grating length will then be 100cm. Thus we can obtain a relatively large increase in the dispersion with a relatively small increase in the grating length and decrease in the bandwidth.

C. Third order dispersion compensation grating

We will also try to synthesize a filter with flat amplitude response and quadratic group delay (third order dispersion compensating filter).[23] The input function is

$$F(\omega) = b(\omega - \omega_0)^2 + i0, \qquad \omega \in \Omega, \tag{25}$$

where b is proportional to the third order dispersion coefficient. This filter turns out to be relatively easy to realize, so we set $\mu = 10^{-4}$. We use the same procedure as in the previous example, but set the grating length to 5cm and the bandwidth of Ω to 0.28nm. The resulting spectra are shown in Figs. 6 and 7. Again, we have obtained a relatively flat amplitude response; the ripple is $\pm1\%$ in Ω. Moreover, the deviation from a quadratic group delay in Ω is less than 0.3ps. The coupling coefficient of the designed fiber grating is shown in Fig. 8. We observe that the grating structure is relatively complex, so that it might be difficult to fabricate in practice. For the grating given in Fig. 8 the reflection phase response was chosen linear. To obtain a different grating structure, we can for example choose a quadratic reflection phase response. In particular, we have specified the dispersion 322ps/nm in reflection, and applied the layer-peeling algorithm to the resulting reflection spectrum. The new grating structure is given in Fig. 9. As expected, the grating is nearly linearly chirped and the modulus of the coupling coefficient is slowly varying compared to that of Fig. 8. In
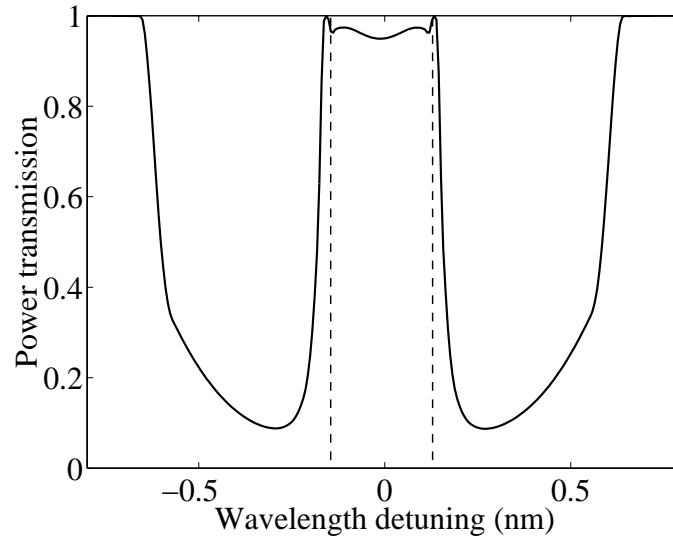
Fig. 6. Power transmission of the fiber grating in example C. The relevant wavelength interval corresponding to frequencies inside Ω is indicated with vertical, dashed lines.
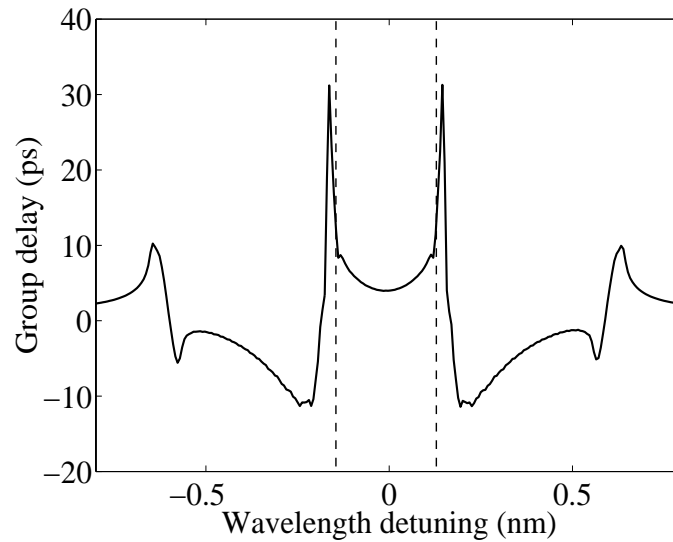
Fig. 7. Transmission group delay of the designed fiber grating in example C. The relevant band Ω is indicated with vertical, dashed lines.

92
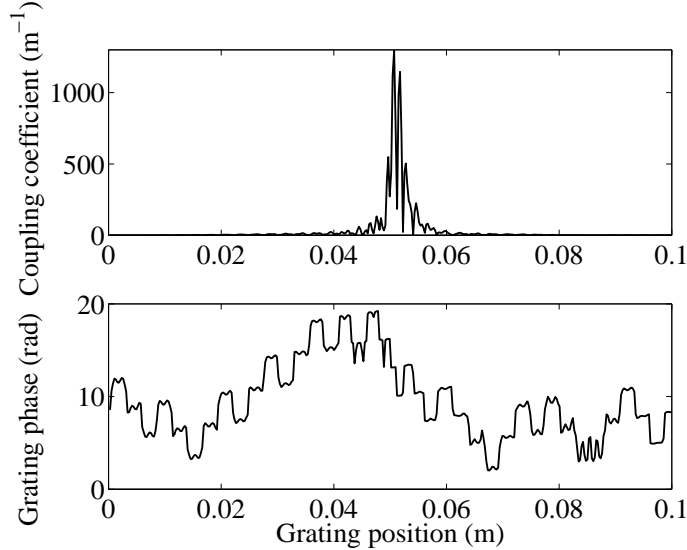
Fig. 8. Magnitude and phase of the complex coupling coefficient associated with the designed grating with nondispersive reflection response (example C).

addition the maximum coupling coefficient value is reduced by a factor 3.4. The associated transmission spectra (power and group delay spectrum) are not plotted as they are virtually identical to the spectra given in Figs. 6-7. This demonstrates the nonuniqueness of the synthesis problem: There is one distinct grating structure for each chosen reflection phase response, and all gratings have identical transmission spectra. If the dispersion in reflection is not relevant to the specific application, we can therefore choose a phase response that makes the grating simple to realize.

If one would like to obtain opposite convexity of the transmission group delay, the power transmission curve would have to grow as the wavelength departs from Ω. Consequently, the power transmission will be smaller in Ω. For the present example, exact opposite dispersion translates into a transmission of 8.7% in Ω. If smaller transmission is not acceptable, one can reduce the specified dispersion or descrease the bandwidth. For example if the bandwidth of Ω is reduced by a factor 4, one gets a transmission of 86% with the exact opposite dispersion as in Fig. 7.

6.   Conclusion

A general method for synthesis of fiber gratings with desired, complex transmission responses in a finite bandwidth window has been described. The necessary minimum phase characteristics is satisfied by the designed grating due to the spectral behavior outside the relevant bandwidth Ω. This behavior decides how difficult it is to realize the filter as a fiber grating. The greater error that can be tolerated in Ω, the easier it is to realize the fiber grating because the spectral behavior outside Ω is more well-behaved.

A general numerical algorithm has been developed, which can be used for the design of practical fiber gratings. Two different transmission responses were specified and applied as

93
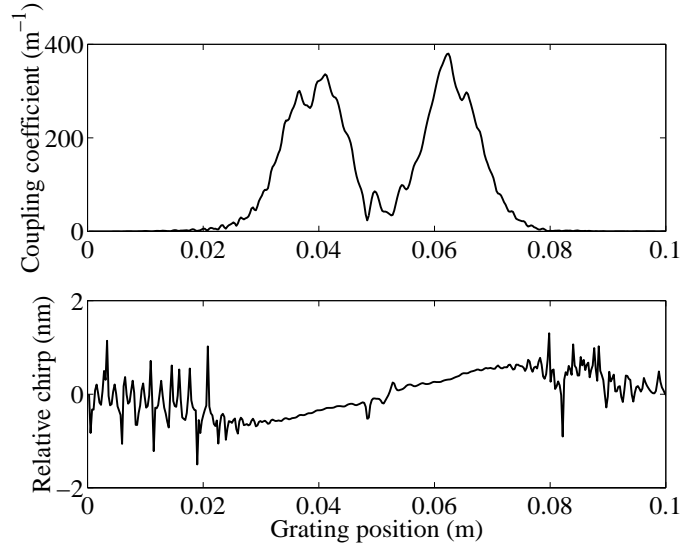
Fig. 9. Magnitude of the coupling coefficient and relative chirp of the designed grating with dispersive reflection response (example C). The chirp is defined relative to the design Bragg wavelength 1550nm.

input to the algorithm. The first filter had nearly flat power transmission and linear group delay, and can therefore be used as a second order dispersion compensator. The second filter was specified as a third order dispersion compensator. We designed two different gratings with this response; one with nondispersive reflection response, and one with constant dispersion. In the latter case, the grating became nearly linearly chirped and simpler to realize. The spectral results in transmission demonstrated that one can design gratings with desired power and group delay responses in transmission in a finite bandwidth. In addition one can specify the reflection group delay independently. For applications where one wants to use the grating in both transmission and reflection at the same time, this means that we can specify the two group delay responses independently. On the other hand, the power reflection and transmission are certainly connected for a lossless grating, and as a result one must sacrifice the freedom in specifying the power reflection outside Ω.

Finally, we note that the method also can be used for design of thin-film filters in transmission and for extrapolation of transfer function data from a limited bandwidth window.

Acknowledgments

References

1. K. O. Hill and G. Meltz, "Fiber Bragg grating technology: Fundamentals and overview," J. Lightwave Technol. **15**, 1263–1276 (1997).

2. T. Erdogan, "Fiber grating spectra," J. Lightwave Technol. **15**, 1277–1294 (1997).

3. R. Feced, M. N. Zervas, and M. A. Muriel, "An efficient inverse scattering algorithm for the design of nonuniform fiber Bragg gratings," IEEE J. Quantum Electron. **35**, 1105–1115 (1999).

4. K. Hinton, "Dispersion compensation using apodized Bragg fiber gratings in transmission," J. Lightwave Technol. **16**, 2336–2346 (1998).

5. E. Brinkmeyer, "Simple algorithm for reconstructing fiber grating from reflectometric data," Opt. Lett. **20**, 810–812 (1995).

6. L. Poladian "Group-delay reconstruction for fiber Bragg gratings in reflection and transmission," Opt. Lett. **22**, 1571–1573 (1997).

7. G. Lenz, B. J. Eggleton, C. R. Giles, C. K. Madsen, R. E. Slusher, "Dispersive properties of optical filters for WDM systems," IEEE J. Quantum Electron. **34**, 1390–1402 (1998).

8. F. Ouellette, "Limits of chirped pulse-compression with an unchirped bragg grating filter," Appl. Opt. **29**, 4826–4829 (1990).

9. B. J. Eggleton, T. Stephens, P. A. Krug, G. Dhosi, Z. Brodzeli, and F. Ouellette, "Dispersion compensation using a fibre grating in transmission," Electron. Lett. **32**, 1610–1611 (1996).

10. N. M. Litchinitser, B. J. Eggleton, and D. B. Patterson, "Fiber Bragg gratings for dispersion compensation in transmission: Theoretical model and design criteria for nearly ideal pulse recompression," J. Lightwave Technol. **15**, 1303–1313 (1997).

11. J. Skaar, "Synthesis of limited bandwidth minimum phase filters," submitted to Inverse Problems, October 2000.

12. M. G. Krein and P. Ya. Nudel'man, "On some new problems for Hardy class functions and continuous families of functions with double orthogonality," Dokl. Akad. Nauk SSSR, **206** 537–540 (1973).

13. M. G. Krein and P. Ya. Nudel'man, "Approximation of functions by minimum-energy transfer functions of linear systems," Problemy Peredachi Informatsii **11**, 37–60 (1975).

14. V. Klibanov, P. E. Sacks, and A. V. Tikhonravov, "The phase retrieval problem," Inv. Probl. **11**, 1–28 (1995).

15. M. Nussenzveig, *Causality and dispersion relations* (Academic Press, New York 1972)

16. A. Papoulis, *The Fourier integral and its applications* (McGraw-Hill, New York 1962), Chapter 10.

17. E. Weisstein, "Eric Weissteins world of mathematics," http://mathworld.wolfram.com/

18. L. Aizenberg, *Carleman's formulas in complex analysis* (Kluwer Academic Publishers, The Netherlands, 1993).

19. A. V. Tikhonravov, "Some theoretical aspects of thin-film optics and their applications," Appl. Opt. **32**, 5417–5426 (1993).

20. A. M. Bruckstein, B. C. Levy, and T. Kailath, "Differential methods in inverse scattering," SIAM J. Appl. Math. **45** 312–335 (1985).

21. N. Young, *An introduction to Hilbert space* (Cambridge University Press, UK, 1988), Chapter 7.

22. G. H. Song, "Theory of symmetry in optical filter responses," J. Opt. Soc. Am. A **11**, 2027-2037 (1994).

23. N. M. Litchinitser, B. J. Eggleton, and G. P. Agrawal, "Dispersion of cascaded fiber gratings in WDM lightwave systems," J. Lightwave Technol. **16**, 1523–1529 (1997).

Chapter 5

Characterization of fiber gratings

Complete characterization of fiber gratings requires knowledge of the complex coupling coefficient or the complex reflection spectrum. If one has measured the complex reflection spectrum, one can for example use the layer-peeling algorithm to compute the coupling coefficient. Conversely, one can use the transfer-matrix approach to obtain the spectrum from the coupling coefficient. Characterization of fiber gratings is not a trivial problem, as optical phase usually is difficult to measure. It would therefore be attractive to use a Hilbert transform or Kramers-Kronig type relation to reconstruct the reflection phase response. However, since the reflection coefficient might have zeros in the "wrong" complex frequency half-plane, this is not possible in general. Even if the responses of certain types of gratings ideally satisfy the minimum phase condition, the phase reconstruction of corresponding practical gratings might be very inaccurate, because small grating imperfections may move the zeros to the "wrong" half-plane as is discussed in Section 5.1.

In Section 5.2 we propose a different method for reconstruction of the phase response from the reflectivity. We make use of some extra *a priori* information in that the modulus of the coupling coefficient is known. The method can be useful for intragrating sensing as only the phase of the coupling coefficient is altered when the grating is exposed to a strain or temperature gradient. Thus if the grating is characterized in advance, this method can be used to obtain the phase of the coupling coefficient, and thereby the strain or temperature profile, by monitoring the power reflectivity alone.

Sections 5.3 and 5.4 contain two different methods for characterization based on interferometry. The first method is extremely simple; one cuts the fiber after the grating, yielding a Fabry-Perot cavity with the grating and the bare fiber end as the mirrors. By measuring the power reflection spectrum of the Fabry-Perot structure, one can retrieve the complex reflection spectrum of the grating. In the second method, a low-coherence approach is used to obtain the complex impulse response of the grating. The complex reflection spectrum is then obtained by a Fourier transform.

For an introduction to the available literature on characterization and phase retrieval of fiber gratings, consult the introductions and references in the respective, following papers. Note that the sign convention on the implicit time dependence in Section 5.2 does not correspond with the sign convention in Chapter 2.

5.1 Phase reconstruction from reflectivity in fiber Bragg gratings

Authors: Johannes Skaar and Helge E. Engan

Phase reconstruction from reflectivity in fiber Bragg gratings

Johannes Skaar and Helge E. Engan

Department of Physical Electronics, Norwegian University of Science and Technology, N–7034 Trondheim, Norway

It is shown that a recently proposed phase-retrieval technique for Bragg gratings [Opt. Lett. **22,** 93 (1997); J. Lightwave Technol. **15,** 1314 (1997)] is not well suited for gratings with imperfections. The reconstructed group delay is in many cases not a more accurate estimate than the simulated group delay of the perfect, designed grating, independently of how small the errors in the grating structure are. The error in the group delay may be especially large near the zeros in the reflection spectrum. © 1999 Optical Society of America

OCIS codes: 060.2340, 060.2770.

For a complete characterization of a fiber Bragg grating (FBG), both the amplitude and the phase of the complex reflection coefficient are needed. The amplitude response or reflectivity is conveniently measured with a spectrum analyzer or a scanning distributed Bragg reflector laser, whereas obtaining the phase response is more complicated. Recently, a phase-retrieval method for obtaining the phase response from the reflectivity spectrum was proposed by Carballar and Muriel.[1,2] The method utilizes the well-known Hilbert transform or dispersion relations that connect the minimum phase and the logarithm of the amplitude spectrum for linear systems.[3,4] The Hilbert transform is easily computed by means of existing numerical packages using fast Fourier transforms or by use of the Wiener–Lee transform.[3] For a transfer function to be minimum phase, it must be zero free in the right-hand half-plane. This condition is always satisfied for the transmission coefficient of a FBG but generally is not true in reflection.[5] Certain grating designs will nevertheless yield minimum phase-reflection coefficients. For such gratings this means that the phase response can be uniquely computed from the reflectivity. In Refs. 1 and 2 Carballar and Muriel therefore assumed *a priori* that the overall grating structure was known (e.g., that it was a uniform grating) to ensure that the minimum phase condition was fulfilled. An experimental grating, however, will have small errors in the grating structure, so we are never guaranteed that the minimum phase condition is satisfied. Here we show that the resulting errors can be significant and that the simulated phase response of the designed minimum phase grating can often be a better estimate. This ideal phase response is usually available since the overall grating design is known *a priori*. Still, it is often a bad estimate of the true phase response. Therefore, this phase-retrieval technique is not well suited for experimental gratings, as was claimed in Refs. 2 and 6. Throughout this Letter the terms ideal grating and actual grating are used for the designed, perfect minimum phase grating and the experimental, nonideal grating, respectively.

A linear system is completely characterized by its impulse response function, $h(t)$. If $h(t)$ represents a causal and stable physical system, it is real, absolutely integrable, and vanishes for $t < 0$. We can therefore define the Laplace transform as

$$H(s) = \int_0^\infty h(t)\exp(-st)\,\mathrm{d}t \qquad (1)$$

and obtain the frequency response or the Fourier transform by evaluating $H(s)$ along the imaginary axis, $s = i\omega$. According to the Titchmarsh theorem,[4] the real and the imaginary parts of $H(i\omega)$ are then related by means of the Hilbert transform. However, we are looking for a relation between the magnitude and the phase of $H(i\omega)$, so we define

$$\tilde{H}(s) = \ln H(s) = \ln|H(s)| + i\,\arg H(s). \qquad (2)$$

In general, $\tilde{H}(s)$ will not be analytic in the right-hand half-plane because $H(s)$ can have zeros. Therefore, the Titchmarsh theorem states that $\tilde{H}(s)$ is not generally a causal transfer function. We must therefore restrict $H(s)$ to be zero free for $\mathrm{Re}(s) > 0$. Then the real and the imaginary parts of $\tilde{H}(i\omega)$, or equivalently the logarithm of the amplitude response and the phase response, will be related by means of a Hilbert transform relation of the type[3]

$$\varphi_{\min}(\omega) = \frac{\omega}{\pi} \int_{-\infty}^{\infty} \frac{\ln|H(i\omega')|}{\omega'^2 - \omega^2}\,\mathrm{d}\omega'. \qquad (3)$$

In Eq. (3), $\varphi_{\min}(\omega)$ is the (minimum) phase response, and we can make sense of the integral by means of the Cauchy principal value. Transfer functions that satisfy Eq. (3) are known as minimum phase functions. If the transfer function is not minimum phase, the contribution to the phase response from the zeros in the right-hand half-plane has to be added to Eq. (3). Let the zeros of $H(s)$ be denoted by $s_n = \sigma_n + i\omega_n$, repeated as necessary for multiple zeros. Then the function

$$H_{\min}(s) = H(s) \prod_{\sigma_n > 0} \frac{s + s_n{}^*}{s - s_n} \qquad (4)$$

is analytic and zero free in the right-hand half-plane and is therefore the minimum phase-shift function corresponding to $|H(i\omega)|$, since

$$\left| \frac{i\omega + s_n{}^*}{i\omega - s_n} \right| \equiv 1.$$

Equation (4) is equivalent to the statement in Ref. 7 that a nonminimum phase filter can be constructed from a minimum phase filter followed by an all-pass filter. From Eq. (4) we deduce that the phase response $\varphi(\omega) = \arg H(i\omega)$ is given by

$$\varphi(\omega) = \varphi_{\min}(\omega) - 2 \sum_{\sigma_n > 0} \arctan\left(\frac{\omega - \omega_n}{\sigma_n}\right), \qquad (5)$$

and the corresponding group delay becomes

$$\tau_g(\omega) = -\frac{d\varphi(\omega)}{d\omega}$$

$$= \tau_{g,\min}(\omega) + 2 \sum_{\sigma_n > 0} \frac{\sigma_n}{\sigma_n^2 + (\omega - \omega_n)^2}. \qquad (6)$$

Thus if there are zeros in the right-hand half-plane the difference between the true group delay $\tau_g(\omega)$ and the minimum group delay $\tau_{g,\min}(\omega)$ can be arbitrarily large for $\omega \approx \omega_n$ and sufficiently small σ_n.

When one is using the phase-retrieval method proposed in Ref. 2, Eq. (6) can have important consequences. Consider, for example, a uniform FBG, the same example as was presented in Refs. 1, 2, and 6. An ideal, uniform FBG will be minimum phase in reflection. This condition is valid for both the forward and the backward reflection coefficients because of its symmetry. Furthermore, there are a number of zeros on the imaginary axis $s = i\omega$, as is evident from their sinc^2-like spectrum. However, when the grating is not perfect, these zeros may be located slightly away from the imaginary axis. This is seen in the reflection spectrum as missing zeros. The probability that one of these zeros will be located in the right-hand half-plane is 1/2, since the zeros of two gratings that are reversed with respect to each other are in the opposite half-plane.[7] When $\sigma_n > 0$ for some n, we must therefore conclude from Eq. (6) that the errors in the reconstructed group delay $\tau_g(i\omega) - \tau_{g,\min}(i\omega)$ can be arbitrarily large for almost-perfect gratings. In other words, some of the peaks in the reconstructed group delay around the perturbed zeros of the spectrum can have large errors. As the grating errors become less, the group-delay error peaks become higher and narrower, and in the limit $\sigma_n \to 0^+$ the peak width approaches zero. However, the peak area remains constant at 2π, as can be seen from Eq. (5). Hence, for each zero that is located somewhere in the right-hand half-plane, we get an integrated error in the group delay of 2π.

For a lossy grating the probability that a zero will be located in the right-hand half-plane is less than 1/2, since the transfer function $H(s)$ will be shifted to the left by the loss coefficient. We may therefore expect a better result from the phase-retrieval method when we have a loss that is large compared with the grating errors. More precisely, if the time-domain loss coefficient is larger than the maximum σ_n, the method will yield the true group delay. In the numerical example below, this delay corresponds to a loss in the grating of more than 80 dB/m, although the grating errors are relatively small. This is a rather large loss,

so it is therefore reasonable to assume that some of the zeros will contribute to errors in the reconstructed group delay. This simple loss model might, however, be somewhat misleading, as grating loss normally is strongly frequency dependent.

To compare the reconstructed phase or group delay from Eq. (3) with the corresponding ideal phase or group delay, we first assume that our ideal grating is symmetric and weak (for example, a uniform grating). Since there are Fourier-transform relations between the grating structure (coupling coefficient) and the reflection spectrum, we can write

$$r_2(\omega) = \exp(ia) r_1(\omega)^* \qquad (7)$$

for the actual grating, where a is a real constant and $r_1(\omega)$ and $r_2(\omega)$ denote the forward and the backward reflection coefficients, respectively. The group delay is proportional to the derivative of the phase response and must therefore satisfy

$$\tau_2(\omega) = -\tau_1(\omega), \qquad (8)$$

where $\tau_1(\omega)$ and $\tau_2(\omega)$ denote the forward and the backward group delays, respectively. Note that the group delay can be negative since the reference plane $z = 0$ is set to the middle of the grating. Note also that $|r_2(\omega)| = |r_1(\omega)|$, which in fact is valid for a general lossless grating.[5] If we want to find an estimate for the group delay, which should be as good as possible for both directions at the same time, according to Eq. (8) we must choose $\tau(\omega) \equiv 0$. In fact, this would be the same as choosing the group delay of the ideal grating as our estimate. We realize this choice by noting that the ideal grating is symmetric, so according to Eq. (7) the group delay must be zero almost everywhere. Since the method in Refs. 1 and 2 finds one estimate, which should be valid for both directions, the resulting group-delay spectrum on average will not be a better estimate than the group-delay spectrum of the ideal grating. Moreover, since the reconstructed, minimum group delay is less than both $\tau_1(\omega)$ and $\tau_2(\omega) = -\tau_1(\omega)$, the expected relative error of the reconstructed group delay is $\{[\tau_1(\omega) - \tau_{\min}(\omega)] + [-\tau_1(\omega) - \tau_{\min}(\omega)]\}/2\tau_1(\omega) = -\tau_{\min}(\omega)/\tau_1(\omega)$, since we have no control over the orientation of the errors. The expected relative error is therefore more than 100% for all ω. These results are independent of how small the errors in the grating are, although the absolute group-delay error of course approaches zero when the grating errors vanish.

For a strong grating, Eqs. (7) and (8) are not valid. Therefore, we analyze a stronger, uniform grating perturbed by slowly varying phase errors of amplitude 0.4 rad in the grating structure by use of coupled-mode theory. The design parameters are otherwise approximately the same as those of the grating presented in Ref. 6. The reflectivity spectra for the ideal and the actual gratings are shown in Fig. 1. The numerical results for the true and the reconstructed group delays in the grating stop band are presented in Fig. 2, together with the group delay of the ideal grating. First, we note that the reconstructed group delay is
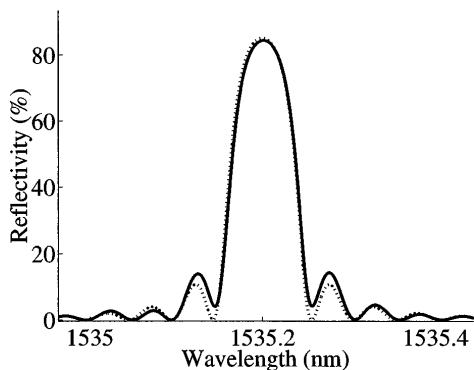
Fig. 1.   Reflectivity spectrum for the actual grating (solid curve) and the ideal uniform grating (dotted curve).
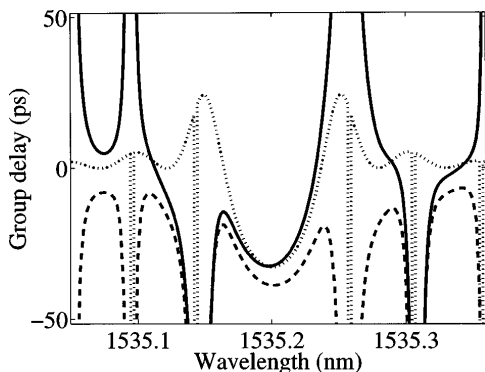
Fig. 2.   Calculated group delay for the actual grating (solid curve), the reconstructed group delay (dashed curve), and the group delay for the ideal uniform grating (dotted curve).

less than the true group delay for all wavelengths, as required from Eq. (6).   Furthermore, we observe that the peaks in the group delay correspond to the (near) zeros in the reflection spectrum.   When the true group delay has a lower peak, the corresponding zero is located to the left of the imaginary axis, $\sigma_n < 0$.   Therefore, the reconstructed group delay corresponds well to the true group delay in the neighborhood of that zero.   However, when the zero is located to the right of the imaginary axis, the true group delay has an upper peak, whereas the reconstructed group delay has a lower peak.   This is because the reconstruction algorithm assumes that the zero is located to the left

of the imaginary axis.   The errors in the group delay near a zero are often of minor interest, since not very much light is ref lected in this area.   Nevertheless, we see from Fig. 2 that the errors from a zero can influence the group-delay spectrum over a range around that zero (e.g., in the stop band).   This distance is increased as the errors in the grating structure become larger, as is evident from Eq. (6).   However, the reconstruction algorithm in this case works better than for an average weak grating, since the rough shape of the group delay in the grating stop band is approximately reconstructed.   This result is due to the fact that a strong grating will in general have not only zeros but also poles.[7]   The contribution to the group delay from the poles will be included in the reconstruction formula [Eq. (3)].   We note, however, that the ideal phase response is still a better estimate in the stop band.   Hence, the ideal, simulated group delay is often a better estimate than the reconstructed group delay.

In general, we must therefore conclude that the phase-retrieval method presented in Refs. 1 and 2 is not well suited for reconstruction of the reflection phase response of experimental gratings, owing to zeros at or near the imaginary axis of the transfer function.   Therefore, when the zeros are sufficiently far from the imaginary axis, we would expect better performance.   However, this is not the case for many kinds of minimum phase FBG, for example, a near-lossless, uniform grating.

J. Skaar's e-mail address is johannes.skaar@ fysel.ntnu.no.

References

1. M. A. Muriel and A. Carballar, Opt. Lett. **22,** 93 (1997).
2. A. Carballar and M. A. Muriel, J. Lightwave Technol. **15,** 1314 (1997).
3. A. Papoulis, *The Fourier Integral and Its Applications* (McGraw-Hill, New York, 1962).
4. H. M. Nussenzveig, *Causality and Dispersion Relations* (Academic, New York, 1972).
5. L. Poladian, Opt. Lett. **22,** 1571 (1997).
6. D. Pastor and J. Capmany, Electron. Lett. **34,** 1344 (1998).
7. G. Lenz, B. J. Eggleton, C. R. Giles, C. K. Madsen, and R. E. Slusher, IEEE J. Quantum Electron. **34,** 1390 (1998).

5.2 Distributed intragrating sensing using phase retrieval

Authors: Johannes Skaar and Helge E. Engan

Distributed intragrating sensing using phase retrieval

Johannes Skaar and Helge E. Engan
Department of Physical Electronics, Norwegian University of Science and Technology
N-7034 Trondheim, Norway
Fax: +47 73 59 14 41, Tel: +47 73 59 44 00

Abstract

A method for measuring a distributed strain or temperature profile along a fiber Bragg grating is proposed. By using an *a priory* knowledge about the index modulation amplitude, the sensing parameters are obtained from the reflectivity spectrum.

Summary

An interesting application of fiber Bragg gratings (FBGs) is to measure a distributed strain or temperature profile along the length of the grating. Several methods for this purpose have been reported in the literature [1-4]. All of them utilize the fact that the measurand can be obtained from the local Bragg wavelength $\lambda_B(z)$ along the grating position z. The function $\lambda_B(z)$ can be obtained by using low coherence interferometry [3, 4] or by recording the complete complex reflection spectrum. By using an inverse scattering method (or an inverse Fourier transform for the case of weak gratings), the wavelength profile $\lambda_B(z)$ may be computed from the complex reflection coefficient.

The phase response or the group delay of a FBG is somewhat difficult to measure, and it is therefore desirable to extract the sensing information from the reflectivity spectrum alone. In [1] the distortion of the reflectivity spectrum due to various kinds of strain gradients is investigated using the transfer matrix method. However, the authors give no method for obtaining the detailed wavelength profile $\lambda_B(z)$ from the spectrum. They note that the spectrum shows no difference if the strain profile is flipped with respect to the grating, and conclude that the strain profile cannot be uniquely calculated from the reflectivity spectrum. In [2] it is therefore *a priori* assumed that the function $\lambda_B(z)$ is either monotonically increasing or monotonically decreasing. Then $\lambda_B(z)$ can be obtained uniquely from the reflectivity spectrum. Because of the *a priori* assumption on $\lambda_B(z)$, not every strain or temperature gradient can be measured.

In this paper, we present a method for obtaining the function $\lambda_B(z)$ from the reflectivity spectrum. Because the index modulation profile of the grating (or the complex coupling coefficient) cannot be computed uniquely from the reflectivity spectrum alone, we need an *a priori* assumption. This assumption is that the coupling coefficient amplitude (or index modulation amplitude) is known, and that it is not symmetric. The former assumption is justified from the fact that usually only the phase of the coupling coefficient, and not the amplitude, is perturbed when the grating is exposed to a temperature or strain gradient. Therefore, if the grating has been characterized initially (for example at fabrication, using optical coherence domain reflectometry [4] or a phase sensitive interferometric spectrum analyzer [5]), we can assume that the coupling coefficient amplitude is known. The latter assumption is easily achieved for example by choosing an asymmetric grating sensor as the one described in the example below. Note that we have made no *a priori* assumption on the function $\lambda_B(z)$ so every strain or temperature profile can in principle be obtained.

In a FBG, the index of refraction along the grating direction z can be modeled by

$$n(z) = n_0(z) + \Delta n(z)\cos\left(\frac{2\pi}{\Lambda}z + \theta(z)\right),\tag{1}$$

where $n_0(z)$, $\Delta n(z)$ and $\theta(z)$ are slowly varying functions compared to the design grating period Λ. The function $n_0(z)$ represents the variation of the mean index, $\Delta n(z)$ is the index modulation amplitude, and $\theta(z)$ accounts for the period deviation from Λ. Since variation of the "dc" index $n_0(z)$ is equivalent to a chirp [6], the information from $n_0(z)$ may be incorporated in $\theta(z)$. Hence, we set $n_0(z) = n_0$, where n_0 equals the mean index over the whole grating, and represent a mean index variation by a gradient in the function $\theta(z)$. It is common to introduce a complex coupling coefficient [6] which contains all z-dependent quantities from (1)

$$\kappa(z) = A \Delta n(z) \exp(-i\theta(z)). \tag{2}$$

The factor A, determined by the unperturbed waveguide structure and the wavelength, may be treated as a constant. For a weak, lossless grating, there is an approximate Fourier transform relation between the complex coupling coefficient $\kappa(z)$ and the complex reflection spectrum $r(\delta)$ [7],

$$r(\delta) = \mathcal{F}\left\{ -\frac{1}{2}\kappa^*\left(\frac{z}{2}\right) \right\}. \tag{3}$$

In (3), $r(\delta)$ is the complex reflection coefficient as a function of the detuning δ, and $\mathcal{F}$ denotes the Fourier transform operator. From (1) we deduce that the local Bragg wavelength is given by

$$\lambda_B(z) = 2n_0\Lambda\left(1 - \frac{\Lambda}{2\pi}\frac{d\theta}{dz} \right). \tag{4}$$

Thus, our aim is to calculate the phase function $\theta(z)$ from the coupling coefficient magnitude $|\kappa(z)|$ and the reflectivity $|r(\delta)|^2$. From (3) this is equivalent to the determination of a complex function when its magnitude and its Fourier transform magnitude is known. This phase retrieval problem has been studied in the literature because of its relevance in a number of applications [8-15]. The most common algorithm for solving this problem is the so-called iterative Fourier transform algorithm, first proposed by Gerchberg and Saxton [8] for determination of the wavefunction phase from a image and diffraction plane pictures in electron microscopy. The method is transforming successively back and forth between the two Fourier domains, holding the magnitudes at the known values. For further details, the reader is referred to the original paper.

In principle, this phase retrieval method may be extended to stronger gratings, when the Fourier transforms must be replaced by the direct and inverse scattering transform. The direct problem, that is to calculate the spectrum from the coupling coefficient, is easily solved by the transfer matrix method [1,6] or a numerical Runge-Kutta solution to the coupled mode equations [6]. The inverse problem may be solved by a numerical solution to the Gel'fand-Levitan-Marchenko coupled integral equations [16]. However, the inverse problem is ill-posed when the reflectivity approaches unity, and will therefore give inaccurate results for noisy input data. In practice, we should therefore restrict our phase retrieval method to relatively weak gratings.

The uniqueness of the above Fourier phase problem has been shown to depend on specific analytic properties on the functions $\kappa(z)$ and $r(\delta)$ [9,10]. However, if the functions $|\kappa(z)|$ and/or $|r(\delta)|$ are symmetric, a two-fold ambiguity arises. This is easily seen from the complex conjugate symmetry of the Fourier transform. On the other hand, it is explained in [11] that in general for the asymmetric situation, if the spatial frequencies of $\kappa(z)$ are sufficiently band-limited with regard to the dimensions of the grids, and if $r(\delta)$ can be measured with sufficient accuracy for large δ, a unique solution can generally be expected. This somewhat loose statement is also supported by numerical simulations in a number of papers [8,12,13]. So we conclude that provided that $|\kappa(z)|$ and $|r(\delta)|$ are asymmetric, we can assume that our solution is unique. The symmetry ambiguity

corresponds to the situation stated in [1] when the authors note that the reflectivity spectrum shows no difference when the strain gradient is flipped with respect to the grating. However, if we choose an asymmetric coupling coefficient magnitude for our grating sensor, the only ambiguity left is when the function $|r(\delta)|$ is symmetric. This rather unusual situation may be handled by slightly perturbing the sensor to see which of the two solutions $\kappa^*(z)$ or $\kappa(z)$ that persist when the reflectivity becomes asymmetric.

Although the Gerchberg-Saxton algorithm has been successfully used in many practical situations, it suffers from certain convergence problems. There are however a large number of alternative algorithms in the literature, which may be used in the situations where the Gerchberg-Saxton algorithm fails. See for example [14,15].

In order to test the phase retrieval method above, we set $\kappa(z) = |\kappa(z)| \exp[-i\theta(z)]$, where

$$|\kappa(z)| = \begin{cases} (z/L) - 2(z/L)^2 + (z/L)^3, & 0 < z < L \\ 0 & , \text{ elsewhere} \end{cases} \tag{5}$$

and

$$\theta(z) = 1.2 \sin\left[10(z/L)^2\right]. \tag{6}$$

A plot of $|\kappa(z)|$ is shown in Figure 1. $\theta(z)$ contains the information of the local Bragg wavelength as a function of z according to (4). From (3), we obtain $r(\delta)$, and a complete information of this grating is therefore known. We then test whether the Gerchberg-Saxton algorithm reconstructs the functions from the magnitudes $|\kappa(z)|$ and $|r(\delta)|$. We use 500 iterations, which results in a computing time of less than 5 sec on a Pentium PC. In most situations, it is sufficient with considerably less iteration. The reconstructed result for the spatial phase function $\theta(z)$ is finally compared to the original one. The numerical results are shown in Figure 2 as local Bragg wavelengths in the grating by means of (4). The effective index is set to $n_0 = 1.5$, the grating length is $L = 10\text{mm}$, and the design Bragg wavelength is $2n_0\Lambda = 1550\text{nm}$. Also shown in the figure is the reconstructed result for a more realistic situation, where noise has been added to the samples of $|\kappa(z)|$ and $|r(\delta)|$. The noise samples are independent, and distributed according to

$$n_r(\delta) = 0.01|r(\delta)| \cdot n(\delta) \tag{7}$$

for $|r(\delta)|$ and similarly for $|\kappa(z)|$. In (7), $n(\delta)$ is a realization of a random, Gaussian process with mean 0 and variance 1. The results show that the reconstructed local Bragg wavelength is indistinguishable from the original for the noise-free situation, since the error is less than 10^{-8} pm. When there is noise, however, we get visible errors at the edges of the grating where the coupling coefficient magnitude is small. Where the coupling coefficient magnitude is large, the errors are relatively small (about 20pm for $0.01 \le z/L \le 0.9$).

The spatial resolution of this method should be approximately the same as the spatial resolution of the initial characterization of $\kappa(z)$, provided that the reflectivity spectrum is measured sufficiently precise at the edges of the grating stopband. By using for example the characterization method described in [4], a resolution of 1mm should be achievable.

In conclusion, we have developed a method for obtaining the distributed strain or temperature distribution along a fiber Bragg grating by measuring the reflectivity spectrum only. The method makes use of some *a priori* information, namely that the index modulation amplitude is asymmetric and known.
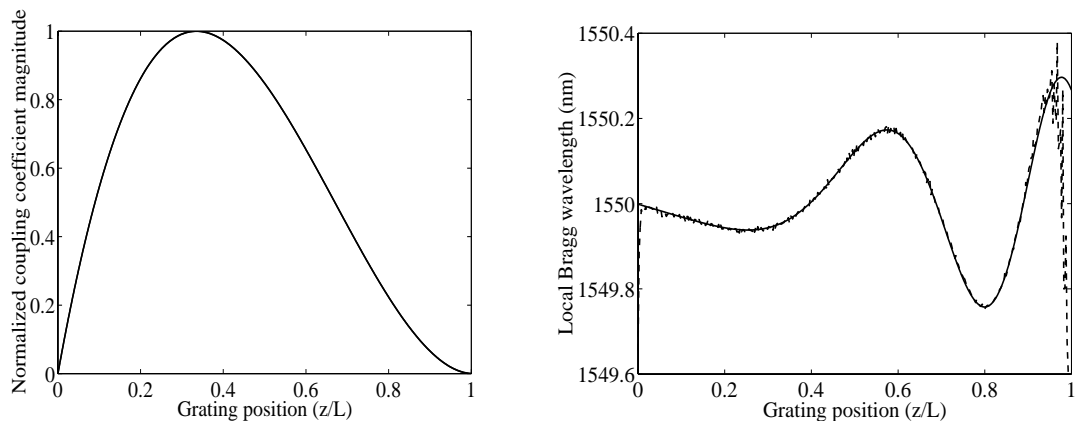
Figure 1: Normalized coupling coefficient magnitude. Figure 2: Local Bragg wavelength in the grating structure, original and reconstructed (solid curve) and reconstructed from noisy modulus data (dashed curve).

References

1. S. Y. Huang, M. LeBlanc, M. M. Ohn, R. M. Measures, "Bragg intragrating structural sensing," Appl. Opt. **34**, 5003-5009 (1995)
2. M. LeBlanc, S. Y. Huang, M. Ohn, R. M. Measures, A. Guemes, A. Othonos, "Distributed strain measurement based on a fiber Bragg grating and its reflection spectrum analysis," Opt. Lett. **21**, 1405-1407 (1996)
3. M. Volanthen, H. Geiger, M. J. Cole, and J. P. Dakin, "Measurement of arbitrary strain profiles within fibre gratings," Electron. Lett. **32**, 1028-1029, 1996.
4. I. Petermann, B. Sahlgren, J. Skaar, P.-Y. Fonjallaz, and R. Stubbe, "Phase distribution measurement of fibre Bragg gratings with white light interferometry," ECOC, Madrid, Spain, September 1998
5. S. Barcelos, M. N. Zervas, R. I. Laming, D. N. Payne, L. Reekie, J.A. Tucknott, R. Kashyap, P. F. McKee, F. Sladen and Wojciechowicz, "High accuracy dispersion measurements of chirped fibre gratings," Electron. Lett. **31**, 1280-1282 (1995)
6. T. Erdogan, "Fiber grating spectra," IEEE J. Lightwave Technol. **15**, 1277-1294 (1997)
7. G. H. Song and S. Y. Shin, "Design of corrugated waveguide filters by the Gel'Fand-Levitan-Marchenko inverse-scattering method," J. Opt. Soc. Amer. **2**, 1905-1915 (1985)
8. R. W. Gerchberg and W. O. Saxton, "A practical algorithm for the determination of phase from image and diffraction plane pictures," Optik **35**, 237-246 (1972)
9. A. M. J. Huiser, A. J. J. Drenth and H. A. Ferwerda, "On phase retrieval in electron microscopy from image and diffraction pattern," Optik **45**, 303-316 (1976)
10. M. V. Klibanov, "Determination of a function with compact support from the absolute value of its Fourier transform, and an inverse scattering problem," Differential Equations **22** 1232-1240 (1987).
11. P. Schiske, "Ein- und Mehrdeutigkeit der Phasenbestimmung aus Bild und Beugungsfigur, " Optik **40**, 261-275 (1974)
12. R. H. T. Bates, "On phase problems I," Optik **51**, 161-170 (1978)
13. A. J. Devaney and R. Chidlaw, "On the uniqueness question in the problem of phase retrieval from intensity measurements," J. Opt. Soc. Am. **68**, 1352-1354 (1978)
14. G. Leone, R. Pierri, and F. Soldovieri, "Reconstruction of complex signals from intensities of Fourier-transform pairs," J. Opt. Soc. Am. A **13**, 1546-1556 (1996)
15. D. C. Dobson, "Phase reconstruction via nonlinear least-squares," Inverse Probl. **8**, 541-557 (1992)
16. P. V. Frangos and D. L. Jaggard, "A numerical solution to the Zakharov-Shabat inverse scattering problem", IEEE Trans. Ant. Prop. **39**, 74-79 (1991).

5.3 A simple method for characterization of fiber Bragg gratings

Author: Johannes Skaar

A simple method for characterization of fiber Bragg gratings

Johannes Skaar

Department of Physical Electronics, Norwegian University of Science and Technology (NTNU)
N-7491 Trondheim, Norway.
johannes.skaar@fysel.ntnu.no

Abstract: A method for characterization of fiber Bragg gratings is described. The group delay and the reflectivity of the grating are obtained from measurement of the spectral reflectivity response of a Fabry-Perot structure consisting of the grating and a reference reflector. The method has been tested numerically, showing good robustness against noise. It has also been tried out experimentally, showing reproducible and promising results.

OCIS codes: (060.2340) Fiber optics components, (050.2770) Gratings.

Introduction

Characterization of fiber Bragg gratings (FBGs) means to determine the complex reflection coefficient or the complex coupling coefficient of the grating. This is not a trivial problem, and there is a large amount of different methods in the literature. The methods are usually based on interferometry, side-scattering, heat-scan or modulation (see e.g. refs [1,2] and the references therein). Whereas these techniques usually are rather complex, Froggatt found a simple approach to the characterization problem of weak gratings [3]. He showed that one can obtain the complex coupling coefficient of the grating from measurement of the interference fringes from the grating and a discrete reference reflector. In his analysis, all multiple reflections are ignored, so the method is only valid for weak gratings and reflectors. In this paper, we analyze a similar structure, namely a Fabry-Perot cavity consisting of two general reflectors, where one of them is the FBG to be characterized, and the other is a reference reflector. We will show that we can obtain the complex reflection spectrum of the FBG, or equivalently the reflectivity and group delay, from measurement of the reflectivity of the Fabry-Perot structure.

Characterization method

Consider a lossless Fabry-Perot-like system consisting of two reflectors, where one reflector has known characteristics, and the other has not. Throughout this paper, we assume that the first reflector (Section 1) is a FBG with unknown characteristics, and the other reflector is characterized and broad band compared to the other, for example a broad band FBG or a bare fiber end, see Fig.1.
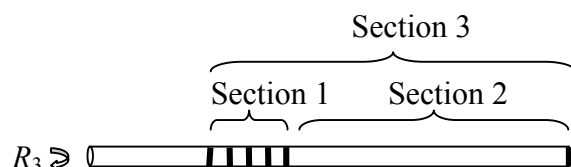
Fig. 1: Fabry-Perot cavity consisting of a fiber Bragg grating and a reference reflector.

Our idea is that the spectral periodicity of the Fabry-Perot fringes in the combined reflection spectrum R_3 is dependent on the effective cavity length. Hence, we may obtain the position of the effective reflection point in reflector 1, or equivalently the desired group delay, from measurement of R_3.

In the following section we analyze the system given in Fig. 1. We define $\delta = \beta - \beta_B$ as a detuning parameter, where β and β_B are the propagation constants for the actual wavelength and the FBG design wavelength, respectively. Furthermore l_j, r_j are the reflection coefficients from the left and the right, respectively, and t_j is the transmission coefficient, all of the jth section. Finally, we define $R_j = |r_j|^2 = |l_j|^2$ as the reflectivity, and L_j as the length of the jth section. By summing all multiple reflections in the Fabry-Perot structure, we easily realize that

$$ t_3 = \frac{t_1 t_2}{1 - r_1 l_2} = \frac{t_1 t_2}{1 - |r_1 l_2| \exp[i(\varphi + 2\delta L_2)]} \tag{1}$$

where $\varphi + 2\delta L_2 = \varphi(\delta) + 2\delta L_2 = \arg r_1 + \arg l_2$. We have explicitly written out the linear term $2\delta L_2$, which corresponds to the round trip propagation in section 2. By calculating $R_3 = 1 - |t_3|^2$, we obtain

$$ R_3(\delta) = 1 - \frac{|t_1 t_2|^2}{1 + |r_1 l_2|^2 - 2|r_1 l_2| \cos(\varphi + 2\delta L_2)} = 1 - \frac{|t_1 t_2|^2}{\left(1 + |r_1 l_2|^2\right)} \cdot \sum_{m=0}^{\infty} \left(g \cos(\varphi + 2\delta L_2)\right)^m, \tag{2}$$

where $g = g(\delta) = 2|r_1 l_2| / \left(1 + |r_1 l_2|^2\right)$. At this point, we assume that the complex reflection and transmission coefficients of the reflectors vary slowly with δ compared to the cosine term in (2). This assumption means that L_2 is so large that the Fabry-Perot fringes in $R_3(\delta)$ varies more rapidly versus δ than the reflector spectra. Then we may band pass filter $R_3(\delta)$ around the angular "frequency" $+2L_2$, obtaining the analytic signal

$$ R_{3,\text{BP}}(\delta) = -h(\delta) \exp[i(\varphi + 2\delta L_2)], \tag{3}$$

where

$$ h(\delta) = \frac{|t_1 t_2|^2}{\left(1 + |r_1 l_2|^2\right)} \cdot \sum_{m=0}^{\infty} \binom{2m+1}{m} \left(\frac{g}{2}\right)^{2m+1} = \sqrt{R_1 R_2} \frac{(1 - R_1)(1 - R_2)}{1 - R_1 R_2} \tag{4}$$

is a real, slowly varying function. Assuming that $0 < R_{1,2} < 1$, we observe that $h(\delta) > 0$. Therefore, from (3) the phase response $\varphi(\delta) = \arg R_{3,\text{BP}}(\delta) - 2\delta L_2 - \pi$ is obtained up to the trivial linear term $2\delta L_2 + \pi$ and the group delay $\tau_g = d\varphi / d\omega$ is obtained up to a constant. Note that the phase response $\varphi(\delta)$ is actually the sum of phase responses of reflector 1 and 2, so the phase response of reflector 1 is found by subtracting the phase response of reflector 2 from $\varphi(\delta)$. If reflector 2 is a bare fiber end, its phase response is zero when ignoring the linear propagation term $2\delta L_2$.

If the reflectivity $R_1(\delta)$ is not known, it may be calculated from R_2 and R_3 by taking the absolute value of eq. (3) and using (4), or by low pass filtering (2), obtaining

$$R_{3,\mathrm{DC}}(\delta) = \frac{R_1 + R_2 - 2R_1 R_2}{1 - R_1 R_2}. \tag{5}$$

As expected, the expression in (5) is symmetric in the two reflectivities, and $R_{3,\mathrm{DC}} \to R_1$ when $R_2 \to 0$. In addition, we observe from (5) that $R_{3,\mathrm{DC}} = R_1 + R_2$ only when both reflectors are weak, $R_{1,2} \ll 1$. Otherwise, the shape of the low-pass filtered Fabry-Perot spectrum will be distorted due to the terms $R_1 R_2$.

For weak reflectors, (3) and (4) reduce to $R_{3,\mathrm{BP}} = -\sqrt{R_1}\sqrt{R_2}\exp[i(\varphi + 2\delta L_2)]$. Hence if the reflection coefficient r_2 is constant with respect to frequency, $R_{3,\mathrm{BP}}$ will be proportional to the complex reflection spectrum of the fiber grating when ignoring the linear propagation phase $2\delta L_2$. The inverse Fourier transform of $R_{3,\mathrm{BP}}(\delta)$ will therefore be proportional to the complex coupling coefficient of the FBG shifted by $2L_2$, since the complex coupling coefficient and the complex reflection spectrum are Fourier transform pairs in the weak grating limit. This is consistent with the result in ref. [113], where Froggatt showed that the Fourier transform of $R_3(\delta)$ is proportional to the complex coupling coefficient for weak gratings in a certain interval. This interval is in our case $[2L_2, 2L_2 + 2L_1]$, and corresponds to the "bandwidth" we must include in the bandpass filtering of $R_3(\delta)$ above.

Note that the obtained reflection coefficient $r_1 = \sqrt{R_1}\exp(i\varphi)$ is the reflection coefficient from the right. The reflection coefficient from the left, l_1, may be calculated from r_1 using the lossless and reciprocity condition $l_1 = -r_1^* \cdot t_1 / t_1^*$ since t_1 is minimum phase [4].

To sum up the algorithm:
i)   The reflectivity $R_3(\delta)$ is measured for the desired wavelength interval.
ii) $R_3(\delta)$ is Fourier transformed. The result is multiplied by a filtering window function centered at the peak corresponding to the angular frequency $+2L_2$. The choice of a window function is not crucial, however its width should be according to the descriptions below. $R_{3,\mathrm{BP}}(\delta)$ is subsequently computed by an inverse Fourier transform.
iii)   The phase response $\varphi(\delta) = \arg R_{3,\mathrm{BP}}(\delta)$ and the group delay $\tau_g = d\varphi/d\omega$ is calculated.
iv)   If desirable, R_1 may be computed using eq. (5).

The window function must be sufficiently wide so that the phase modulation of the Fabry-Perot fringes due to $\varphi = \varphi(\delta)$ is included, but so narrow that the higher order variation in (2) is removed. This compromise is possible when $\varphi(\delta)$ varies slowly compared to $2\delta L_2$. In practice however, the important compromise is between numerical stability and resolution in $r_1(\delta)$. If large resolution in $r_1(\delta)$ is desirable, the window function must be correspondingly wide. On the other hand, the stability of the method increases with decreasing window width, as more noise is suppressed.

Numerical and experimental examples

In order to test our algorithm, we analyze a structure consisting of a raised cosine apodized, 0.5nm linear chirped FBG of length $L_1 = 2\,cm$, an end reflection of 3.5%, and a cavity length $L_2 = 5\,cm$. The spectral responses $r_1(\delta)$ and $l_3(\delta)$ is calculated using transfer matrix and coupled mode theory [5]. From the calculated spectrum $R_3 = |l_3|^2$ we construct the "measured" data including noise

$$R_m(\delta) = R_3(\delta)\big(1 + An_s(\delta)\big) + An_d(\delta), \tag{6}$$

where n_s and n_d are realizations of Gaussian processes with mean 0 and variance 1. The 1000 noise samples in (6) are independently distributed. We construct the "measured" R_m in this way to simulate source and detector noise in a measurement process with a scanning DBR laser. The reflectivity R_1 of the FBG, and R_m are shown in Fig. 2. By applying R_m as input to our algorithm, we compute the group delay, and compare to the original group delay resulting from the coupled mode theory. The size of the filtering window (Blackman window) has been chosen so that the wavelength resolution of $r_1(\delta)$ becomes approximately 30pm. The resulting group delays for $A = 0$ and $A = 0.02$ are shown in Fig. 3, demonstrating that the reconstructed group delays only have small errors for both the noisy and noise-free situation. The reconstructed group delay is not identical to the true group delay for noise-free input data because we have filtered away some information of R_3 through the use of the window function. This fact demonstrates the trade-off between accuracy and stability. Because we want high stability, we sacrifice some of the accuracy in the sense that rapid variation in $r_1(\delta)$ is lost.
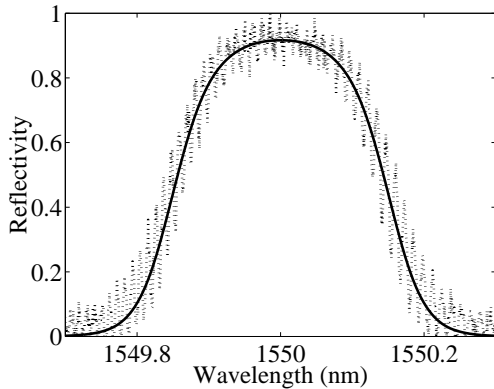
Fig. 2: The dotted curve shows the reflectivity R_m of the Fabry-Perot configuration including errors according to eq. (6) with A=0.02. The solid curve represents the reflectivity R_1 of the apodized, linearly chirped FBG.
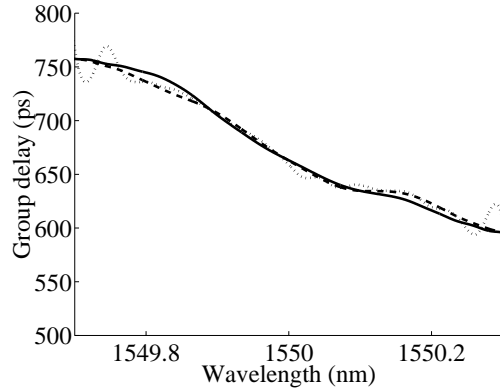
Fig. 3: Retrieved group delays (dashed and dotted curves) compared to the true group delay of the FBG (solid curve). The dotted curve is computed from noisy data (A=0.02), whereas the dashed curve is computed from noise-free data.

We also note the requirements of the scanning DBR laser. Because it must be able to resolve the Fabry-Perot fringes, its resolution should be roughly

$$\Delta\lambda = \frac{\lambda^2}{2L_3 n_{\text{eff}}} \qquad (7)$$

where n_{eff} denotes the effective index of refraction in the core. For our case, (7) yields a resolution of about 13pm.

Finally, we have measured the reflectivity spectrum of a configuration consisting of an apodized FBG and a bare end reflection using a scanning DBR laser. The resulting spectrum is applied as input to our algorithm. The experiment is repeated several times in order to test its reproducibility. The results for three measurements are shown in Fig. 4 and Fig. 5. As can be seen, the reproducibility is good in the area where the reflectivity of the grating is significantly different from zero. Outside the grating spectrum however, the reproducibility is bad, as expected from (3) and (4) since the amplitude of the Fabry-Perot fringes h is near zero. Moreover, we observe a "DC" level of roughly 650ps. This corresponds to about 13cm propagation in the fiber, which means that the distance between the average effective reflection point in the grating and the bare fiber end is about 6.5cm.
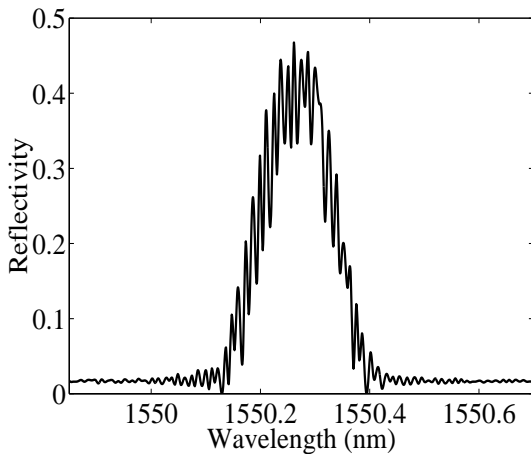
Fig. 4: Measured reflectivity of an apodized FBG and the end reflection.
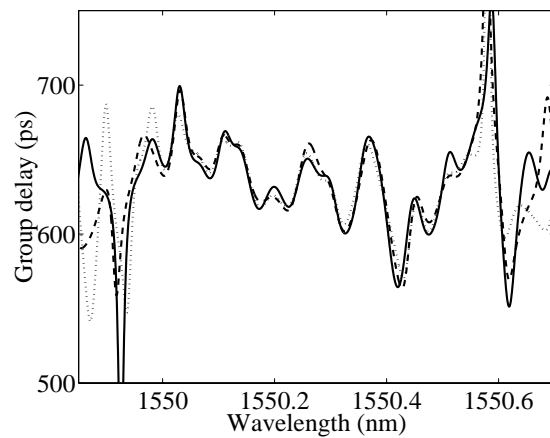
Fig. 5: Retrieved group delay of an apodized FBG. The three curves correspond to three independent measurements.

This characterization method may also be used for distributed intragrating sensing, since a distributed strain or temperature profile, or equivalently the local Bragg wavelength of reflector 1 may be calculated from the complex reflection spectrum r_1 by using an inverse scattering algorithm (or an inverse Fourier transform in the case of weak FBG).

Conclusion

We have developed a method for characterization of FBGs. By measuring the spectrum of a FBG interfering with a bare end reflection, the group delay can be computed for all wavelengths where the reflectivity of the grating is not very close to 0 or 1.

Acknowledgements

References

1. N. Roussel, S. Magne, C. Martinez, and P. Ferdinand, "Measurement of index modulation along fiber Bragg gratings by side scattering and local heating techniques," Opt. Fiber. Tech. 5, 119-132 (1999).
2. D. Sandel, R. Noé, G. Heise, and B. Borchert, "Optical network analysis and longitudinal structure characterization of fiber Bragg grating," IEEE J. Lightwave Tech. 16, 2435-2442 (1998).
3. M. Froggatt, "Distributed measurement of the complex modulation of a photoinduced Bragg gratings in an optical fiber," Appl. Opt. 35, 5162-5164 (1996).
4. L. Poladian, "Group delay reconstruction for fiber Bragg gratings in reflection and transmission," Opt. Lett. 22, 1571-1573 (1997).
5. T. Erdogan, "Fiber grating spectra," IEEE J. Lightwave Tech. 15, 1277-1294 (1997).
6. J. Skaar, "Measuring the group delay of fiber Bragg gratings by use of end-reflection interference," Opt. Lett. 24, 1020-1022 (1999).

5.4 Characterization of fiber Bragg gratings by use of optical coherence-domain reflectometry

Authors: I. Petermann, J. Skaar, B. Sahlgren, R. Stubbe, and A. Friberg

Characterization of Fiber Bragg Gratings by Use of Optical Coherence-Domain Reflectometry

E. Ingemar Petermann, *Student Member, IEEE,* Johannes Skaar, *Student Member, OSA,* Bengt E. Sahlgren, Raoul A. H. Stubbe, *Member, OSA,* and Ari T. Friberg, *Fellow, OSA*

Abstract—A method based on optical low coherence reflectometry for complete characterization of fiber Bragg gratings (FBG's) is presented. It is shown that the measured signal corresponds to the impulse response of the grating filter, and the measurement therefore yields all information about the device. Experiments have been carried out with a novel dual-channel interferometer. The results are in excellent agreement with the theory, demonstrating the versatility of the method for characterization of fiber gratings.

Index Terms—Gratings, interferometry, optical fibers, optical fiber measurement, optical interferometry, reflectometry.

I. INTRODUCTION

SINCE the demonstration of the transverse holographic method in 1989 [1], many improvements have been realized for the fabrication of fiber Bragg gratings (FBG's). In particular, new methods to produce long gratings with complex structures have been developed [2], [3]. Long fiber gratings are very sensitive to perturbations and require a practical characterization method for their actual refractive index envelope and local periodicity. One method of characterizing FBG's is to measure the reflection spectrum with a spectrum analyzer. However, this does not yield a complete characterization unless the phase response is obtained as well. Another characterization method is optical coherence-domain reflectometry (OCDR), which in recent years has been used in several ways to perform measurements on fiber gratings [4], [5].

Using a frequency-domain method it has recently been established that optical low coherence reflectometry (OLCR) is directly related to the inverse Fourier transform of the complex reflection spectrum of the device under test [6]. In this paper, we restate this fact in the frame work of linear systems theory and use the result to fully characterize fiber Bragg gratings. The advantage of our method is its simplicity and generality.

Once the complex reflection spectrum is calculated from the measured OLCR data using the Fast Fourier Transform (FFT), the index modulation profile (both amplitude and phase), which is proportional to the coupling coefficient in coupled mode theory, may be obtained with the help of an inverse scattering method. In particular, a numerical solution to the Gel'Fand–Levitan–Marchenko (GLM) coupled equations is well suited for this problem [7]. However, the inverse scattering problem is ill-posed, and may give inaccurate results in the case of strong gratings and noisy data. In the case of weak gratings, the coupling coefficient and the reflection spectrum are simply a Fourier transform pair [8], so the complex envelope of the OLCR data directly corresponds to the complex coupling coefficient.

In order to verify the theory, measurements have been carried out with aid of a novel dual-channel interferometer. The two channels are used to produce differential data, thus reducing the system noise. A number of different gratings with easily predictable profiles have been analyzed and for one grating, the reflection spectrum has also been obtained with a tunable DBR laser yielding the same result as with our method.

A rigorous mathematical analysis of the OLCR characterization method is given in the Appendix. Section II contains a description of the experiments and the obtained results. The main conclusions are summarized in Section III.

II. EXPERIMENTS

A. Experimental Setup

A verification of the theory was carried out using a two-channel interferometer capable of interrogating a test grating at two positions simultaneously. By using the information from two positions, it is possible to make differential measurements with the benefit of suppressing noise due to, e.g., thermal fluctuations in the system itself. Of course this somewhat limits the spatial (phase) measurements that can be performed in the front and rear parts of the grating, but this information is in most cases not so important.

A schematic two-dimensional (2-D) drawing showing the working principle of the interferometer is depicted in Fig. 1 (for a detailed description, see [9]). The light from the source and grating under study is split into two channels by beamsplitter a. A translatable retroreflector b is used to alter the length of both reference paths simultaneously. A second retroreflector c changes the distance between the two interrogation points in the grating by increasing the reference path length in one channel and the length of the test path in the other. Each channel is split into two complementary outputs that are fed into differential detectors. The electrical signal from each detector is then proportional to the corresponding interference
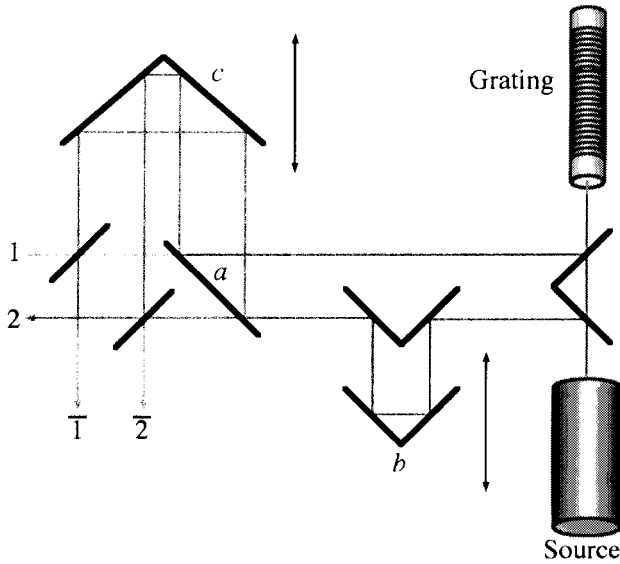
Fig. 1. Schematic 2-D equivalent drawing of the interferometer. Each channel has two complementary outputs.

signal. As shown in the Appendix, this signal is directly related to the real part of the impulse response of the investigated grating.

In all experiments, both interrogation points were scanned simultaneously along the grating and from the resulting data, the differential phase between these points throughout the grating was calculated. For a fiber Bragg grating the impulse response can be written on the form

$$h_c(\tau) = h_{\mathrm{env}}(\tau) e^{i\omega_b \tau} \qquad (1)$$

where

$$h_{\mathrm{env}}(\tau) = |h_{\mathrm{env}}(\tau)| e^{i\Phi(\tau)} \qquad (2)$$

is the complex slowly-varying envelope of the impulse response and ω_b the average Bragg frequency. In this context, it is convenient to view the impulse response as a function of scanning position instead of time, i.e.

$$h_c(z) = h_{\mathrm{env}}(z) e^{i\omega_b n_{\mathrm{eff}} z/c} \qquad (3)$$

where c is the speed of light in vacuum and n_{eff} the effective refractive index in the fiber.

In a general case, the absolute value and phase of the envelope in (2) is obtained by first calculating the imaginary part of the impulse response from its experimentally determined real part using the Hilbert transform. Since the impulse response of a grating is approximately sinusoidal with the Bragg frequency ω_b, the absolute value of $h_{\mathrm{env}}(z)$ may in the present case instead be approximated by the average of the local maxima of the real part in the vicinity of z. Accordingly, if the distance between the two interrogation points is denoted by d and the measured phase difference by $\Delta\Phi(z)$, the phase $\Phi(z)$ of the impulse response envelope is taken as

$$\Phi(z) = \int^z \frac{\Delta\Phi(z)}{d}\, dz \qquad (4)$$
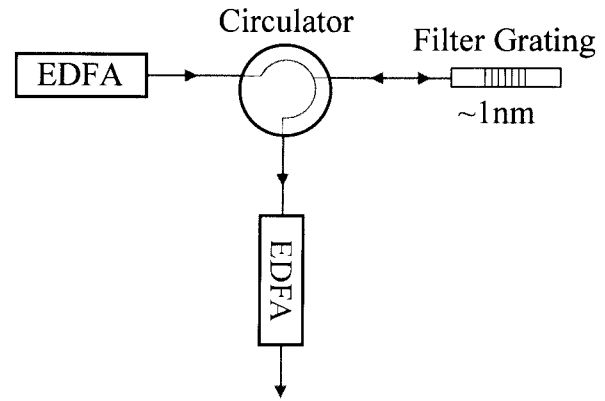
Fig. 2. White light source used in fiber grating characterization.

or, since we are dealing with sampled data

$$\Phi(z_n) = \sum_{i=1}^{n} \frac{\Delta\Phi(z_i)}{d} \Delta z \qquad (5)$$

where z_i is the i:th sample, n is the number of samples and Δz is the spatial distance between two samples.

The white light source used for the measurements consisted of two erbium-doped fiber amplifiers and a filter grating connected as shown in Fig. 2. The ASE of the first amplifier is guided to the filter through a circulator, is reflected, and then amplified by the second amplifier. With a filter grating bandwidth of 1 nm, the light eventually reaching the interferometer has a (vacuum) coherence length of approximately 1 mm and a power of several mW.

If only one channel is used, this coherence length determines the spatial resolution that can be obtained. When obtaining differential measurements, however, this is not the case. The spatial resolution is then rather determined by the sample distance Δz as well as by the resolution of the detectors. Furthermore, spatial variations with a period corresponding to a multiple of the distance between the two interrogation points will be suppressed.

The time it takes to obtain one measurement is only limited by the speed of the scanning movement and the sampling frequency for a given sample distance Δz. In our experiments, we used a scanning speed of approximately 0.25 mm/s and a sampling rate near the Nyqvist limit. For a typical 10 cm long grating the whole process of obtaining raw data and calculating the phase difference and envelope then took less than 10 minutes using a 200 MHz Pentium computer. Of course this time can be substantially shortened by using higher translation speeds and more powerful computer and data acquisition hardware.

B. Results

Some preliminary experiments confirming the functionality of the setup are given in [10]. Furthermore, a weak uniform grating containing three phase shifts of magnitudes $-90°$, $+90°$ and $-50°$ was fabricated. As can be seen in Fig. 3, a differential measurement with the interferometer yields three peaks corresponding to the phase shifts. Without the phase shifts, the curve would be a straight line with an offset
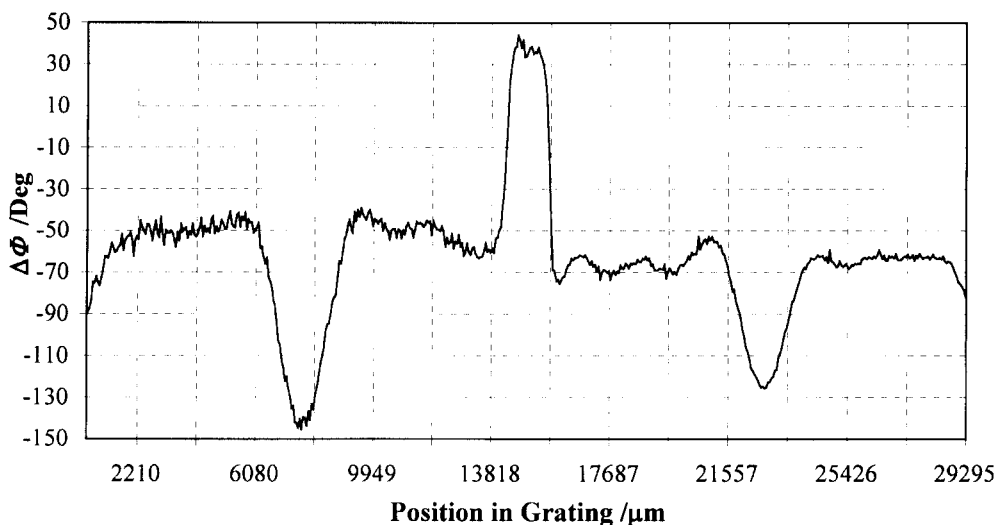
Fig. 3. Measured phase difference for a uniform grating with phase shifts $-90°$, $+90°$ and $-50°$.
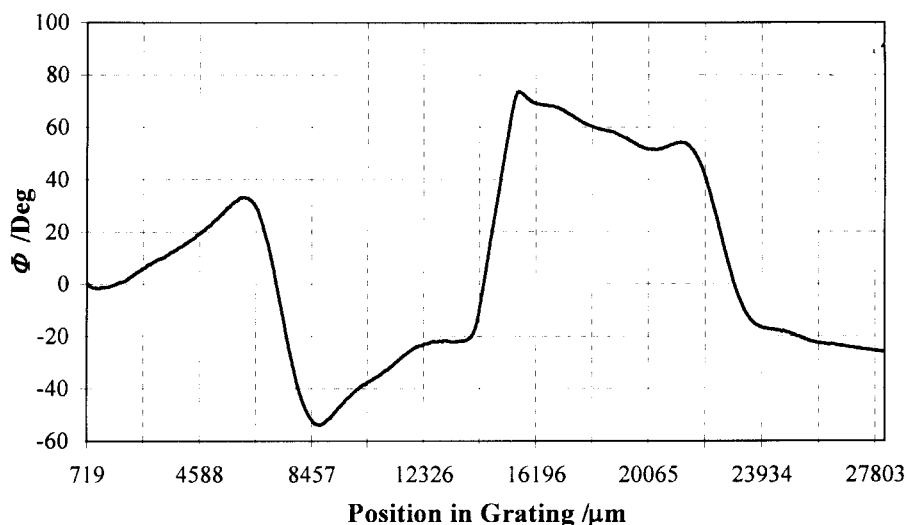
Fig. 4. Phase of the index modulation of the grating from Fig. 3.

depending on the distance between the interrogation points. In the present case, the phase difference decreases by 90° as soon as the first interrogation point passes the first phase shift. When the second interrogation point follows, the difference returns to the initial value. As long as the distance between these points is larger than the coherence length of the source, the FWHM of these peaks can thus be used to estimate the distance. In the present case it is approximately 1.5 mm (cf. Fig. 3). A slow modulation of the phase that lowers the constant level by about 20° toward the end of the grating can be seen. The most probable cause of this is that the fiber was not perfectly aligned during the writing process.

Since the grating is weak, the phase of the index modulation is directly obtained by integrating the phase difference. The phase difference offset gives rise to an unwanted linear term that can be eliminated by choosing a suitable zero level. This corresponds to moving the reference plane for the reflection coefficient, or equivalently adding a constant time delay. The phase difference zero level is in this case set to 60°, which

gives a modulation phase according to Fig. 4, where the three phase shifts once again clearly can be seen.

Fig. 5 shows the impulse response envelopes, which in this case are the same as the index modulation envelopes measured by the two channels. Since a phase shift works as a broad band reflector within the grating, there is a peak (positive or negative) for each phase shift in the envelope as well. As seen from (A11) and (A12) these unwanted peaks are obviously due to the fact that the source spectrum $S(\omega)$ is not constant for all frequencies at which the reflection spectrum $r(\omega)$ is significantly different from zero, i.e., the source is not entirely "white". The peaks can therefore be reduced by using a light source with broader spectrum.

Fig. 6 shows the phase difference data for a 10 cm long chirped grating. As can be seen, there is a slowly varying modulation on the signal here as well. As expected, the average derivative is not zero as was the case for a uniform grating. In order to simulate a simple sensor, another measurement was done on the same grating when heating one end with a
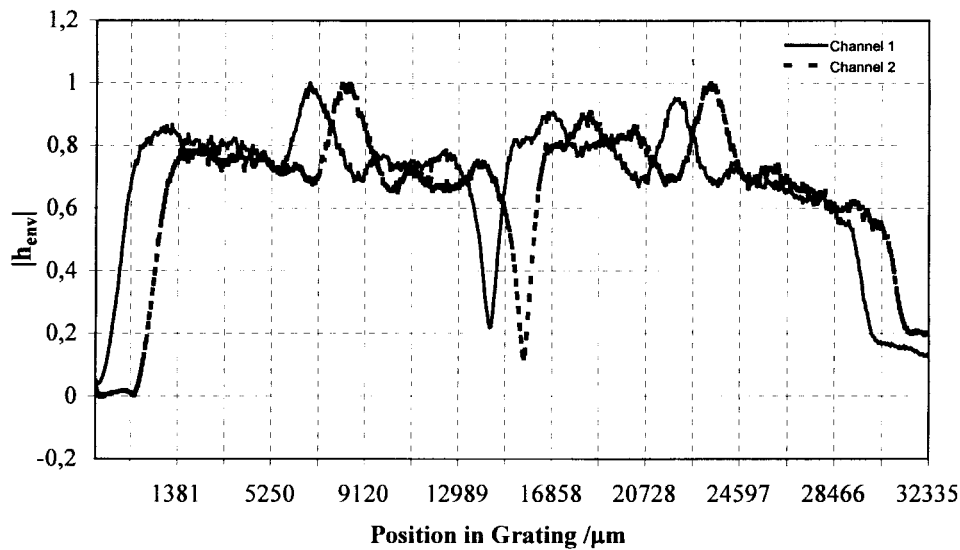
Fig. 5. Impulse response envelopes from the two channels for the grating in Fig. 3.
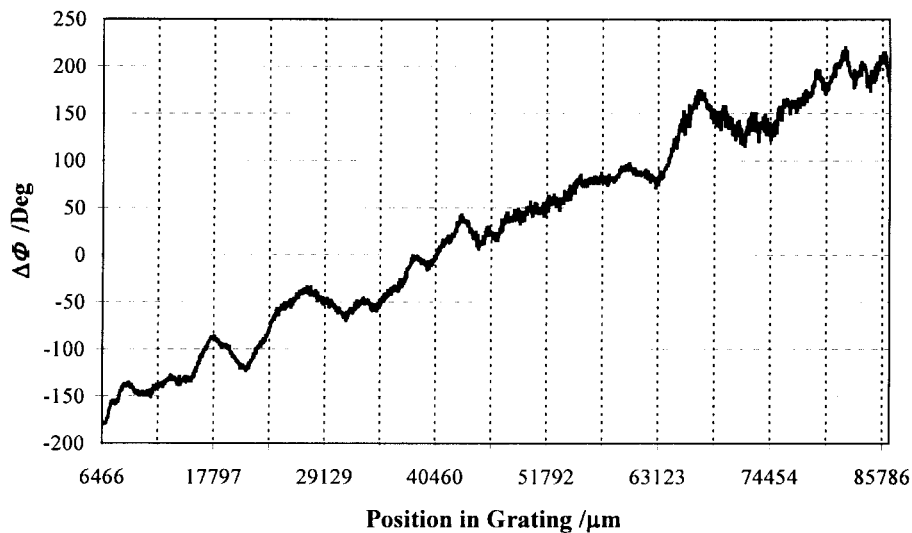
Fig. 6. Measured phase difference for a 10-cm chirped grating.

soldering iron, thus changing the chirp profile according to the heat gradient. The difference of these two measurements is plotted in Fig. 7. Obviously, this data could be used to determine the heat gradient along the fiber. This particular experiment was merely done to show the principle, though, and no proportionality constant between chirp and heat was calculated. The induced chirp happened in this case to be of the same orther of magnitude, but with a different sign, as compared to the original chirp. The slow modulation disappears due to the subtraction in this plot and the noise in the measurement is revealed. Evidently, the fluctuation is typically ±25°.

Performing a Fourier transform on the measured impulse response of the unheated grating yields the reflectance spectrum depicted in Fig. 8. The group delay is defined as the derivative of the phase spectrum with respect to frequency and can be seen in Fig. 9. As expected, the linearly chirped grating yields a group delay curve that is almost linear with a slope

that corresponds to the chirp. As a last experiment, a weak uniform 10 cm grating with Bragg wavelength 1551.1 nm was fabricated. The reflectance spectrum as calculated from the white light interferometer data is given by the solid line in Fig. 10. The spectrum of the same grating was also measured with a tunable DBR-laser with a result corresponding to the dashed line in Fig. 10. As can be seen, the agreement between these two measurements is excellent. In Fig. 11, the group delay calculated from the interferometer data is shown. As opposed to the group delay spectrum for a chirped grating, this is more or less constant. The peaks are caused by the phase shifts that occur when the reflectance spectrum equals zero.

III. CONCLUSION

It has been shown, theoretically as well as experimentally, that low coherence interferometry is a versatile tool for characterizing fiber Bragg gratings. The output of the interferometer corresponds to the impulse response of the grating. From
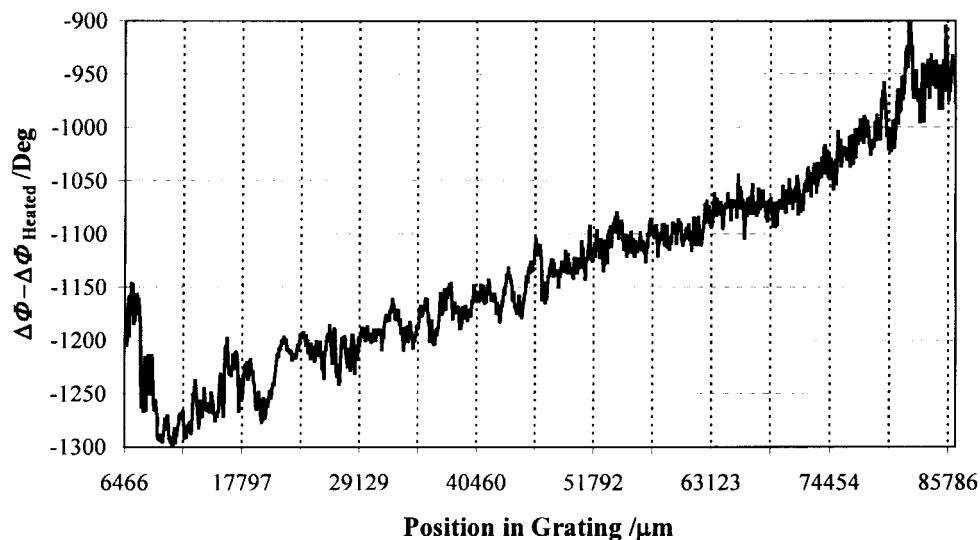
Fig. 7. Subtraction of a second measurement with heated grating from the data in Fig. 6 reveals the noise to be typically $\pm 25°$.
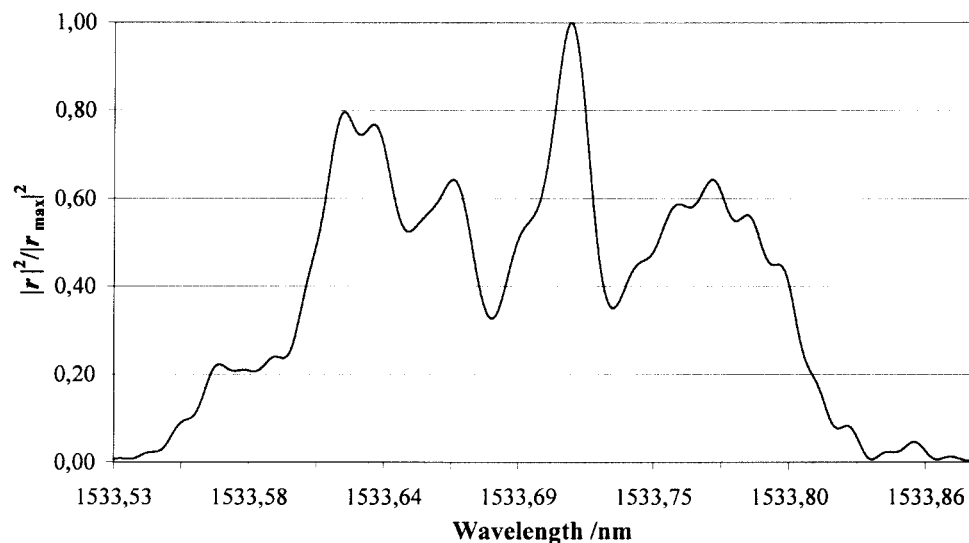
Fig. 8. Reflectance spectrum of the same chirped grating as in Fig. 6.

this, we obtain the reflection spectrum and the group delay spectrum. In the case of a weak grating, the measured impulse response directly corresponds to the index modulation amplitude and phase (or the complex coupling coefficient). For stronger gratings it is necessary to use an inverse scattering method to obtain the same spatial information.

In the experimental verifications, a dual-channel interferometer has been used, giving the benefit of reducing noise originating from e.g. thermal fluctuations in the interferometer itself. The measurements show a noise corresponding to approximately $\pm 25°$ in spatial phase. This value is by no means a limit: most of the noise probably comes from fluctuations in the velocity of the scanning interferometer arm and further improvements to this movement would probably also take away a substantial part of the noise.

APPENDIX

The basis of the theory is an ordinary Michelson interferometer used with a white light source as shown in Fig. 12. In

the following, we apply a linear systems approach to derive the important result that the detector signal as a function of reference mirror position corresponds to the impulse response of the device under investigation.

At a given point the light from the source is represented by a random complex field $E(t)$. It is characterized by the autocorrelation function

$$\Gamma_{EE}(\sigma) = \langle E^*(t)E(t+\sigma) \rangle \qquad (A1)$$

where $\langle \cdots \rangle$ denotes the time average. Light coming from the interferometer arm containing the fiber grating will interfere with light from the (broadband) reference mirror at the beamsplitter. Each arm is characterized by a respective impulse response, which for the reference arm is a simple time delay τ corresponding to the time it takes for the light to travel twice the length of the arm. According to the theory of linear systems [11], the electric fields at the beamsplitter are thus given by

$$E_1(t) = E(t - \tau) \qquad (A2)$$
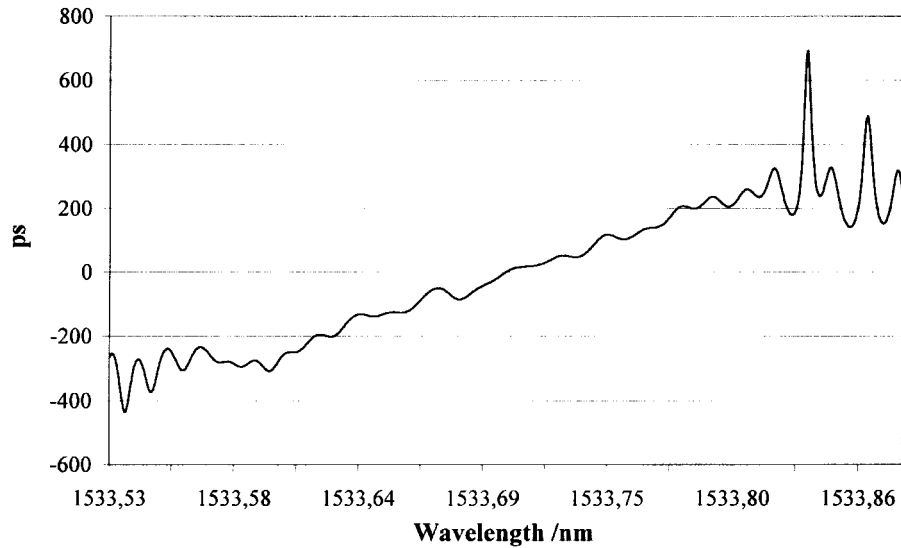
Fig. 9. Group delay for the chirped grating in Fig. 6.
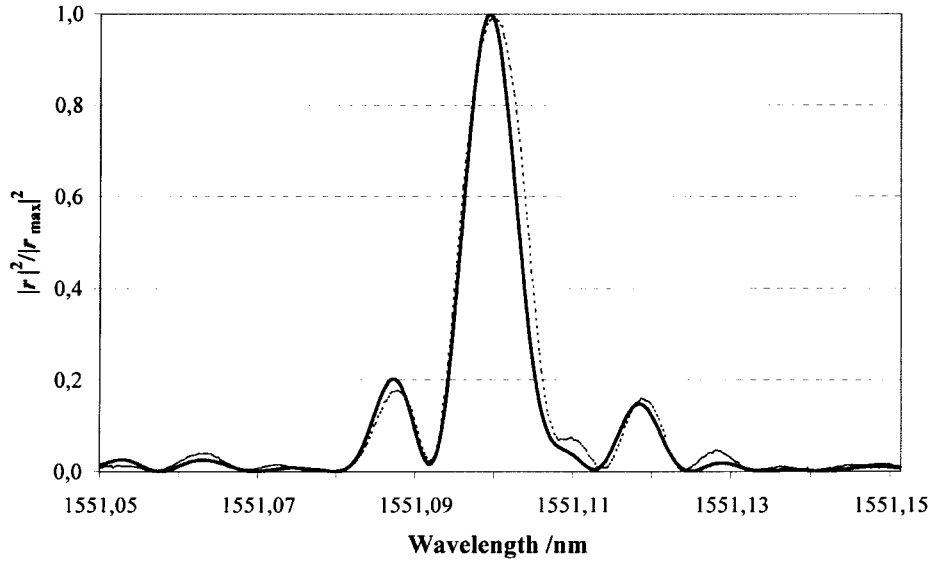
Fig. 10. Reflectance spectrum of a uniform grating, calculated from the OCDR data (solid curve), and measured by the DBR laser (dashed curve).

and

$$E_2(t) = E(t) * h_c(t) = \int_{-\infty}^{\infty} E(t')h_c(t-t')\,dt' \qquad \text{(A3)}$$

where $*$ denotes the convolution integral and $h_c(t)$ is the complex impulse response of the interferometer arm containing the device under investigation. Note that $h_c(t-t') = 0$ for $t < t'$ due to causality. The total field at the beam splitter becomes

$$E_{12}(t) = E_1(t) + E_2(t). \qquad \text{(A4)}$$

We are interested in the detector signal, which is proportional to the average power of $E_{12}(t)$

$$\begin{aligned} I_{\text{det}}(\tau) &= \langle |E_{12}(t)|^2 \rangle \\ &= \langle |E_1(t)|^2 \rangle + \langle |E_2(t)|^2 \rangle + 2 \cdot \Re \langle E_1^*(t)E_2(t) \rangle \end{aligned}$$

$$\text{(A5)}$$

$\Re$ denoting the real part. The first two terms in (A5) are trivial, since they are constant powers independent of the delay τ. We recognize the last interference term as a cross-correlation of $E_1(t)$ and $E_2(t)$, which will be dependent of τ, i.e.

$$I(\tau) \equiv \Re \langle E_1^*(t)E_2(t) \rangle = \Re \Gamma_{E_1 E_2}(0). \qquad \text{(A6)}$$

This interference detector signal is determined by the properties of the source field $E(t)$, impulse response $h_c(t)$ and delay τ.

On substituting (A2) and (A3) into the expression for $\Gamma_{E_1 E_2}(0)$ obtained in analogy with (A1), we find

$$\Gamma_{E_1 E_2}(0) = \left\langle E^*(t-\tau) \cdot \int_{-\infty}^{\infty} E(t')h_c(t-t')\,dt' \right\rangle. \qquad \text{(A7)}$$

Since the source has a finite power, the mean-square value $\langle |E(t)|^2 \rangle$ is finite for all t and we may interchange the order
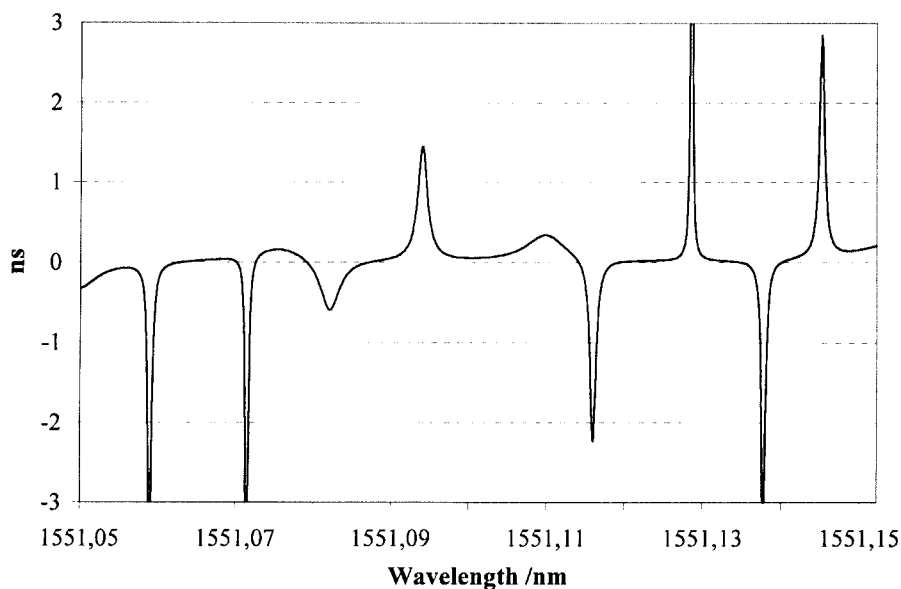
Fig. 11. Group delay for the uniform grating in Fig. 10.
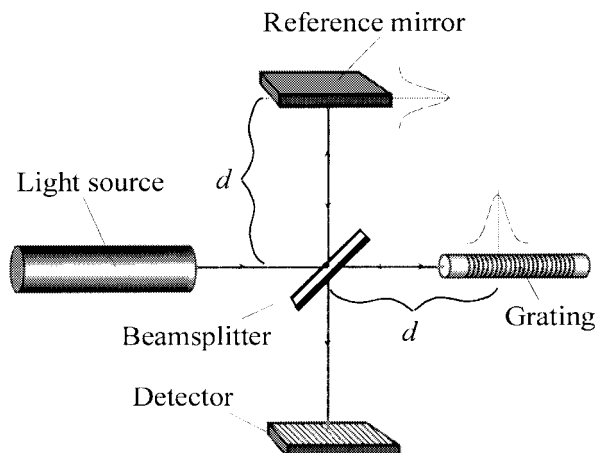
Fig. 12. White light interferometer.

of averaging and integration [11]

$$\Gamma_{E_1 E_2}(0) = \int_{-\infty}^{\infty} \langle E^*(t - \tau)E(t - t') \rangle h_c(t') \, dt'$$

$$= \int_{-\infty}^{\infty} \Gamma_{EE}(\tau - t')h_c(t') \, dt' \qquad (A8)$$

where the last equality follows from (A1) and noting that $E(t)$ is stationary.

By Fourier transforming (A8), we obtain

$$F\{\Gamma_{E_1 E_2}(0)\} = r(\omega) \cdot S(\omega) \qquad (A9)$$

where $S(\omega) = F\{\Gamma_{EE}(t)\}$ is the power spectral density of the source due to the Wiener–Khintchine theorem and $r(\omega) = F\{h_c(t)\}$ is the reflection coefficient of the device under investigation. Hence

$$\Gamma_{E_1 E_2}(0) = F^{-1}\{r(\omega) \cdot S(\omega)\} \qquad (A10)$$

and

$$I(\tau) = \Re F^{-1}\{r(\omega) \cdot S(\omega)\}. \qquad (A11)$$

The same formula is also deduced in the frequency domain in [6]. Note that the result is general and valid for any optical filter and source spectrum.

Now, in OLCR the spectral bandwidth of the source is often much larger than the bandwidth of the device under investigation. Hence $S(\omega)$ may be treated effectively as a constant near the Bragg frequency $\omega = \omega_b$ characterizing the grating, yielding

$$I(\tau) = \Re S(\omega_b) \cdot F^{-1}\{r(\omega)\}. \qquad (A12)$$

Since $S(\omega)$ is real, we obtain

$$I(\tau) = \text{const} \cdot \Re h_c(\tau). \qquad (A13)$$

Hence, ignoring a background power, the data from the white light interferometer corresponds to the real part of the impulse response of the device under investigation, provided the spectrum of the source is constant over the device bandwidth. The imaginary part of $h_c(\tau)$ is generally obtained from the real part in terms of the Hilbert transform [12].

References

[1] G. Meltz, W. W. Morey, and W. H. Glenn, "Formation of Bragg gratings in optical fibers by a transverse holographic method," *Opt. Lett.*, vol. 14, no. 15, p. 823, 1989.

[2] A. Asseh, H. Storøy, B. E. Sahlgren, S. Sandgren, and R. Stubbe, "A writing technique for long fiber Bragg gratings with complex reflectivity profiles," *J. Lightwave Technol.*, vol. 15, pp. 1419–1423, 1997.

[3] M. J. Cole, W. H. Loh, R. I. Laming, M. N. Zervas, and S. Barcelos, "Moving fiber/phase mask-scanning beam technique for enhanced flexibility in producing fiber gratings with uniform phase mask," *Electron. Lett.*, vol. 31, no. 17, p. 1488, 1995.

[4] M. Volanthen, H. Geiger, M. J. Cole, R. I. Laming, and J. P. Dakin, "Low coherence technique to characterize reflectivity and time delay as a function of wavelength within a long fiber grating," *Electron. Lett.*, vol. 32, no. 8, pp. 757–758, 1996.

[5] P. Lambelet, P .Y. Fonjallaz, H. G. Limberger, R. P. Salathé, C. Zimmer, and H. H. Gilgen, "Bragg grating characterization by optical low-coherence reflectometry," *IEEE Photon. Technol. Lett.*, vol. 5, p. 565, 1993.

[6] U. Wiedmann, P. Gallion, and G.-H. Duan, "A generalized approach to optical low-coherence reflectometry including spectral filtering effects," *J. Lightwave Technol.*, vol. 16, pp. 1343–1347, July 1998.

[7] P. V. Frangos and D. L. Jaggard, "A numerical solution to the Zakharov-Shabat inverse scattering problem," *IEEE Trans. Antennas Propagat.*, vol. 39, pp. 74–79, 1991.
[8] H. Kogelnik, "Filter response of nonuniform almost-periodic structures," *Bell Syst. Tech. J.*, vol. 55, pp. 109–126, 1976.
[9] I. Petermann, "Fiber grating analysis with white light interferometry," Master's thesis, Royal Inst. Technol., Stockholm, Sweden, TRITA-FYS 2167, ISSN 0280-316X, 1997.
[10] I. Petermann, B. Sahlgren, J. Skaar, P.-Y. Fonjallaz, and R. Stubbe, "Phase distribution measurement of fiber Bragg gratings with white light interferometry," in *Proc. 24th European Conf. Optic. Commun.*, Paper WdA09, 1998, pp. 399–340.
[11] S. Haykin, *Communication Systems*, 3rd ed.   New York: Wiley, 1994.
[12] G. Arfken, *Mathematical Methods for Physicists*, 3rd ed.   New York: Academic., 1985.

E. Ingemar Petermann (S'98) was born in Österhaninge, Sweden, in 1972. He received the M.Sc. degree in engineering physics from the Royal Institute of Technology, Stockholm, Sweden, in 1997 and is currently pursuing the Ph.D. degree at ACREO AB, Stockholm, in cooperation with the Department of Physics—Optics at the same university.

His main research interests are characterization of fiber Bragg gratings and modeling and simulation of wave propagation in periodical structures.

Johannes Skaar, photograph and biography not available at the time of publication.

Bengt E. Sahlgren was born in Stockholm, Sweden, in 1960. He received the M.Sc. degree in mechanical engineering from the Royal Institute of Technology, Stockholm, in 1987.

He is currently employed as a Research Scientist at ACREO AB, Stockholm. He has ten years of scientific experience in the field of fiber optics. His main research interests are manufacturing techniques of fiber Bragg gratings and fiber optical sensor systems.

Mr. Sahlgren is a member of the European Optical Society and the Swedish Optical Society.

Raoul A. H. Stubbe was born in Norrköping, Sweden, in 1961. He received the M.Sc. and Ph.D. degrees in engineering physics from the Royal Institute of Technology, Stockholm, Sweden, in 1985 and 1991, respectively.

He is currently employed as a Research Scientist at ACREO AB, Stockholm. He has more than ten years of scientific experience in fiber optics and holds several patents in the field. His main interest is applications of fiber Bragg gratings for optical sensor systems and telecommunication.

Dr. Stubbe is a member of the European Optical Society, the Swedish Optical Society, and the Optical Society of America (OSA).

Ari T. Friberg received the Ph.D degree in optics from the University of Rochester, Rochester, NY, in 1980 and the Ph.D. degree in technical physics from the Helsinki University of Technology, Helsinki, Finland, in 1993.

He has worked at universities in Helsinki, Rochester, London, U.K., and Berlin, Germany. In the 1990's, he was with the Academy of Finland before being appointed Professor of Physics at the University of Joensuu, Finland. Since 1997, he has been Professor of Physics at the Royal Institute of Technology, Stockholm, Sweden. His main research interests deal with physical optics, coherence, and laser technology.

Dr. Friberg is a Fellow of the Optical Society of America (OSA), as well as a Topical Editor of the *Journal of the Optical Society of America* and Associate Secretary of ICO.

Chapter 6

Thesis summary and future work

In this chapter we will summarize the previous chapters with a special emphasize on the results. We will also try to draw lines into the future.

6.1 Summary

In Chapter 2 we derived the coupled-mode equations that govern the coupling between the forward and backward propagating waves in a fiber grating. The connection between the mathematical model and the physical grating was examined. We defined the complex coupling coefficient $q(z)$ and found that its modulus and phase correspond to the index modulation amplitude and phase, respectively. Once the mathematical model was established, we could use it as a starting point for analyzing the reflection and transmission response of an arbitrary grating. We observed that there is a Fourier relation between the coupling coefficient and the reflection spectrum for weak gratings. For uniform gratings we found exact closed-form expressions for the reflection and transmission coefficients. When analyzing nonuniform, general gratings, one must use numerical tools as the well-known numerical integration method or the transfer-matrix method. As an alternative, we also presented a discrete method that is the direct counterpart to the discrete layer-peeling algorithm for the inverse (synthesis) problem. We ended this chapter by examining the different mathematical properties of the reflection and transmission spectra in addition to some properties of the transform between $q(z)$ and the spectra.

Chapter 3 was devoted to the inverse scattering problem of finding the grating structure from a desired, complex reflection spectrum. First we applied a genetic algorithm to the problem. In this optimization method, each grating corresponds to an individual. By evolution through several generations, the performance of the individuals (gratings) becomes better. The performance or fitness of the individuals was computed by a merit function. The method is general and it is easy to weight different trade-offs as for example dispersion and skirt steepness. The main disadvantage is the computing time; it is considerably slower than most other approaches to the synthesis problem.

The next paper in this chapter contained a description of the layer-peeling algorithm for designing gratings. The essence of this method is the following causality argument: The impulse response of the grating evaluated at time $\tau = 0^+$ corresponds directly to

the front end of the coupling coefficient since the light does not have time to propagate deeper into the structure. Since the initial segment of $q(z)$ now can be determined, one can propagate the fields to the next section using the coupled-mode equations or the transfer matrix. Then, one is in the same situation as at the beginning, since the effect of the first layer is "peeled off". The process is continued until the entire grating structure is reconstructed. In our paper we described two variants of the same method, what we called the discrete and continuous layer-peeling algorithm. The discrete technique was simplified compared to a previously published version of it, and it was shown how it can be implemented exactly on a computer once the grating model is discretized into a stack of discrete reflectors. Moreover, the continuous version was derived and an error in the literature was corrected. The discrete and continuous variants were compared, and we found that the discrete layer-peeling algorithm is significantly faster than its continuous counterpart, whereas the continuous algorithm offers some advantages in flexibility.

To demonstrate the generality of the layer-peeling inverse scattering approach, we utilized it for the design of optical thin-film filters in the last paper of Chapter 3. We designed both filters consisting of arbitrary index layers (with indices ranging between certain limits) and filters consisting of layers with only two different indices. Since the algorithm is so fast, it is particularly useful for filters with many layers.

Chapter 4 contained a similar synthesis problem. We designed grating filters working in transmission with an arbitrary complex response inside a finite bandwidth. The synthesis problem turned out to be that of obtaining a minimum phase transfer function approximating a desired, complex function in a finite interval. In the first paper, we solved this general continuation problem and developed a numerical algorithm. Dependent on the required asymptotic behavior of the transfer function at infinite frequency, we got two different variants of the method. For asymptotic value different from zero, the synthesis method was completely general and rigorous. For asymptotic value equal to zero, the method was not suitable for all kinds of filters as the designed filters in some cases get large energy.

The minimum phase design method was then applied to the synthesis of fiber gratings in the next paper. The algorithm was modified to obtain a passive filter, and practical gratings with desired transmission characteristics were designed. In particular, we designed gratings that can be used as dispersion compensators in transmission. Several trade-offs are present in the design process. In particular, we demonstrated that the power transmission in the pass band, the dispersion, and the bandwidth are closely connected. For a dispersion compensator, one usually wants large transmission and also large dispersion. To obtain this the bandwidth of the filter must be relatively small.

In Chapter 5 we proposed different methods for complete characterization of gratings. First we analyzed a method for phase reconstruction from reflectivity that has appeared in the literature. In this method, one assumes *a priori* that the reflection coefficient satisfies the minimum phase condition. For certain types of gratings, as uniform gratings, this condition is fulfilled, and consequently one can use the logarithmic Hilbert transform to reconstruct the reflection phase response. However, it turns out that small grating imperfections may move the reflection zeros to the "wrong" half-plane, and then the response is not minimum phase anymore. It is shown that the reconstructed phase response often is more inaccurate than the phase response of the corresponding ideal

grating. Consequently, this method is not suitable for experimental gratings.

In the next paper we proposed a different method for the characterization. We assumed that the modulus of the coupling coefficient is known *a priori*. Then, if the coupling coefficient is not symmetric, one can retrieve the phase of the coupling coefficient from the power reflectivity spectrum. The phase retrieval is performed by using an iterative Fourier transform algorithm. This method may be useful for intragrating sensing according to the following scheme: Initally one must fabricate a weak grating with an asymmetric index modulation amplitude and characterize it using a method for complete characterization (for example one of the methods in Section 5.3 or 5.4). Then one can use the grating as a sensor: By recording the power reflection spectrum one can compute the grating phase using the iterative Fourier transform algorithm since the coupling coefficient amplitude is known. Only the phase and not the amplitude of the coupling coefficient is altered when the grating is exposed to a change in the strain or temperature profile. The temperature or strain profile is encoded in the phase of the coupling coefficient or the Bragg wavelength profile.

The two final papers contained descriptions of complete characterization methods. The first method is the simplest; one cuts the fiber after the grating yielding a Fabry-Perot cavity with the grating and the bare fiber end reflection as the mirrors. By looking at the phase of the Fabry-Perot spectral fringes, one can read out the effective cavity length and thus the group delay of the grating. The power reflection spectrum is obtained from the lowpass-filtered Fabry-Perot spectrum. The method was tested on numerical examples with noise and also experimentally, yielding good stability and reproducibility.

The idea of the final characterization method is to use low-coherence light to probe the grating at different positions. We showed that the measured signal is proportional to the impulse response of the grating, and thus one gets the complex spectrum by a Fourier transformation. Several gratings were characterized experimentally using a dual-channel interferometer. An excellent agreement between the square modulus of the measured spectrum and the power reflection spectrum measured by a scanning DBR (Distributed Bragg Reflector) laser was demonstrated.

6.2   Future work

One interesting issue is the impact of noise in inverse scattering algorithms. For several applications, it is desirable to reconstruct the grating profile from a measured complex reflection spectrum, and hence it is desirable to analyze how noise in the measurements is amplified through the reconstruction process. It would also be useful to include some *a priori* information on the coupling coefficient in order to regularize the solution yielding better numerical stability.

As noted in the appendix of Section 3.2, the FIR windowing procedure is not necessarily optimal for the synthesis of finite length gratings. Strictly speaking, the windowing procedure does not apply to Bragg gratings due to the infinite length of the grating impulse response. Therefore, it would be useful to investigate how one can make a goal spectrum exactly realizable for a grating of length L. For example, one could try to find the realizable spectrum that is closest to the goal spectrum in the least-square sense. By

combining such a fitting procedure with the layer-peeling algorithm, one ends up with a design method that finds the grating structure of length L whose reflection spectrum is optimal with respect to the goal spectrum. Such a method would be particularily suitable for designing short gratings.

The algorithm for synthesis of minimum phase functions could be used in other fields, for example for designing thin-film filters in transmission or transmission lines. Moreover, the numerical solution to Krein-Nudelman's problem could be used for extrapolation of causal filter functions or design of general filters. It would be interesting to investigate how the extrapolation technique complies with noise for different values of μ.

It remains an open question which method that would be the most practical for intragrating sensing. One could in particular test the methods in Section 5.2 and Section 5.3 experimentally for this purpose. Both methods are promising due to relatively good stability against noise, and because it is only necessary to record a power reflectivity spectrum.

Bibliography

[1] K. O. Hill, Y. Fujii, D. C. Johnsen, and B. S. Kawasaki, "Photosensitivity in optical fiber waveguides: Application to reflection filter fabrication," Appl. Phys. Lett. **32,** 647–649 (1978).

[2] P. J. Lemaire, R. M. Atkins, V. Mizrahi, and W. A. Reeed, "High pressure H2 loading as a technique for achieving ultrahigh UV photosensitivity and thermal sensitivity in GeO2 doped optical fibers," Electron. Lett. **29,** 1191–1193 (1993).

[3] G. Meltz, W. W. Morey, and W. H. Glenn, "Formation of Bragg gratings in optical fibers by a transverse holographic method," Opt. Lett. **14,** 823–825 (1989).

[4] K. O. Hill and G. Meltz, "Fiber Bragg Grating Technology: Fundamentals and Overview," J. Lightwave Technol. **15,** 1263–1276 (1997).

[5] R. Stubbe, B. Sahlgren, S. Sandgren, and A. Asseh, in *Photosensitivity and Quadratic Nonlinearity in Glass Waveguides (Fundamentals and Applications)* (Postdeadline papers, Portland, OR, 1995), p. PD1.

[6] A. Asseh, H. Storøy, B. E. Sahlgren, S. Sandgren, and R. Stubbe, "A writing technique for long fiber Bragg gratings with complex reflectivity profiles," J. Lightwave Tech. **15,** 1419–1423 (1997).

[7] J. A. R. Williams, K. S. I. Bennion, and N. J. Doran, "Fiber dispersion compensation using a chirped in-fibre Bragg grating," Electron. Lett. **30,** 985–987 (1997).

[8] I. Baumann, J. Seifert, W. Nowak, and M. Sauer, "Compact all-fiber add-drop multiplexer using fiber Bragg gratings," IEEE Photon. Technol. Lett. **8,** 1331–1333 (1996).

[9] D. R. Hjelme, H. Storøy, and J. Skaar, in *Trends in Optics and Photonics Series* (OSA, 1998), pp. 280–284.

[10] A. D. Kersey, M. A. Davis, H. J. Patrick, M. LeBlanc, K. P. Koo, C. G. Askins, M. A. Putnam, and E. J. Friebele, "Fiber grating sensors," J. Lightwave Technol. **15,** 1442–1463 (1997).

[11] J. T. Kringlebotn, J. L. Archambault, L. Reekie, and D. N. Payne, "Er^{3+}:Yb^{3+}-codoped fiber distributed-feedback laser," Opt. Lett. **19,** 2101–2103 (1994).

[12] T. Erdogan, "Fiber Grating Spectra," J. Lightwave Technol. **15,** 1277–1294 (1997).

127

[13] R. Kashyap, *Fiber Bragg Gratings* (San Diego, CA: Academic Press, 1999).

[14] A. Othonos and K. Kalli, *Fiber Bragg Gratings: Fundamentals and Applications in Telecommunications and Sensing* (Boston: Artech House, 1999).

[15] A. W. Snyder and J. D. Love, *Optical Waveguide Theory* (Chapman & Hall, 1983).

[16] H. Kogelnik, "Filter response of nonuniform almost-periodic structures," Bell Sys. Tech. J. **55,** 109–126 (1976).

[17] D. Marcuse, *Theory of Dielectric Optical Waveguides* (New York: Academic, 1991).

[18] L. Poladian, "Resonance Mode Expansions and Exact Solutions for Nonuniform Gratings," Phys. Rev. E **54,** 2963–2975 (1996).

[19] H. Kogelnik, in *Theory of Optical Waveguides, Guided-Wave Optoelectronics*, T. Tamir, ed., (New York: Springer-Verlag, 1990).

[20] L. A. Weller-Brophy and D. G. Hall, "Analysis of waveguide gratings: application of Rouard's method," J. Opt. Soc. Am. A **11,** 2027–2037 (1985).

[21] R. Feced, M. N. Zervas, and M. A. Muriel, "An efficient inverse scattering algorithm for the design of nonuniform fiber Bragg gratings," IEEE J. Quantum Electron. **35,** 1105–1115 (1999).

[22] G.-H. Song, "Theory of symmetry in optical filter responses," J. Opt. Soc. Am. A **11,** 2027–2037 (1994).

[23] L. Poladian, "Group-delay reconstruction for fiber Bragg gratings in reflection and transmission," Opt. Lett. **22,** 1571–1573 (1997).

[24] D. M. Pozar, *Microwave engineering* (Addison-Wesley, 1993).

[25] E. Brinkmeyer, "Simple algorithm for reconstructing fiber grating from reflectometric data," Opt. Lett. **20,** 810–812 (1995).

[26] G. Lenz, "Dispersive properties of optical filters for WDM systems," IEEE J. Quantum Electron. **34,** 1390–1402 (1998).

[27] G.-H. Song and S.-Y. Shin, "Design of corrugated waveguide filters by the Gel'fand-Levitan-Marchenko inverse-scattering method," J. Opt. Soc. Am. A **2,** 1905–1915 (1985).

[28] P. V. Frangos and D. L. Jaggard, "A numerical solution to the Zakharov-Shabat inverse scattering problem," IEEE Trans. Antennas. Propagat. **39,** 74–79 (1991).

[29] P. V. Frangos and D. L. Jaggard, "Inverse scattering: Solution of coupled Gel'fand-Levitan-Marchenko integral equations using succesive kernel approximations," IEEE Trans. Antennas. Propagat. **43,** 547–552 (1995).

[30] E. Peral, J. Capmany, and J. Marti, "Iterative solution to the Gel'fand-Levitan-Marchenko equations and application to synthesis of fiber gratings," IEEE J. Quantum Electron. **32,** 2078–2084 (1996).

[31] L. Poladian, "Simple grating synthesis algorithm," Opt. Lett. **25,** 787–789 (2000).

Publication list

Journal publications

1. J. Skaar, B. Sahlgren, P.-Y. Fonjallaz, H. Storøy, and R. Stubbe, "High-reflectivity fiber-optic bandpass filter designed by use of the iterative solution to the Gel'Fand-Levitan-Marchenko equations," Opt. Lett. **23**, 933-935 (1998).

2. J. Skaar and K. M. Risvik, "A genetic algorithm for the inverse problem in synthesis of fiber gratings," J. Lightwave Technol. **16**, 1928-1932 (1998).[1]

3. D. R. Hjelme, H. Storøy, and J. Skaar, "Reconfigurable all-optical crossconnect node using synthesized fiber Bragg gratings for both demultiplexing and switching," in OSA Trends in Optics and Photonics Series (TOPS) **20**, Optical Networks and Their Applications, ISBN 1-55752-545-5, Richard A. Barry, ed., 280-284 (1998).

4. J. Skaar and H. E. Engan, "Phase reconstruction from reflectivity in fiber Bragg gratings", Opt. Lett. **24**, 136-138 (1999).[1]

5. J. Skaar, "Measuring the group delay of fiber Bragg gratings by use of end reflection interference", Opt. Lett. **24**, 1020-1022 (1999).

6. I. Petermann, J. Skaar, B. Sahlgren, R. Stubbe, and A. Friberg, "Characterization of fiber Bragg gratings by use of optical coherence-domain reflectometry," J. Lightwave Technol. **17**, 2371-2378 (1999).[1]

7. J. Skaar, "A simple method for characterization of fiber Bragg gratings," submitted to OSA Trends in Optics and Photonics Series (TOPS) **33**, Bragg Gratings, Photosensitivity, and Poling in Glass Waveguides, submitted October 1999.[1]

8. J. Skaar and T. Erdogan, "Synthesis of thick optical thin-film filters using a layer-peeling inverse scattering algorithm," submitted to Applied Optics, June 2000.[1]

9. J. Skaar, "Synthesis of limited bandwidth minimum phase filters," submitted to Inverse Problems, October 2000.[1]

10. J. Skaar, "Synthesis of fiber Bragg gratings for use in transmission," accepted for publication in Journal of the Optical Society of America A, submitted June 2000.[1]

11. J. Skaar, L. Wang, and T. Erdogan, "On the Synthesis of Fiber Bragg Gratings by Layer Peeling," to appear in IEEE Journal of Quantum Electronics, February 2001.[1]

Conference publications

12. J. Skaar and K. M Risvik, "A genetic algorithm for the inverse problem in synthesis of fiber gratings," European Workshop on Optical Fibre Sensors, Scotland, July 1998.

13. D. R. Hjelme, H. Storøy, and J. Skaar, "Reconfigurable all-fiber all-optical cross-connect node using synthesized fiber Bragg gratings for both demultiplexing and switching," Optical Fiber Communication Conference (OFC), San Jose, California, February 1998.

14. H. Storøy, J. Skaar, R. Stubbe, and B. Sahlgren, "Fibre optic Bragg grating band stop filters for WDM applications," in Norwegian Conference on Electro-optics, Geiranger, 1997.

15. I. Petermann, B. Sahlgren, J. Skaar, P.-Y. Fonjallaz, and R. Stubbe, "Phase distribution measurement of fibre Bragg gratings with white light interferometry," European Conference on Optical Communications (ECOC), Madrid, Spain, September 1998

16. P.-Y. Fonjallaz, J. Skaar, B. Sahlgren, H. Storøy and R. Stubbe, "Optimised fibre Bragg grating filters for telecommunications", Summer School on Photosensitivity in Optical Waveguides and Glasses, Switzerland, July 1998.

17. J. Skaar and H. E. Engan, "Distributed intragrating sensing using phase retrieval," in 13th International Conference on Optical Fiber Sensors (OFS 1999), Kuongju, S. Korea, Proceedings of SPIE Vol. 3746, 588-591 (1999).[1]

18. J. Skaar and H. E. Engan, "Distributed temperature or strain sensing from the reflectivity spectrum of a fiber Bragg grating," in Norwegian Electro-optics Meeting, Balestrand 1999.

19. J. Skaar, "Characterization of fiber Bragg gratings by use of end reflection interference," in Bragg Gratings, Photosensitivity, and Poling in Glass Waveguides, OSA Technical Digest (Optical Society of America, Washington DC, 1999), pp. 242-244.

20. T. Kjerre, Ø. Farsund, J. Skaar, K. Pran, G. B. Havsgård, and G. Wang, "Experimental technique for strain gradient measurement with embedded fiber Bragg gratings by use of a tunable external cavity laser," in 14th International Conference on Optical Fiber Sensors (OFS 2000), Venice, Italy, Paper P3-11.

Thesis

21. J. Skaar, "Synthesis and analysis of optical fiber Bragg gratings," Diploma thesis, The Norwegian University of Science and Technology, December 1997.

---

[1]The paper is included in this thesis.